CALIFORNIA INSTITUTE OF TECHNOLOGY

EARTHQUAKE ENGINEERING RESEARCH LABORATORY

A MATHEMATICAL MODEL FOR CALCULATION OF THE RUN-UP OF TSUNAMIS

BY

KENNETH LEON HEITNER

A REPORT ON RESEARCH CONDUCTED UNDER A GRANT FROM THE NATIONAL SCIENCE FOUNDATION

PASADENA, CALIFORNIA

1969

A MATHEMATICAL MODEL FOR CALCULATION OF THE RUN-UP OF TSUNAMIS

Thesis by

Kenneth Leon Heitner

In Partial Fulfillment of the Requirements

For the Degree of

Doctor of Philosophy

California Institute of Technology

Pasadena, California

1969

(Submitted May 19, 1969)

ACKNOWLEDGEMENT

The author wishes to acknowledge the guidance of Dr. George W. Housner in carrying out the work discussed in this thesis. He also wishes to acknowledge the financial support of the National Science Foundation, the State of California, and the R. C. Baker Foundation

ABSTRACT

To understand the engineering implications of possible wave run-up resulting from tsunamis, a formulation of the run-up process capable of giving quantitative answers is required. In this thesis, a new mathematical run-up model suitable for computer evaluation is proposed and tested. The two-dimensional model uses a flow constrained so that the horizontal velocity is uniform in depth. However, unlike the usual shallow water theory, the terms representing the kinetic energy of the vertical motion are retained. It is shown that this formulation allows a solitary-like wave to propagate as well as giving a more accurate indication of wave breaking. An 'artificial viscosity' term is used to allow the formation of hydraulic shocks. The effects of bottom friction are also included. The model is derived for a linear beach slope, in Lagrangian coordinates. A finite element formulation of the problem is derived that is suitable for digital computer evaluation.

Calculations with the model agree satisfactorily with experimental results for the run-up of solitary waves and bores. The model is used to obtain run-up data on tsunami-like waves, which show the danger of large run-up from low initial steepness waves on shallow slopes. However, the data also show that bottom friction values can significantly attenuate run-up, especially on shallow slopes.

Waves generated by a dipole-like displacement of the simulated ocean floor show that the run-up is usually larger when the upwards displacement is nearest the beach than when the downwards displacement is nearest the beach.

TABLE OF CONTENTS

INTRODUCTION

The consideration of tsunamis (seismic sea waves) is comparatively new in the engineering of man-made structures. Increased population and increased construction, particularly of nuclear reactor power plants, has led engineers to give more attention to protection against earthquakes and related natural phenomena.

Tsunamis are large ocean waves generated by movement of the ocean floor in undersea earthquakes. These waves propagate to the ocean shoreline, where they are capable of doing great damage. Large ocean waves, generated by earthquake induced landslides, as referenced by Wiegel (25), are also classed as tsunamis.

At present, the ocean shoreline regions are the sites of a high degree of development. They are the locations for large power plants and other industries desiring to use the ocean as a thermal sink. They are the interface between waterborne and land transportation systems, and they are also regions of great population centers. In order to prepare suitable structural designs for these areas, one should know about the probabilities of tsunamis at a certain site and the depth of inundation and water velocities that could be expected if a tsunami did occur. Then, valuable or vital structures could be protected from the tsunami or designed to resist it with acceptable levels of damage. However, the desired information is very difficult to obtain because of the complexity of the overall tsunami problem.

Tsunamis may be generated unpredictably in many areas of undersea earthquake activity. The basic generating mechanism is a tectonic displacement of the ocean floor which displaces the water from its equilibrium with respect to the gravity field. Studies by Iida (6) indicate that an average of one tenth of the seismic energy is coupled into the tsunami wave energy, and that significant tsunamis are to be expected only with earthquakes of magnitude greater than 6.5.

The displacements are usually small with respect to the depth of the water, measured in tens of feet, so that equivalent problems of elevations or depressions in the water's surface may be considered. Since the tectonic displacement is estimated to occur with a velocity of approximately one foot per second, the displacements occur rapidly compared to the time needed by the water to flow away. There is an extensive literature on tsunami generation and propagation and the papers of Carrier (2) and Keller (10) are typical works dealing with the theory of tsunami generation by considering simple geometries of bottom deformation.

Experimental studies of tsunami generation have also been made. Wiegel (25) studied waves generated by initial elevations and depressions in the water's surface, as well as block masses, simulating landslides, entering the water. Takahasi (20) studied waves from single circular sources and arrays of circular sources.

The generation of actual tsunamis is quite complex and is not well known, only the most basic features have been identified. The typical dimensions of a significant tsunami can be deduced from

the data compiled by Iida (6), on many tsunamis. The height of the tsunami at generation is of the order of the vertical bottom displacement, which for a large earthquake typically is 1-10 feet, but may be as much as 50 feet. The water is usually deep, one to two miles, or 10^4 feet. The characteristic length is of the order of the size of the disturbed area, which for a very large earthquake may be 50-200 miles across, or 10^5 to 10^6 feet. This means the longest wave lengths in the tsunami waveform are of this size.

Because the wave height is much less than the depth, small amplitude theory may be used to study the wave motion in mid-ocean. The longer wave lengths travel at the upper limiting velocity $\sqrt{gd}$, where d is the ocean depth, which in mid-ocean is approximately 500 feet per second. Destructive tsunamis may travel long distances, for example, the tsunami generated just offshore by the Chilean earthquake of May 1960 caused destruction and loss of life in Hawaii and in Japan. However, the travel time of the tsunami is long enough to allow the evacuation of distant areas where the tsunami is expected to strike if there is an efficient warning system.

The shorter wave lengths will propagate slower, be more subject to internal damping, and contain less energy than the longer waves, and they probably can be neglected far from the tsunami source.

The propagation of the tsunami across the ocean is often studied by drawing refraction diagrams based on the ocean bottom contours. Wadati (23) gives examples of these diagrams used to calculate the travel times of tsunamis for the purposes of the Pacific

Tsunami Warning System. Such refraction charts also give the magnification of the wave height due to refraction, assuming the energy between rays is conserved. Refraction diagrams are also drawn for regions near shore to examine the wave behavior there.

The largest gap in knowledge about the generation and propagation of tsunamis is the lack of full scale measurements on a tsunami in the deep ocean. However, as described by Vitousek (21), the problems of obtaining such measurements via pressure transducers on the ocean floor are not simple.

As the tsunami approaches a shoreline, the wave grows in height, especially if the depth transition is gradual and only a small fraction of the wave energy is reflected seaward. Kajiura (7) gives a thorough discussion of this problem for a wide range of transition geometries.

Depending on the particular coastline, two things may happen. First local resonances may be excited. These are often seen in the frequency spectrum of local tide gauge records obtained during the disturbance. These resonances are caused by energy being trapped between steep depth transitions and steep (highly reflective) shorelines. They also occur in harbors, bays, and other relatively enclosed bodies of water excited by the tsunami. Numerous calculations of resonant frequencies have been made with the hope of finding a correspondance with the peaks of the tide gauge spectrum, but the analysis of the three-dimensional problem is very difficult.

Where the tsunami impinges on a beach, the so called run-up problem occurs. This is of practical importance because additional

magnification of the wave occurs and it may climb up the beach a considerable distance. Also, this process determines what sort of reflected wave occurs, an important consideration in trying to study resonances. If one of the boundaries of a resonant cavity returns only a small fraction of the energy it receives, the accumulation of energy in the cavity can only be very slow and may not even occur at all.

In trying to evaluate the engineering implications of the tsunami problem, it was felt that a better formulation of the run-up process would be of value. It would be very informative if the characteristics of distant or local tsunamis were known or could be assumed, the waves produced used as input to the run-up process, and the run-up heights and velocities calculated. Comparisons between two sites could be made to determine which would be more desirable in the event of such a projected tsunami; or the influence of bottom friction on run-up could be evaluated, etc. The available mathematical models seemed unsuitable for this purpose. Hence the objective of the research described in this thesis was to develop a model by means of which practical results could be calculated. This would then complement experimental models in investigating tsunami run-up.

The model would have to be more complete in its description of the hydrodynamics of run-up than present mathematical models in order to provide practical information on run-up heights and water velocities. This would require numerical solution techniques, since analytic solutions for these problems are quite limited. However, the model would not be an attempt to completely reproduce the hydro-

dynamics of the prototype, as is often done in scale model experiments. Approximations that would obscure the less significant detailed flow phenomena would be acceptable and useful in keeping the amount of numerical computation within reasonable limits. The result would be a useful tool for studying the implications of tsunami run-up on structural design.

THE RUN-UP PROBLEM

The run-up problem can be defined as what happens when waves on the free surface of the ocean impinge on a shoreline. The most general form of this problem can be posed mathematically, as done by Stoker (19) as a general free surface flow in a vessel of arbitrary shape. However, a general solution to this problem, either analytically or numerically, is at present impossible. Even modelling such a problem experimentally is a large and difficult job.

The usual first step in simplifying this problem is to eliminate the horizontal dimension parallel to the beach. The shoreline is made straight and the wave motion is perpendicular to it. This means that certain refraction, diffraction, and reflection phenomena cannot be studied. However, in many cases these processes occur separately from the actual run-up and can be studied by themselves.

Even this reduced problem is usually further simplified by having an incoming wave in a region of constant depth, joined by a linear slope as the profile of the beach. A number of studies of this problem have been made, as summarized by LeMéhauté (13). They reflect the two usual approaches to any problem in that both experimental models and mathematical models are discussed.

Experimental results basic to the run-up problem are given by Savage (17) and Saville (18), who measured the run-up of periodic waves on beaches of varying slope, roughness, and permeability. The results, however, are for waves which are rather steep compared to tsunami waves and for beaches which are steep compared to

continental slopes along many shorelines. It is difficult to model waves of very small steepness accurately, especially on very small slopes. On the smaller scale of the model, the frictional effects are quite different from those of the prototype. Also, surface tension and the wetting action of the beach material introduce many complicating factors. Large models avoid these problems, but require more costly facilities.

Hall and Watts (5), and Kishi and Saeki (11) measured the run-up of solitary waves, which are steep. Recently, Miller (14) measured the run-up of bores moving towards the beach. These data are not of direct application to the tsunami run-up problem, but they do provide results against which to test a run-up theory.

Mathematical analysis of the run-up problem usually leads to expansion solutions for certain types of waves, i.e., small amplitude or shallow water waves. In general, small amplitude theory is used offshore, with (nonlinear) shallow water theory used near the beach. A typical example of this is the work of Carrier (2), in which the tsunami is assumed to originate from a point disturbance and the resulting run-up is calculated. Keller (10) gives results for sinusoidal wave run-up based on small amplitude theory. However, all these results have the common limitation of not allowing the wave to break and form a bore. Breaking can be predicted, but the flow after breaking is not given. Also only frictionless cases can be treated, and only linear slopes.

To allow for the breaking waves, numerical solutions have

been attempted where the bore was 'fitted' between the incoming wave and the undisturbed water. This was first done by Keller, Levine, and Whitham (9) for a bore approaching a beach. It was a test of the approximation of Whitham (24) which allowed the variation in the strength of a bore to be derived from the shallow water theory and the associated shock conditions. Freeman and LeMéhauté (4) used this 'fitted' shock to study the run-up of solitary waves.

Amein (1) used this method to study long waves running up on a beach, as well as separate theoretical calculations of the strength of the bore. Additional methods of dealing with breaking waves are summarized by LeMéhauté (13).

In attempting to improve on the run-up models available, it is thought a new model should include the kinetic energy of the vertical component of the flow, which had not been included in prior model studies. It should also model the effects of bottom friction and be extendable to a general beach profile. The model should also allow for breaking waves. Assuming such a model could be derived and that it was suitable for numerical calculations, it then would be tested against known results, as well as used to study aspects of the tsunami run-up problem.

The discussion of the development of the new model is broken down into several steps. First, the theoretical background and justification of the model is given. Then a finite element version of the model is derived and its numerical evaluation is discussed. Last, the model is shown to reproduce known results indicating its usefulness. It is then used to investigate some features of tsunami run-up.

PROPOSED MODEL THEORY

Simplifying Assumption

In considering how to analyze the run-up problem, it becomes clear that the vertical dimension (water depth) cannot be an independent variable as this hopelessly complicates the problem, but neither can it be eliminated from the problem completely. One must make a suitable assumption about the flow which allows the equations to be integrated (averaged) vertically, yet preserves the physics required to model the run-up process. One way to achieve this is to approximate the horizontal velocity distribution by a finite number of terms in the vertical direction, i.e.,

$$u(x,y,t) \approx \sum_{i=0}^{i=N} y^i u_i(x,t) \qquad (1)$$

where N is a small integer like 0, 1, 2, or 3, u is the horizontal velocity, x is the horizontal coordinate, y is the vertical coordinate, and t is time. The equations then can be integrated vertically, since the y dependence is now explicit. The resulting problem, in one space dimension and time, is reasonable to solve numerically, as demonstrated by work in flood waves and other problems, see Stoker (19) and Richtmyer (15).

The simplest assumption is that the flow is constrained so the horizontal component of fluid velocity is constant over the depth, i.e., $N = 0$, and this forms the basis for the present study. This is reasonable for long waves approaching a beach, since it is a basic result of long wave (shallow water) theory. For steeper waves, such as solitary

waves, the distribution of horizontal velocity is not constant and the assumption of constrained flow is more approximate. However, a comparison of the solitary wave theory of Laitone (12) (which has no constraint) with a solitary-like wave from the constrained flow equations shows the approximation in profile shape is good, see Figure I, also Appendix B. Only near the limiting solitary wave, $H/d \sim 0.71 - 0.72$, does any appreciable difference show up.

An important point is that the kinetic energy of the vertical flow is not neglected as it is in shallow water theory. It has been noted by LeMéhauté (13) that shallow water theory tends to predict breaking sooner than is observed experimentally; in fact, it causes every waveform to break. On the other hand, the constrained flow gives more realistic results in that it includes the effects of the vertical kinetic energy of the flow.

The model should approximate cnoidal wave forms if the variation of horizontal velocity with depth is not too large. It becomes invalid for surface waves of less than 3-5 times the depth in wavelength, which have a non-constant distribution of horizontal velocity. However these are not of interest here. See Appendix D.

The equations of constrained flow are readily derived from the general equations of motion and continuity. The flow is incompressible so the density is constant and this allows the equations to be simplified by setting the density equal to unity. The flow in Figure II, where the horizontal velocity u is not a function of the vertical coordinate y, (i.e., $u = u(x,t)$), then is described by the continuity equation

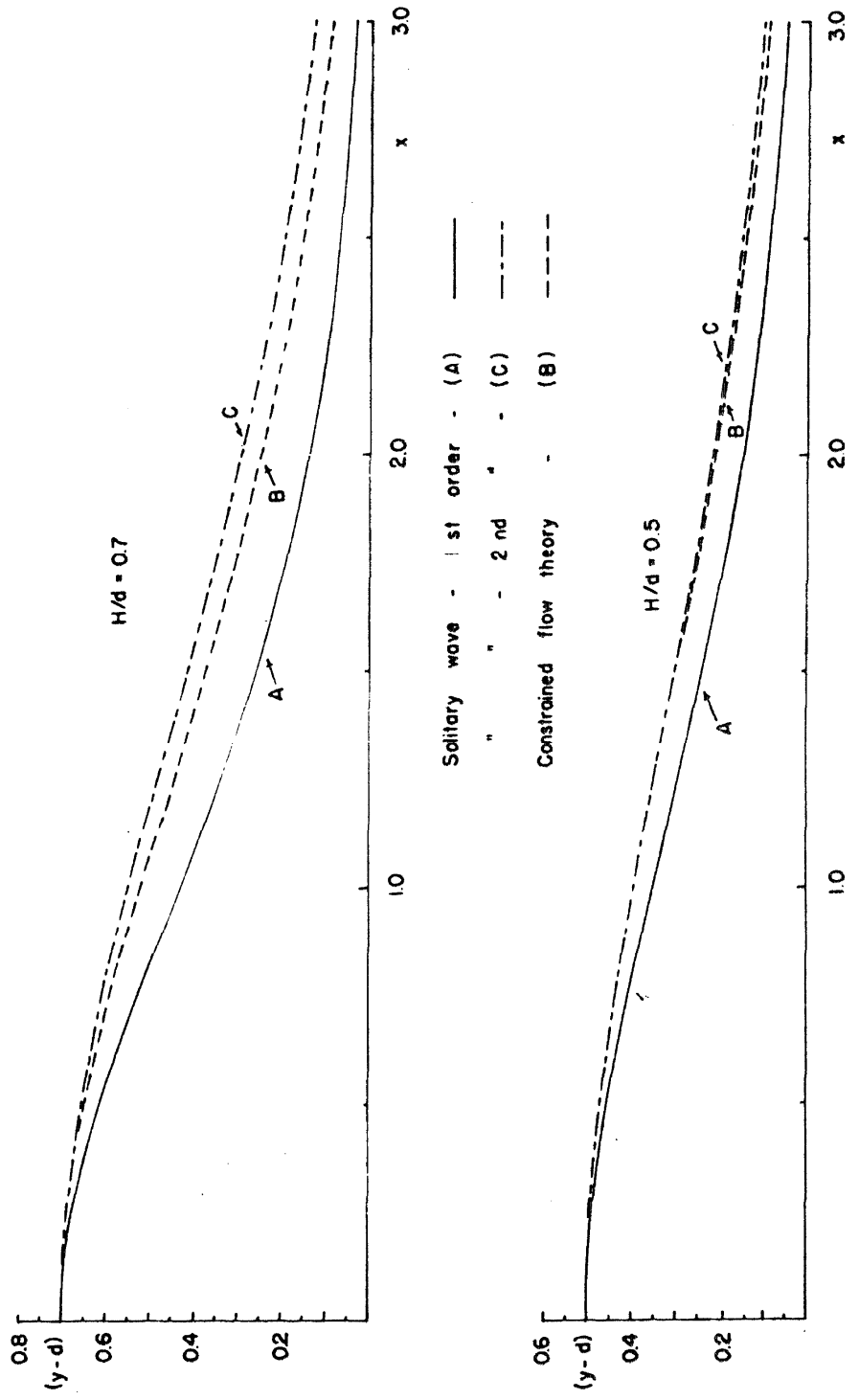

Figure 1. Comparison of Solitary Wave Theory and Constrained Flow Theory

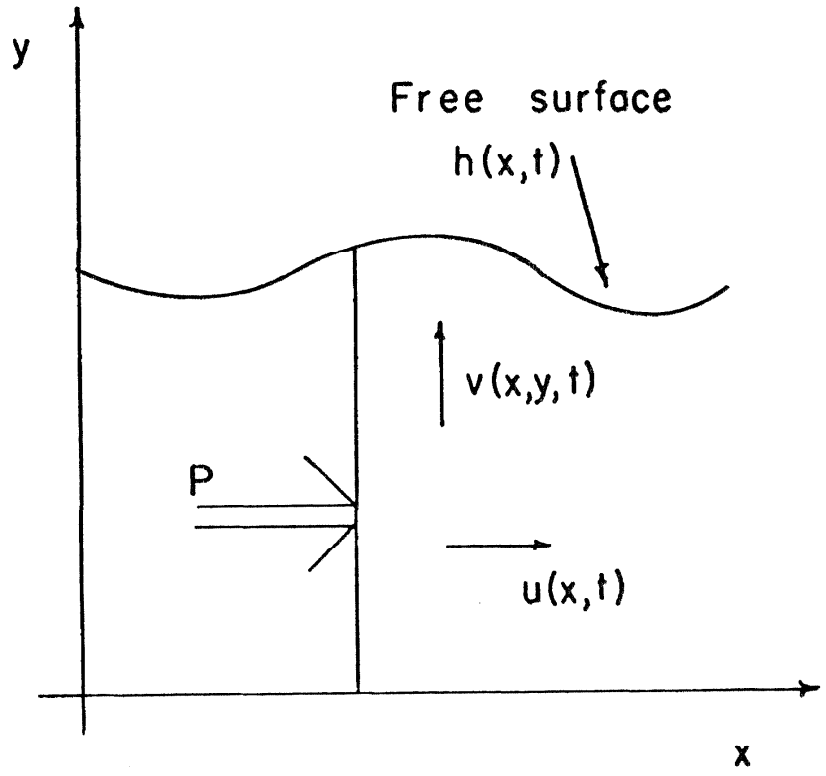

Figure II. Basic Flow Quantities

$$u_x + v_y = 0 \tag{2}$$

where v is the vertical velocity and x is the horizontal coordinate. This integrates to

$$yu_x + v = f(x,t) \tag{3}$$

where f is an arbitrary function of x and t. Since $v = 0$ at $y = 0$ for a flat bottom, then

$$v = - yu_x \tag{4}$$

Substituting in the vertical momentum equation and including a gravity field $-g$, one has

$$dv/dt = -g-(\partial p/\partial y) \tag{5}$$

where p is the pressure.

Equation (4) can be differentiated

$$dv/dt = y(u_x^2 - u_{xt} - uu_{xx}) \tag{6}$$

and combined with (5), and since the y dependence is explicit and $p = 0$ at $y = h(x,t)$, the free surface, two integrations will give the total force P on a vertical section

$$P = gh^2/2 + h^3(u_x^2 - u_{xt} - uu_{xx})/3 \tag{7}$$

The second integration averages the pressure distribution vertically. If this pressure distribution were allowed to act on unconstrained fluid, it would cause the horizontal fluid velocity to vary over the depth. This would violate the original constraint placed on the

flow. Thus the approximation involved in averaging the vertical pressure distribution is consistent with the constrained flow.

When the pressure force P and the horizontal momentum of the fluid in a vertical section (u^2h) are considered, the average horizontal momentum equation results

$$(uh)_t + (u^2h + P)_x = 0 \tag{8}$$

The well known shallow water continuity equation is valid

$$h_t + (uh)_x = 0 \tag{9}$$

Note that equation (8) is the momentum equation for shallow water flow with additional terms representing the vertical kinetic energy of the constrained flow.

'Artificial Viscosity' Term

Equations (8) and (9), however, will still not provide a correct model for the run-up flow, as they represent a system with no energy dissipation. In real run-ups, the waves may become steep and break, forming hydraulic shocks with high energy dissipation. The detailed flow within these shocks is complex but we are interested only in its overall effect on the flow preceeding and following it. Hence, we do not try to model the dissipation mechanism within the shock, but merely try to represent its gross effects.

Analytically, this could be done by considering the shock as a discontinuity in the solution between two essentially separate problems, with momentum and continuity preserved across the shock. Numerically, this requires a complex shock 'fitting' procedure. It is somewhat simplified if the shock is progressing into

still water, as does an initial wavefront, but it would yet be necessary to consider return flows and the formation of subsequent shocks.

A more useful approach introduces an 'artificial viscosity' term. In this method, a suitable term is added to the momentum equation which represents the energy dissipation in the regions of sharply changing flow quantities, i.e., shock discontinuities. The term selected here is in effect an 'artificial viscous force' F at any cross section, whose magnitude is

$$F = \ell^2 h(\partial u/\partial x)^2 \tag{10}$$

A more general term would be proportional to density, so as to make the shock width independent of it. Here, the density is taken as unity to be consistent with equations (2) to (9). Equation (9) now reads

$$(uh)_t + (u^2 h + P + F)_x = 0 \tag{11}$$

The motivation for selecting this form for the term is made plausible by examining a simplified profile of a shock. The fluid enters the shock in Figure III(a) from the left at high speed and its velocity drops as it flows through the shock region. The gradient of the velocity (absolute value) has a profile as shown in Figure III(b). This gives a characteristic profile to the curve for F (Figure III(c)); i.e., F is small away from the shock region, but has a sharp peak in the region of rapidly varying flow. The choice of exponents for $(\partial u/\partial x)$ and the factor h merely are weightings to make the shock width independent of strength, as shown in Appendix A.

The factor ℓ^2 controls the width of the shocks that form.

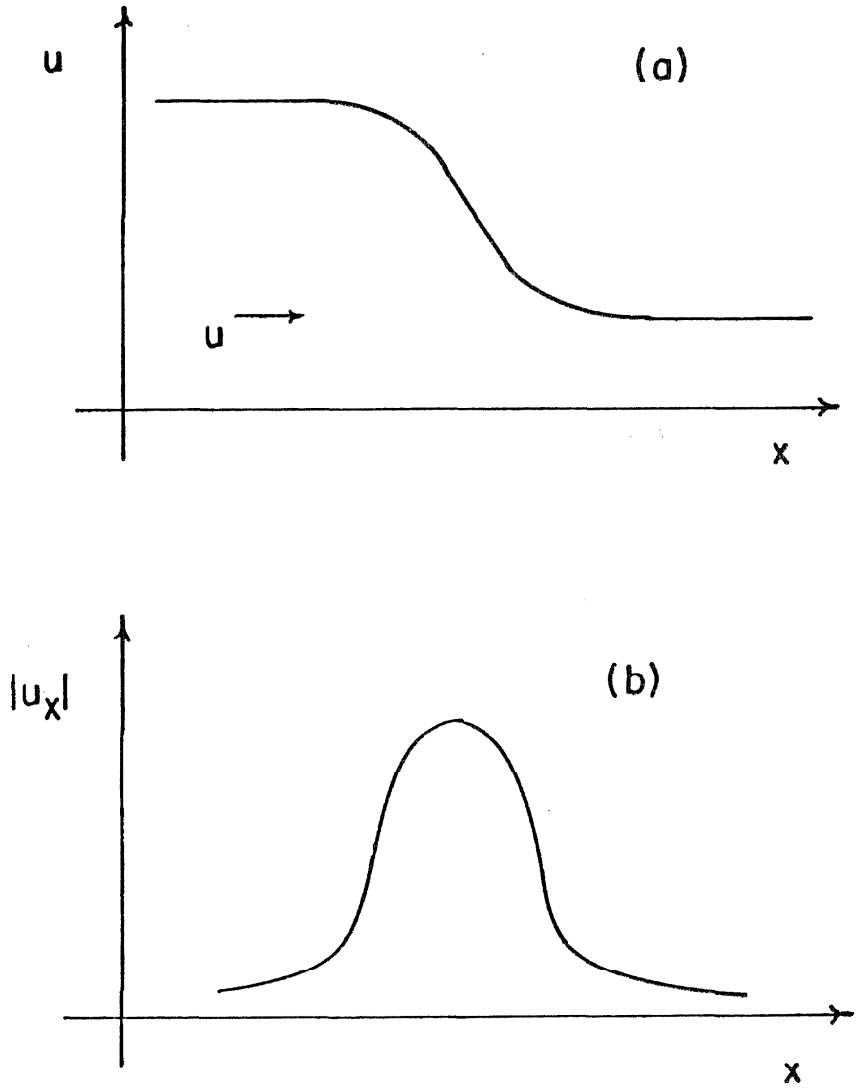

Figure III (a,b). Profiles of 'Artificial Viscosity' Terms Through a Shock

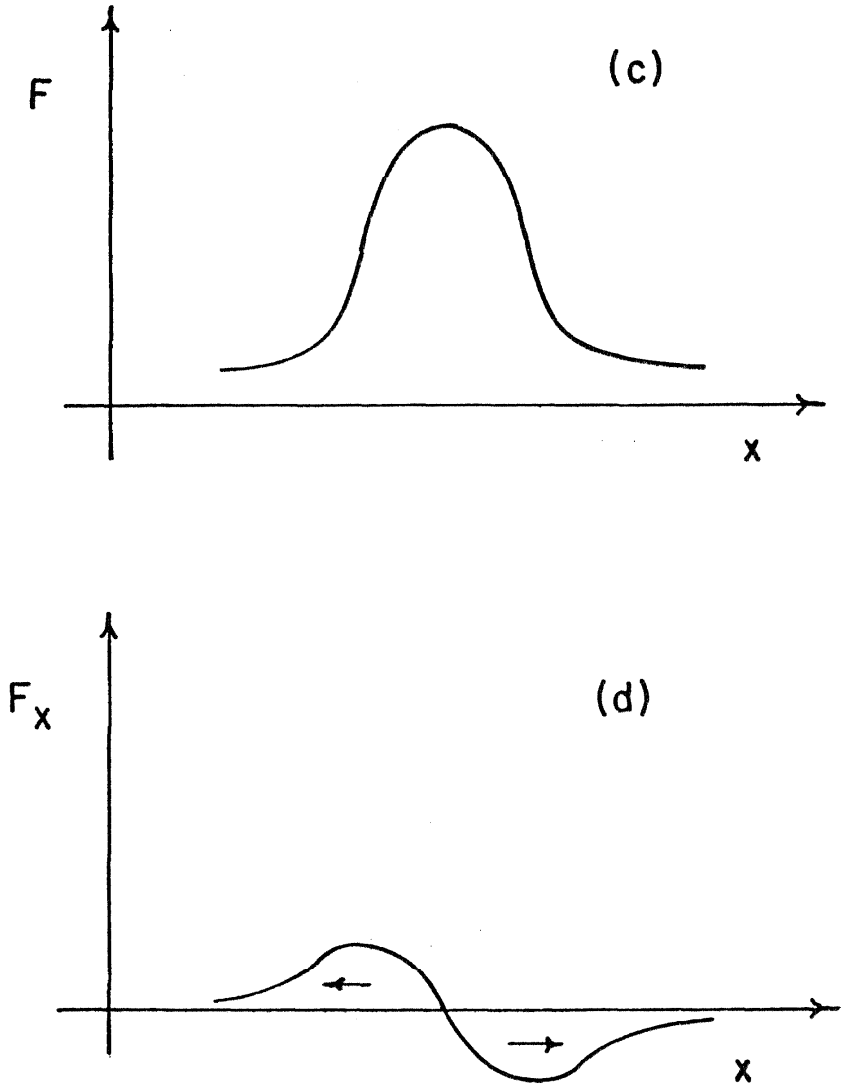

Figure III (c,d). Profiles of 'Artificial Viscosity' Terms Through a Shock

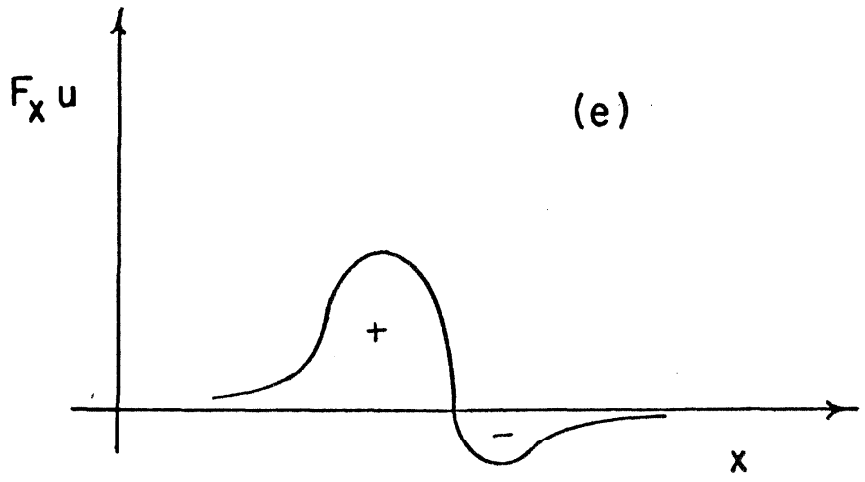

Figure III (e). Profiles of 'Artificial Viscosity' Terms Through a Shock

This also can be seen in Appendix A, where the 'artificial viscosity' term is solved with the shallow water equations to give a shock-like solution, whose slope width is 2ℓ. In the actual examples solved numerically, the presence of the additional terms for the kinetic energy of the vertical flow complicates the effect of the 'artificial viscosity' term. However, larger values of ℓ^2 still give wider shocks.

The gradient of the force, F_x, Fig. III (d)), is the force field the fluid must work against, with local energy dissipation $F_x u$ (Figure III(e)). See Appendix C. The net energy dissipated will be positive, thus accounting for the losses in the shock.

Away from the shock, $\partial u/\partial x$ is very small and the 'artificial viscosity' term has negligible effect. The net force across the shock is zero, so the momentum equation still represents conservation of momentum across the shock. The continuity equation is unmodified and still valid. Hence the shock conditions for an infinitesimal (width) shock are preserved in this finite shock.

Velocity gradients also occur in expansion waves where there is no dissipation, but in this case the 'artificial viscosity' term should have no effect, i.e., it should be small or zero. Hence, a modified term

$$F = \ell^2 h(\partial u/\partial x)^2 He(-\partial u/\partial x) \qquad (12)$$

gives the desired results, where He, the Heavyside function is equal to unity for arguments greater than zero and equal to zero for arguments less than zero.

Numerical solutions for the constrained flow with the 'artificial viscosity' term show that they give the desired modeling of the overall shock structure in the flow. Figures IV(a, b) show typical shock profiles obtained with different values of the shock width coefficient ℓ. In Figure IV(b), larger oscillations downstream of the shock are noticed. These oscillations represent energy produced in the shock, not dissipated by the 'artificial viscosity' term, propagating away from the shock as waves. The 'artificial viscosity' term coefficient must be large enough to reduce these trailing waves to acceptable amplitudes, as in Figure IV(a). This behavior is due to the terms for the kinetic energy of the vertical flow being present. It is not seen in the solution in Appendix A, where the shock width decreases with the shock width coefficient, but remains constant in shape.

An explanation of this phenomena is that the vertical velocity of the fluid as it rides up the crest of the wave is too large for a smooth flow and it tends to overshoot and excite the trailing oscillations as in the case of an undular bore. However, in a real bore of sufficient strength, this overshoot is directed forward and produces the 'roller'action which the constrained flow cannot model.

Figure V shows that the shocks generated behave almost as the theoretical infinitesimal (width) shocks do in terms of the relationship between shock strength and shock velocity. The points representing the calculations lie very close to the theoretical curve, indicating the accuracy of the 'artificial viscosity' method.

The 'artificial viscosity' method was originally developed by Von Neumann and Richtmyer (22) for the analysis of shock waves in

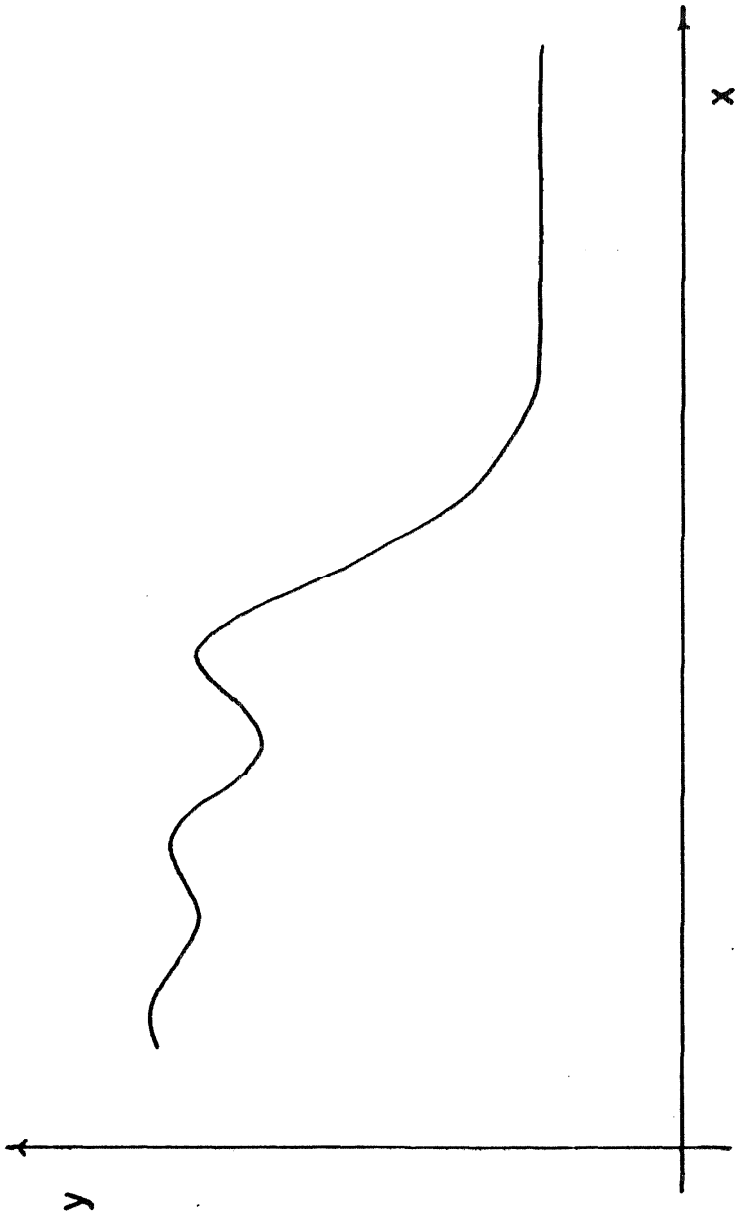

Figure IV(a). Computed Shock Profile. Fr = 2.5, $(\ell/h_1)^2 = 10.0$.

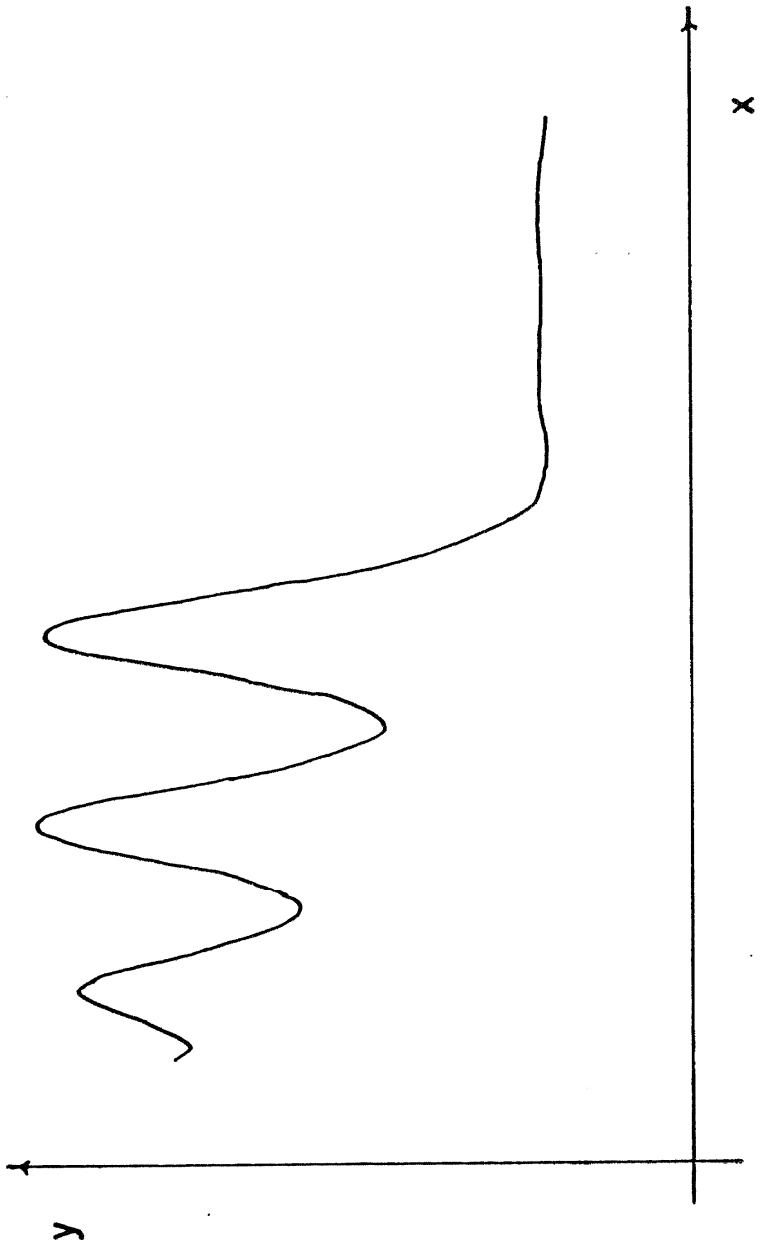

Figure IV(b). Computed Shock Profile. Fr = 2.5, $(\ell/h_1)^2 = 1.0$.

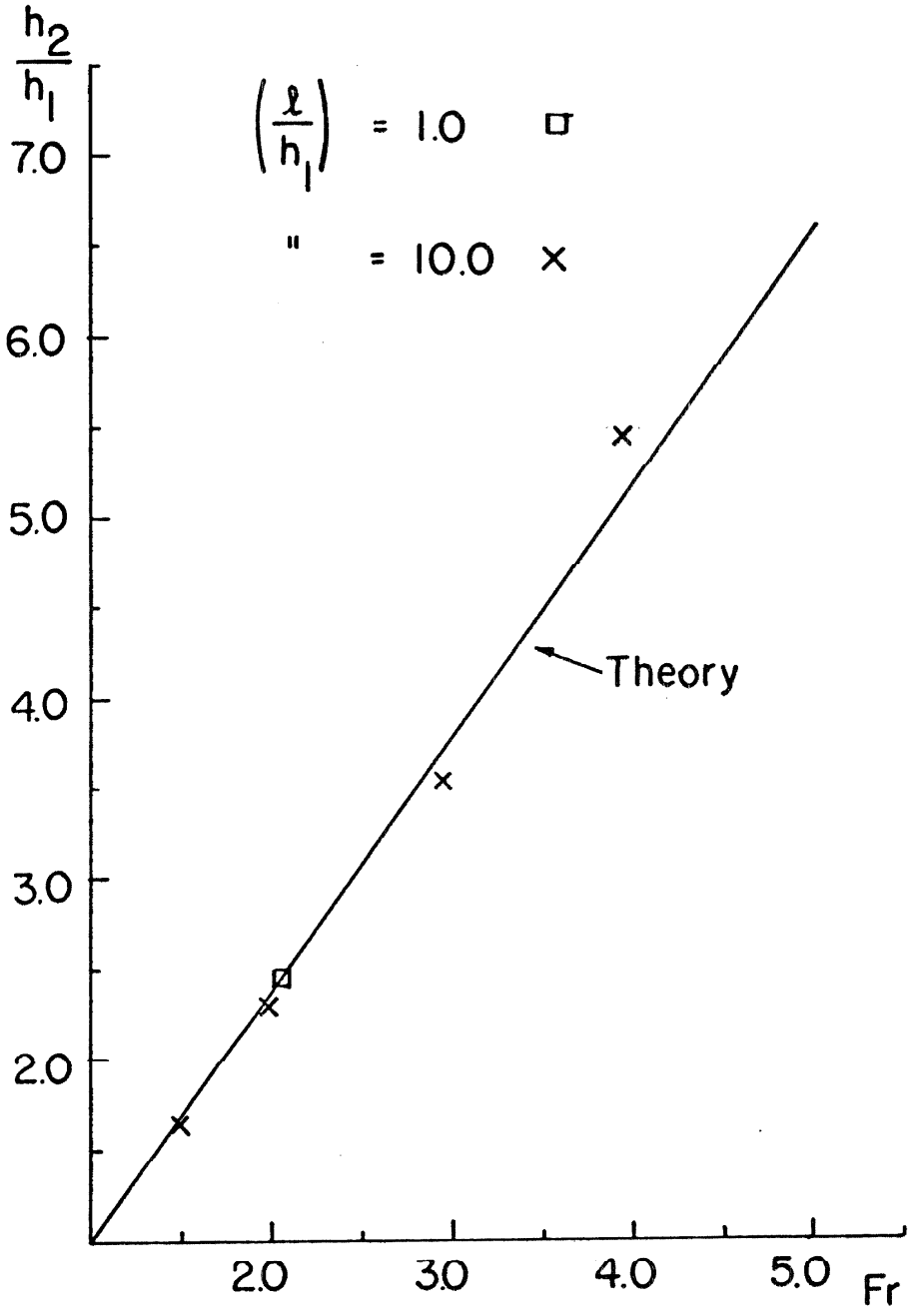

Figure V. Comparison of Computed Height Ratios for Given Froude Number vs. Theory.

gasdynamics. The term used here agrees with that recommended by Richtmyer (15), but it has been modified for hydraulic flow for this investigation. Richtmyer (15) gives detailed discussion on how the method approximates theoretical results for gasdynamics.

Bottom Friction Term

A further significant influence on the hydrodynamics of the run-up is the bottom friction, however, the friction laws operating here are not well known. A simple friction rule is used in this study with the hope of simulating some of the basic effects of the bottom friction. The local shear stress τ at the bottom is taken to be

$$\tau = Ku^2 \tag{13}$$

The friction coefficient K is calculated from the friction rule for steady flow in an open channel of a given depth and bottom roughness. K is thus a function of the depth of the water and the bottom material properties. The details of how this is applied are covered in the cases discussed.

This particular rule was chosen primarily because it allows comparison with the usual steady flow definitions of friction coefficients and friction factors. However, the formulation of the problem does not preclude the use of more accurate friction laws as they are defined.

Lagrangian Coordinates

In visualizing the solution of a run-up problem, it is obvious

that the physical domain of the problem changes as the solution progresses. In an Eulerian coordinate system, this causes complications in numerical calculations, as mesh points have to be added and subtracted during the solution. On the other hand, for modeling a wave tank, or any fixed quantity of fluid, a Lagrangian scheme is more natural. The Lagrangian independent variable is attached to the fluid particles, which are conserved. Hence, the domain of the problem is constant and the numerical calculation simplified.

The Lagrangian scheme also has the advantage that one dependent variable, (x, the instantaneous horizontal coordinate of a particle whose location at $t = 0$ was a, i.e., $x(a,0) = a$), defines the solution for all time. The continuity equation is thus eliminated.

It should be pointed out that previous computational work for the run-up problem has been in Eulerian coordinates.

Summary

The purpose of the section has been to define the approximations of the run-up hydrodynamics used in the model formulation, so as to allow them to be distinguished from the errors in solving the model equations numerically. The basic approximations are the replacement of the general two-dimensional flow by the constrained flow, and the allowance of discontinuous shock solutions by means of an 'artificial viscosity' term. Also, a simple friction law is used to approximate bottom friction effects.

In the next chapter, these approximations are applied directly to the flow to allow the specification of a system of finite elements,

whose equations serve as a mathematical analog for the flow. The finite elements help to keep the physics of the process in view and the resulting equations lend themselves to numerical solution methods. This is in lieu of first deriving the continuum equations to represent the approximated flow, and then proceeding to solve them with a numerical solution technique, which may not be well defined for the resulting system.

DERIVATION OF FINITE ELEMENT SYSTEM

Definition of a Typical Element

When making a numerical solution of a physical problem there is a conceptual advantage in formulating the problem by means of finite elements. In the problem under consideration, a finite element is a particular mass of fluid whose internal flow field is specified so as to facilitate a numerical solution of the problem. Initially, before the fluid has been disturbed, the finite element is the mass of fluid between the vertical plane at x_i and the vertical plane at $x_{i+1} = x_i + DX$.

When the fluid is disturbed by wave propagation we consider the front and back faces of the finite element to displace and to deform out of plane. The fluid particles adjacent to one of these faces will experience a horizontal velocity which can be approximated by equation (1)

$$u(x,y,t) = \sum_{i=0}^{i=N} y^i u_i(x,t) \qquad (1)$$

where as noted earlier, N is a small integer like 0, 1, 2, or 3. The vertical velocity will be determined by integrating the equations of flow vertically, since in the approximate expression for u, y is explicit.

To obtain an accurate solution it is desirable that the fluid motion specified within the finite element be as near as possible to the true fluid motion. On the other hand, to simplify the numerical

solution it is desirable to specify a simplified flow pattern within the element. The aim is to obtain a satisfactory accuracy with a minimum amount of computing.

It appears for this problem that a reasonable compromise is the simplest case, $N = 0$, giving

$$u(x,y,t) \approx u(x,t) \tag{14}$$

that is the constrained flow discussed in the previous section. However, for certain future investigations, it may be necessary to prescibe a more complex element deformation, where the series in equation (1) is carried to $N = 2$ and $N = 3$.

To be able to derive the equations governing the motion of the elements, it is necessary to be able to specify the fluid flow within the element so the fluid's kinetic and potential energies are specified, preferably in terms of the displacement of the element's vertical boundaries. The equations of motion can then be derived by means of Lagrange's equation.

To examine how this is done, one first considers Figure VI(a), where the vertical element boundaries are shown in a general constrained flow over a linear beach slope. The element boundaries do not affect the constrained flow and remain vertical. The location of these boundaries define where the fluid is, and can serve as a Lagrangian variable that describes the fluid flow.

However, the specification of the fluid motion in Figure VI(a) is not complete, since the free surface shape is unknown. The only way the internal flow of the element can be prescribed is to simplify

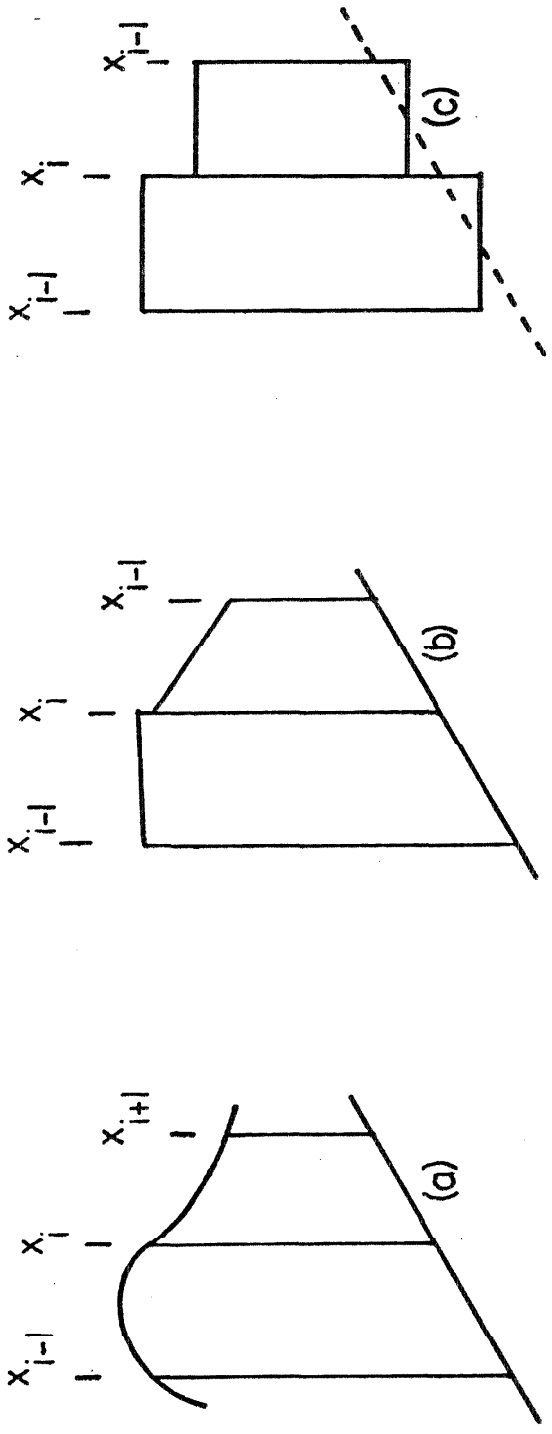

Figure VI (a) General Element on Linear Slope
(b) 'Linear Slope' Element on Linear Slope
(c) 'Simplest' Element on Linear Slope.

its shape by approximating the top and bottom boundaries with simple functions.

In Figure VI(b), the approximating function is linear. It provides an exact description of the bottom contour in this case of a linear beach slope. However, even this simple function does not allow complete specification of the element by its vertical boundaries. If the vertical boundaries are fixed, the free surface can still rotate to different slopes, though mass conservation (or continuity) requires the center (average height) to remain fixed. Thus there is a fluid motion not described by the vertical boundary positions.

Only the very simplest element form, shown in Figure VI(c), allows specification of the element in terms of the vertical boundary positions. The approximating function is a constant. Since the position of the lower boundary of the element is determined by the contour of the beach, continuity determines the height of the fluid in the element in terms of the vertical boundary positions. Thus, the shape of the element is completely determined. This simple element is the basis of all the calculations done in this model.

A higher order element could be defined so that it was completely specified by the vertical boundaries of the element, but this would involve the numerical evaluation of considerably more complicated expressions in application. To achieve a given over-all accuracy in solving the equations, the trade-off to be considered is evaluating a simple expression more often than a more complicated

higher order expression. It usually favors the simple expression, which is easier to derive and program into the computer. The investigation of higher order elements should be considered in future work.

While the equations for the element could be derived for a general beach contour, the equations are somewhat simpler for a linear beach slope. All calculations done here were for a linear slope. The general contour should be considered in future work.

Thus Figure VII(a) defines the 'ith' element used for the calculations. It is a rectangular mass of fluid between the two boundaries located at x_i and x_{i+1}. The centerline of the element, at $\frac{1}{2}(x_i + x_{i+1})$, intersects the beach slope at the bottom of the element. The top of the element is h_i above that level.

Derivation of the Equations of Motion

If there is some fixed quantity of fluid, c_i in the element, the position of the fluid is defined by the Lagrangian coordinates x_i and x_{i+1}. The height (h_i) of the fluid above E is obtained from the continuity equation

$$h_i(x_{i+1} - x_i) = c_i \tag{15}$$

since c_i is constant. For any smaller section of the element, for example, up to the line HJ

$$y(x_{i+1} - x_i) = \text{constant} \tag{16}$$

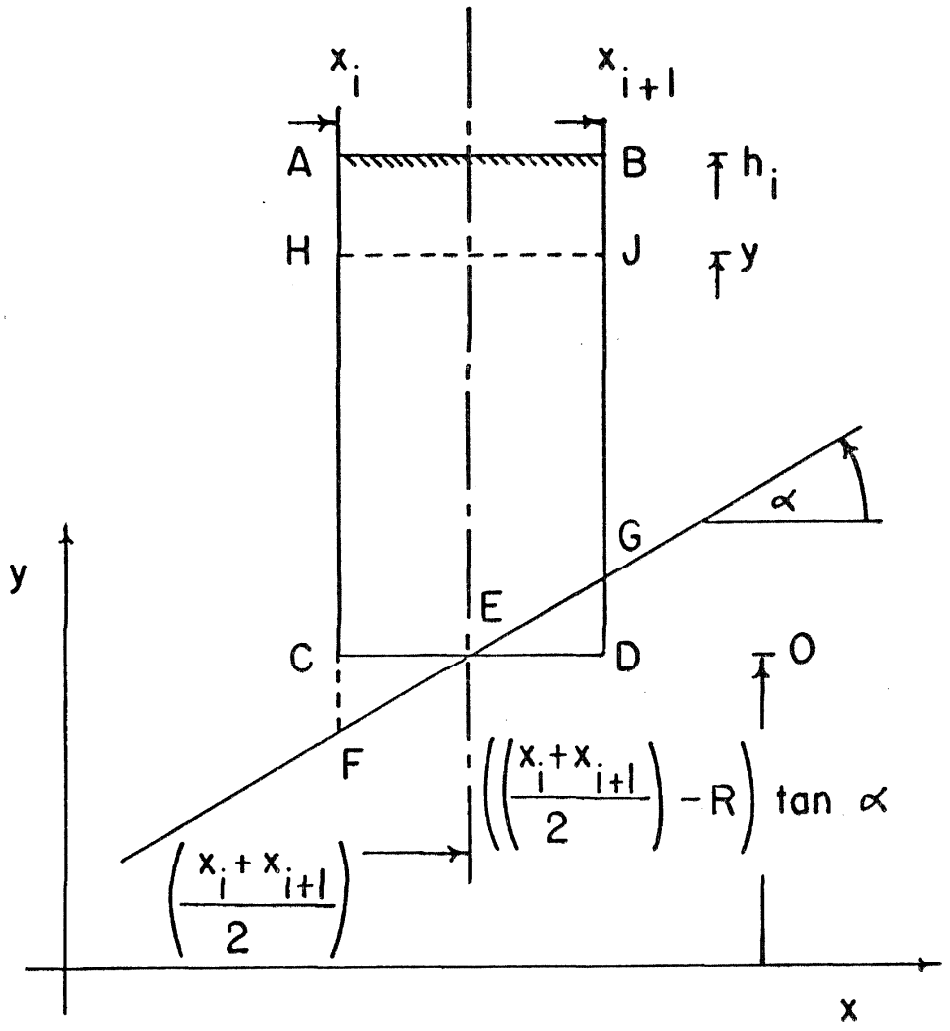

Figure VII(a). The 'ith' Element.

also.

Differentiating (15) and (16) with respect to time gives

$$\dot{h}_i(x_{i+1} - x_i) + h_i(\dot{x}_{i+1} - \dot{x}_i) = 0 \tag{17}$$

$$v(x_{i+1} - x_i) + y(\dot{x}_{i+1} - \dot{x}_i) = 0 \tag{18}$$

From this it can be seen that h_i and $\dot{h}_i$ are functions of the x_i's and the $\dot{x}_i$'s.

$$h_i = c_i/(x_{i+1} - x_i) \tag{19}$$

$$\dot{h}_i = -c_i(\dot{x}_{i+1} - \dot{x}_i)/(x_{i+1} - x_i)^2 \tag{20}$$

Also seen is that the dependence of v on y is explicit, i.e.,

$$v = \dot{h}_i y/h_i \tag{21}$$

However, this has neglected the vertical motion of the point E as it moves along the slope with velocity $\frac{1}{2}(\dot{x}_{i+1} + \dot{x}_i)$ horizontally. Adding in the vertical component one has

$$v = \dot{h}_i y/h_i + \frac{1}{2}(\dot{x}_{i+1} + \dot{x}_i) \tan \alpha \tag{22}$$

To derive the equations of motion, one can write the Lagrangian for this finite degree of freedom system. The horizontal kinetic energy is taken to be the kinetic energy of the fluid moving with the velocity of the mass center; the kinetic energy of motion with respect to the mass center is not included as this is a relatively small quantity for the problems considered here.

$$KE_{hor_i} = \frac{1}{2} c_i [\frac{1}{2} (\dot{x}_{i+1} - \dot{x}_i)]^2 \tag{23}$$

The vertical kinetic energy is a result of the vertical velocity (v) distribution:

$$KE_{vert_i} = \frac{1}{2} (x_{i+1} - x_i) \int_o^{h_i} v^2 \, dy$$

$$= \frac{1}{8} c_i (\dot{x}_i + \dot{x}_{i+1})^2 \tan^2\alpha - [\frac{1}{4} c_i^2 (\dot{x}_{i+1}^2 - \dot{x}_i^2) \tan\alpha] / (x_{i+1} - x_i)^2$$

$$+ [\frac{1}{6} c_i^3 (\dot{x}_{i+1} - \dot{x}_i)^2] / (x_{i+1} - x_i)^4 \tag{24}$$

The potential energy is the mean height of the element times its weight

$$PE_i = g c_i \{\frac{1}{2} h_i + [\frac{1}{2} (x_i + x_{i+1}) - R] \tan\alpha\} \tag{25}$$

where R is the intercept of the slope and the x-axis. In terms of the x_i's

$$PE_i = g c_i \{\frac{1}{2} c_i / (x_{i+1} - x_i) + [\frac{1}{2} (x_{i+1} - x_i) - R] \tan\alpha\} \tag{26}$$

The total Lagrangian is formed by the 'ith' box

$$L_i = KE_{hor_i} + KE_{vert_i} - PE_i \tag{27}$$

By inspection, only L_{i-1}, L_i, and L_{i+1} contribute to the 'ith' equation, which if we define the entire Lagrangian $\overline{LT}$ as

$$\overline{LT} = \sum_{\text{all } i} L_i \tag{28}$$

is of the form

$$d(\partial \overline{LT}/\partial \dot{x}_i)/dt = \partial \overline{LT}/\partial x_i \qquad (29)$$

This leads to a typical equation of motion of the form

$$\begin{aligned}
&\left\{c_i(1+\tan^2\alpha)/4 - c_i^3/[3(x_{i+1}-x_i)^4]\right\}\ddot{x}_{i+1} \\
&+\{(c_i/4+c_{i-1}/4)(1+\tan^2\alpha)+c_i^3/[3(x_{i+1}-x_i)^4]+c_{i-1}^3/[3(x_i-x_{i-1})^4] \\
&\quad + c_i^2\tan\alpha/[2(x_{i+1}-x_i)^2] - c_{i-1}^2\tan\alpha/[2(x_i-x_{i-1})^2]\}\ddot{x}_i \\
&+\{c_{i-1}(1+\tan^2\alpha)/4 - c_{i-1}^3/[3(x_i-x_{i-1})^4]\}\ddot{x}_{i-1} \\
&= -2c_i^3(\dot{x}_{i+1}-\dot{x}_i)^2/[3(x_{i+1}-x_i)^5] - c_i^2 g/[2(x_{i+1}-x_i)^2] \\
&\quad - 2c_{i-1}^3(\dot{x}_i-\dot{x}_{i-1})^2/[3(x_i-x_{i-1})^5] - c_{i-1}^2 g/[2(x_i-x_{i-1})^2] \\
&\quad - c_i^2(\dot{x}_{i+1}-\dot{x}_i)^2\tan\alpha/[2(x_{i+1}-x_i)^3] \\
&\quad - c_{i-1}^2(\dot{x}_i-\dot{x}_{i-1})^2\tan\alpha/[2(x_i-x_{i-1})^3] - \tfrac{1}{2}(c_i+c_{i-1})g\tan\alpha \qquad (30)
\end{aligned}$$

At the end of a sloping beach, where the fluid surface intersects the bottom, a different approximation is used for the element shape. The free surface is still considered as level, but the actual beach slope is used for the element bottom. The resulting element, defined by Figure VII(b), is triangular in shape. Its position is defined by the coordinate x_n of its vertical boundary and it moves without distortion.

This simplifies the calculation of the Lagrangian. With reference to Figure VII (b), if the volume is c_n, then

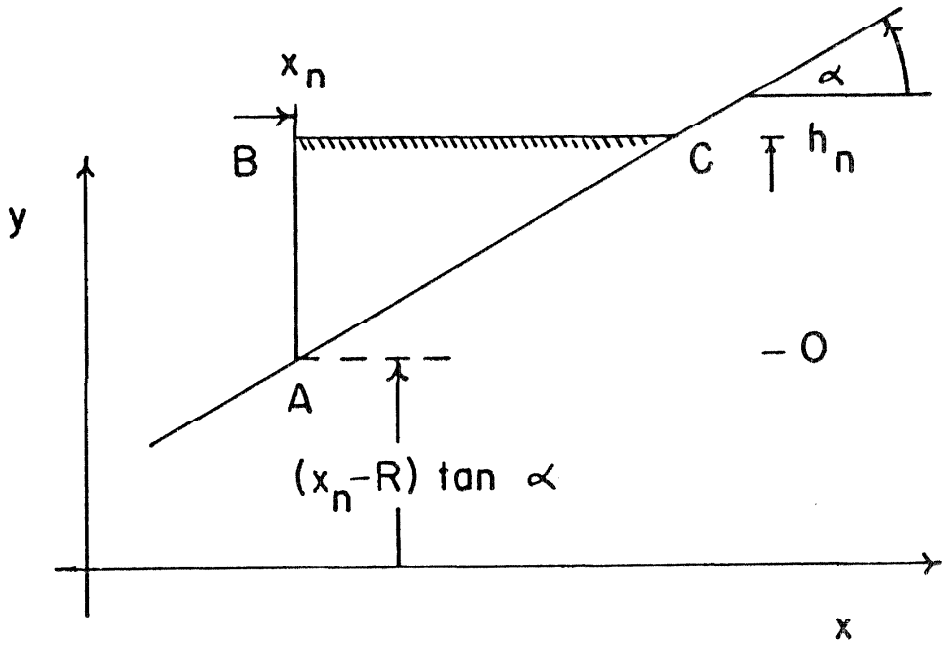

Figure VII(b). The 'nth' Element.

$$c_n = h_n^2/(2 \tan \alpha) \tag{31}$$

$$KE_{hor_n} = c_n \dot{x}_n^2/2 \tag{32}$$

and

$$KE_{vert_n} = c_n(\dot{x}_n \tan \alpha)^2 \tag{33}$$

The potential energy is still the weight of the element times the height of the centroid of ABC above the datum

$$PE_n = gc_n[(x_n - R)\tan \alpha + 2h_n/3]$$

$$= gc_n\{(x_n - R)\tan \alpha + [2(2c_n \tan \alpha)^{1/2}/3]\} \tag{34}$$

When this Lagrangian is used, the 'nth' equation is found to be slightly different from equation (30). It only includes x_n and x_{n-1}, and their derivatives.

'Artificial Viscosity' and Bottom Friction

The 'artificial viscosity' and bottom friction terms may be added to the finite element equations as additional forces contributing to the equilibrium of the 'ith' vertical boundary. From the continuum form for the 'artificial viscosity' term, $F = \ell^2 h(\partial u/\partial x)^2 He(-\partial u/\partial x)$, ℓ^2 is allowed to be a constant (K'), specified in the numerical solution to give a certain shock width. For the 'ith' element

$$h_i = c_i(x_{i+1} - x_i) \tag{35}$$

and

$$\partial u/\partial x = (\dot{x}_{i+1} - \dot{x}_i)/(x_{t+1} - x_i) \tag{36}$$

Since $(x_{i+1} - x_i) > 0$, $He(-\partial u/\partial x)$ may be represented by $He(\dot{x}_i - \dot{x}_{i+1})$.

Acting on the 'ith' boundary is a negative force from the 'ith' element and a positive force from the '(i-1)th' element. The direction of these forces is the same as the pressure forces acting on the boundary. Hence, the following terms are added to the right-hand side of equation (30), the basic element equation of motion

$$K'[-c_i(\dot{x}_{i+1} - \dot{x}_i)^2 He(\dot{x}_i - \dot{x}_{i+1})/(x_{i+1} - x_i)^3$$

$$+ c_{i-1}(\dot{x}_i - \dot{x}_{i-1})^2 He(\dot{x}_{i-1} - \dot{x}_i)/(x_i - x_{i-1})^3] \tag{37}$$

The bottom friction is considered in a similar manner. The shear stress is a function of the horizontal velocity and the friction coefficient, i.e., $\tau = Ku^2$. Since the friction term is only providing an estimate of the friction losses, considering it to act in the horizontal direction is sufficient, especially on the small beach slopes in question. The friction force acting on each element is taken as $\overline{DX}\, Ku^2$, where $\overline{DX}$ is the initial width of an element. This produces two additional force terms on the right-hand side of equation (25) resulting from the friction force on each element being transmitted to the boundaries of that element. They are

$$-K(\overline{DX})\,[(\dot{x}_{i+1} + \dot{x}_i)^2 \operatorname{sign}(\dot{x}_{i+1} + \dot{x}_i) + (\dot{x}_i + \dot{x}_{i-1})^2 \operatorname{sign}(\dot{x}_i + \dot{x}_{i-1})] \tag{38}$$

where

$$\text{sign } a = \begin{cases} 1 \text{ if } a \geq 0 \\ -1 \text{ if } a < 0 \end{cases} \tag{39}$$

The use of the sign function indicates that the friction force opposes the flow.

Use of the Finite Elements in a Model Tank Analog

In order to use the scheme so far described to study wave run-up, a model tank was considered, typically as shown in Figure VIII(a). This tank consists of a flat section with a sloped beach. However, for other calculations, a simpler tank with just a flat bottom and a vertical wall at the far end was used. In still a third case, the entire length of the tank was sloped. The derivation of the finite element equations covers all of these cases with only minor changes.

In any case, the tank is divided into n elements, $\overline{DX}$ wide, for an initially level free surface. The constants in the finite element equations, i.e., c_i $(i = 1,\ldots,n)$, $\tan \alpha$, R, etc., are evaluated for the system of equations based on the dimensions of the tank and how it is divided. This includes the bottom friction and 'artificial viscosity' coefficients. This system of equations becomes the mathematical analog of the wave tank in question.

Because of the interest in the solution in the vicinity of the intersection of the free surface and the beach slope, it would seem logical to use a finer element size there. However, the large vari-

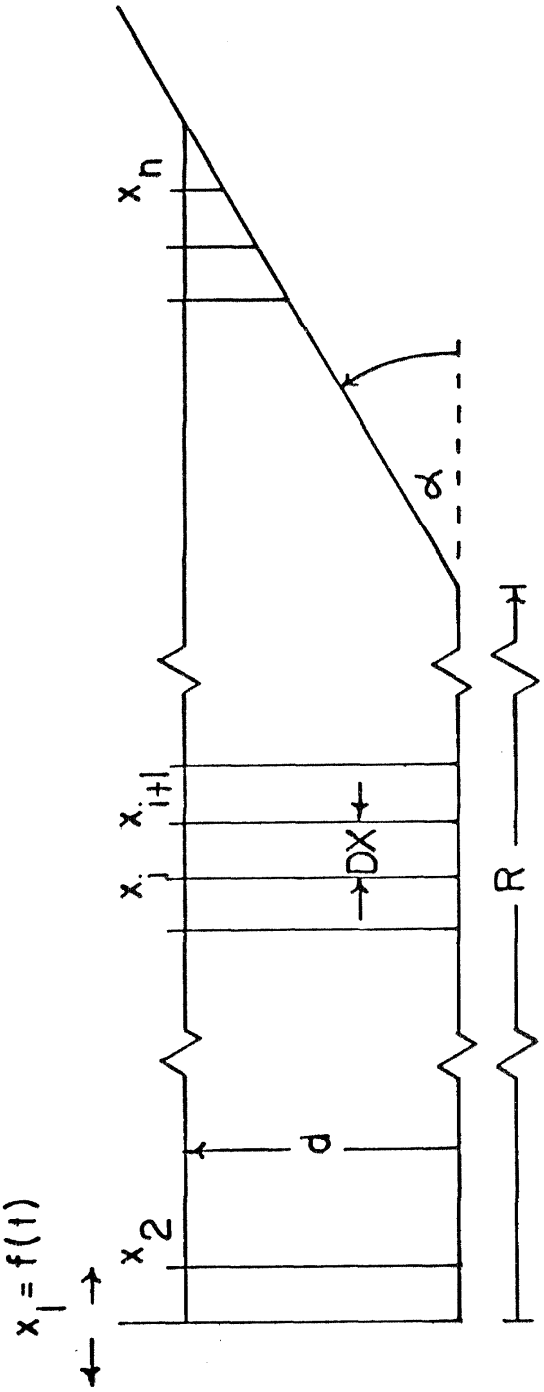

Figure VIII(a). Typical 'Wavetank' Model.

ations in the local depth in this region causes the element width to become very small at times. This requires very small time steps to integrate the equations stably, as will be seen later. The use of smaller elements would only worsen this situation, so the uniform initial element width was maintained.

Using the Model Tank Analog

In order to produce waves in the tank, x_1 is prescribed as a function of time. It acts as a piston wavemaker and by controlling its motion a wide variety of waveforms can be produced. The motion of the wavemaker is usually deduced from the known results about horizontal fluid particle motion for various waveforms. These will be described in the specific cases of interest.

For solutions of the system of ordinary differential equations to exist, initial values of x_i and $\dot{x}_i$, $i = 1,\ldots,N$, must be given. In all cases, the calculations were begun with a still tank and all of the excitation was supplied by the wavemaker input. Thus, the initial conditions were simply, $x_i = i\overline{DX}$, $\dot{x}_i = 0$.

This system of equations must then be solved. In this work, the solution was by digital computer and will be discussed in the next chapter. The solution consists of the x_i's as functions of time.

However, it is desirable to recover the free surface profile as a function of time, because its behavior is most often recorded in experiments and used as a basis for theoretical discussion. The surface profile at any time is defined by the x_i's and obtained by calculating the h_i's from the continuity equation (15). Since this is

in reference to the bottom of the tank, a sloped region has

$$h_i = c_i/(x_{i+1} - x_i) + [\tfrac{1}{2}(x_{i+1} + x_i) - R] \tan \alpha \qquad (40)$$

See Figures VII(a,b). The free surface profile is then defined as a curve passing through the points $(\frac{1}{2}(x_{i+1} + x_i), h_i)$. For the end point defined by the 'nth' element on a sloping beach, the intercept of the beach slope and the top of the element is used. A smooth curve can be passed through the points by an appropriate interpolation procedure.

Treatment of Multiple Slopes

One limitation of the derivation given for a linear beach slope is in its direct application to modeling a tank with two regions of different slope, such as shown in Figure VIII(a). As the solution progresses, sufficiently large horizontal displacements of the elements may take place so that an element defined on one slope may be on another. In this case, the equations referring to that element would be in error, the error size depending on how far the element went into the other region.

Fortunately, this can be overcome in an actual numerical computation by having the computer check at each time step which region the element is in and modify the numerical evaluation of the element equations accordingly. The location of an element is defined by its center, i.e., $\frac{1}{2}(x_{i+1} + x_i)$ for the 'ith' element.

Even with this correction, error still results from the equa-

tions being solved stepwise in time. In the course of one time step, an element may cross into a new region. However, the equations are not modified until the next time step, and are in error for part of the one time step. This manifests itself as small error waves, generated at transitions between different slopes. In most cases, these waves were considerably smaller than the phenomena of interest, and did not affect the results. However, in certain cases, dealing with small wave amplitudes, these were very definitely noticeable and interferred with the waves under study.

This is illustrated in Figure VIII(b), where in the original tank a certain wave is generated, but is smaller than the error wave generated at the transition. The most direct cure to this problem is to modify it so it can be studied on a single slope. This means transforming the wave to the correct size for the greater depth of the modified tank using small amplitude theory.

An alternative method of dealing with the error is to reduce the element size. This is a natural way of reducing errors from the 'finiteness' of the system, but must be paid for in computer time.

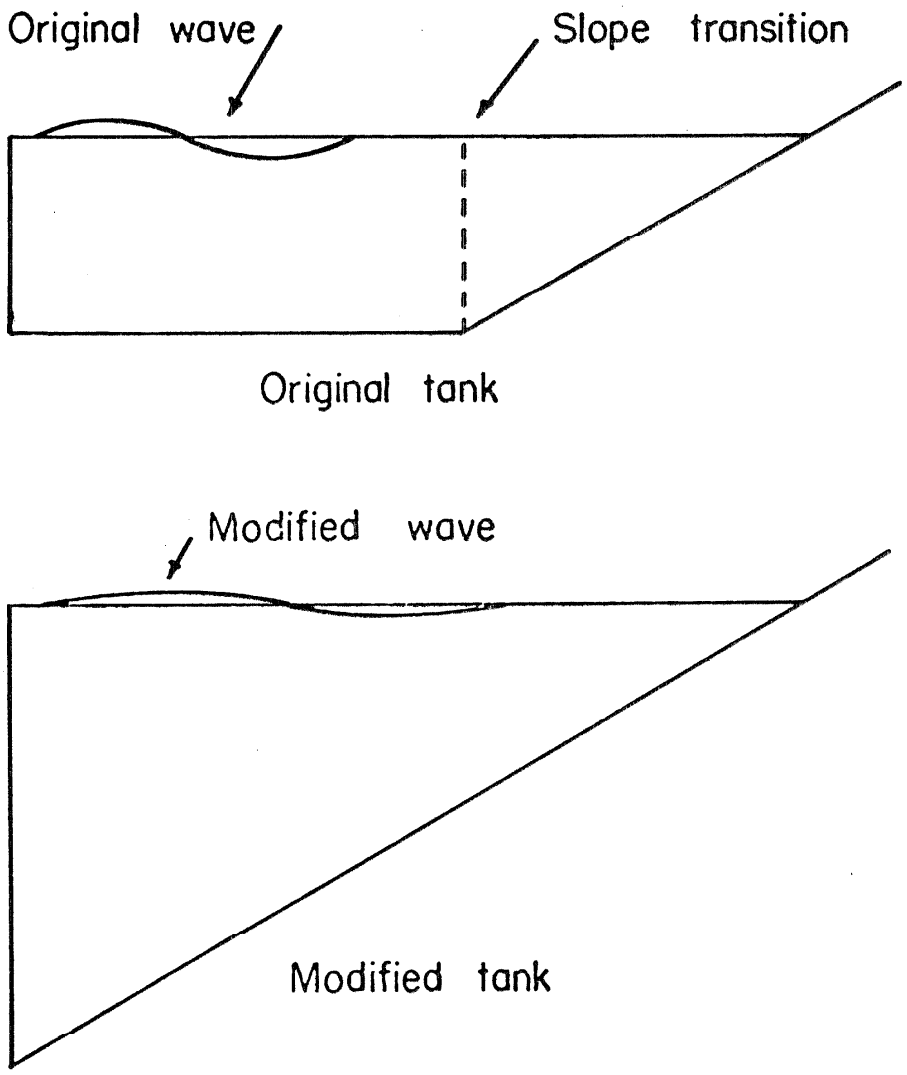

Figure VIII(b). Elimination of Transition Using a Tank with One Slope.

COMPUTATIONAL PROCEDURES

Solution Mechanics

In order to solve the finite element system of second order nonlinear ordinary differential equations, the system is viewed as follows

$$[A(x_i, \dot{x}_i)]\{\ddot{x}_i\} = \{B(\dot{x}_i, x_i)\} + \{f(t)\} \tag{41}$$

Equation (41) represents the n equations of motion, where $[A]$ is a matrix function of the x_i's and the $\dot{x}_i$'s, while $\{\ddot{x}_i\}$ consists of the accelerations arranged as a vector. $\{B\}$ and $\{f(t)\}$ are the right-hand sides of the equations of motion and the driving function arranged as vectors.

The system is converted to first order by defining

$$\{x_{i+n}\} = \{\dot{x}_i\} \tag{42}$$

so that

$$[A(x_i, x_{i+n})]\{\dot{x}_{i+n}\} = \{B(x_i, x_{i+n})\} + \{f(t)\} \tag{43}$$

Since at any given time the matrix $[A]$ can be numerically inverted, we essentially have

$$\{\dot{x}_{i+n}\} = [A]^{-1}\{B\} + [A]^{-1}\{f(t)\} \tag{44}$$

($[A]$ is a tridiagonal matrix and so the inversion is not difficult.) Equations (42) and (44) then represent a first order system of 2n equations in standard form for numerical solution.

The actual integration is by Adam's method, with Runga-Kutta starting. The truncation error for the schemes used was $\overline{DT}^4$, where $\overline{DT}$ is the time step size.

Stability Criteria

The numerical integration of this system is restricted by a stability criteria. This is because the system is essentially hyperbolic, in that it propagates disturbances at a finite speed. The time steps must be sufficiently small so that

$$\overline{DT} < \text{Cons}\ (\overline{DX}/c) \tag{45}$$

Here $\overline{DX}$ is the width of an element, $\overline{DX} = (x_{i+1} - x_i)$, and c is the local small wave speed. ($c = \sqrt{gd}$, where d is the local depth.) Cons is a constant of order one which depends on the exact scheme and which is affected by the presence of the 'artificial viscosity' term. See Richtmyer (15). Also, in Lagrangian coordinates, $\overline{DX}$ varies locally as the solution progresses, the smallest value being critical. It was found prudent to use $K = 1/10$ to $1/50$ for $c = \sqrt{gd}$, where d was the initial maximum depth and $\overline{DX}$ the initial element width, to determine a safe $\overline{DT}$ for all time.

Details on Computation

The computer is programmed to do most of the work in any given investigation. Usually, only numerical values of parameters are fed in as data, with functional forms involved specified by the

program. Several different subroutines defining specific tank geometries and waveforms were used to investigate specific problems. The computer facilities can provide graphical outputs as well as numerical outputs for these problems. Additional notes on the programs used may be found in Appendix E.

Since the computer times for such calculations are not trivial, they may be estimated on the following basis. To evaluate one equation for one time step requires about 200 operations (additions and multiplications), which take about ten microseconds apiece on the IBM 7094 computer used. Thus, such a step takes about two milliseconds.

From this, the time to do a problem is determined. The tank is divided into n elements, which determines the element width $\overline{DX}$. The stability criteria, taking into account the depth (and hence, wave speed), gives a maximum size for the time step. If the wave propagation is to be studied for a certain time, usually until reflected waves interfere, the number of time steps ($\overline{NT}$) is determined. (This is also related to the depth and wave speed.) The computer execution time is approximately $n(\overline{NT})/500$ seconds.

DISCUSSION OF SPECIFIC CALCULATIONS WITH MODEL

Checks on Wave and Shock Propagation

The complete computer model can be tested to see if it reproduces the phenomena associated with water waves. A typical check is to produce small amplitude long waves. These are found to propagate undistorted with constant velocity as predicted by the linear wave equation. If generation of short surface waves is attempted, the model would not give such good results because the surface waves have a large variation in horizontal velocity with depth, which the model cannot allow.

For larger amplitude long waves, the nonlinear effects become significant, with the waves steepening into shocks. Shocks may also be generated directly by moving the wavemaker piston at constant velocity into the tank. Figures IV(a,b) show the results of such calculations done to test the shock behavior. It is noted that for larger values of the 'artificial viscosity' coefficient the shock tends to a smooth transition, with the required energy being dissipated in the jump. As the value of the coefficient is decreased, the transition has small waves on the downstream side. These seem to result from the fact that the shock does not dissipate enough energy and the excess energy tends to propagate downstream in the little waves. However, the motion of the waves is attenuated and they become smaller away from the shock.

Weak hydraulic shocks tend to propagate waves downstream in a similar manner. However, for stronger shocks, where the flow is

unsteady in reference to the shock coordinates and is complicated by rotation and air entrainment, a direct comparison with the 'artificial viscosity' shocks is of doubtful value.

Other comparisons between the computed shocks and the real shocks should only concern their overall properties. From the basis given in Chapter III, 'Proposed Model Theory,' it seems clear the shocks should behave as the infinitesimal (width) shocks. It is pointed out that the use of the 'artificial viscosity' term essentially allows the momentum and continuity conditions to be satisfied across the shock. Again, this is indicated by Figure V, showing how the computed shocks agree with the theory in the relation between shock height ratio and Froude number.

The only other parameter of the shock would be its thickness, as influenced by the choice of the 'artificial viscosity' coefficient, ℓ^2. As seen in Appendix A, this determines the approximate width of the shock to be about 2ℓ. Experimental data from Chow (3) indicate that the width of the shock region is three to five times the height of the jump for Froude numbers from 2.0 to 8.5. Since the thickness of the computed shocks can be varied, this criteria could be met in the generation of any particular shock.

However, all of this is based on steady flow patterns (in reference to the shock coordinates). In wave run-ups, the shocks form from steepening waves and their strength continually varies in time as the flow progresses. One can only assign nominal widths to the shocks at the beginning of a calculation and see if the results look reasonable. If not, then a new choice of shock width is made. Usually

this is not a very critical matter. The shock width does not affect the flow around the shock very strongly, since the amount of energy dissipated in the shock is not a function of its width.

The shock width assigned must be large enough so the transition covers several elements. Otherwise, the 'artificial viscosity' term is not evaluated and instability results since the energy supposed to be dissipated in the shock is not accounted for properly. It usually appears as rather large oscillations downstream of the transition. The elements become very narrow (in attempting to represent the large amplitudes) and the stability criteria is violated, causing the numerical calculation to fail.

However, if the shock width is made overly large, it will interfere with the flow. In the prototype flow, the shocks are narrow compared to the other significant wave lengths. If the shock width coefficient ℓ was the same size as a wave that should propagate unattenuated, the 'artificial viscosity' term would incorrectly cause this wave to loose energy. Thus ℓ must be smaller than the significant wave lengths in the problem.

The usual proceduce is to assign shock widths close to the minimum required for stable computation, i.e., several element widths. This may produce wider shocks than would actually occur in a real flow, but they are still much shorter than the significant wave lengths in the problem and do not cause unrealistic attenuation of the desired wave motion.

Solitary Waves - Generation

To examine how the model would work for predicting run-up results, it was first used to study solitary wave run-up. Solitary wave calculations could be conducted with a minimum of computer time and the results of experimental investigations in this field were available for comparison.

However, several drawbacks should be noted. First, the experimenters do not give data on the bottom friction involved in their studies, only descriptions of the materials used for the beach slope. Also, the flows were in tanks narrow enough so that the wall friction might have a significant effect. Thus, the friction coefficient for the experiments is difficult to deduce.

Another difficulty is that in a finite time, only an approximation of the solitary wave is produced by a wave generator. This tends to produce a profile with a 'bump,' as shown in Figure IX. The 'bump' falls behind the main wave as they propagate away from the wavemaker and in a long tank the two will separate. This results in a good solitary wave profile. However, this requires a great deal of computer time. Therefore, in this calculation the solitary wave is not given sufficient time to separate itself entirely from the 'bump,' and this may have some small influence when the wave reaches the beach slope.

The solitary wave is generated by a finite displacement of the wavemaker, theoretically over an infinite period of time. The first order motion of Laitone (12), where the horizontal velocity is constant over the depth is of the form

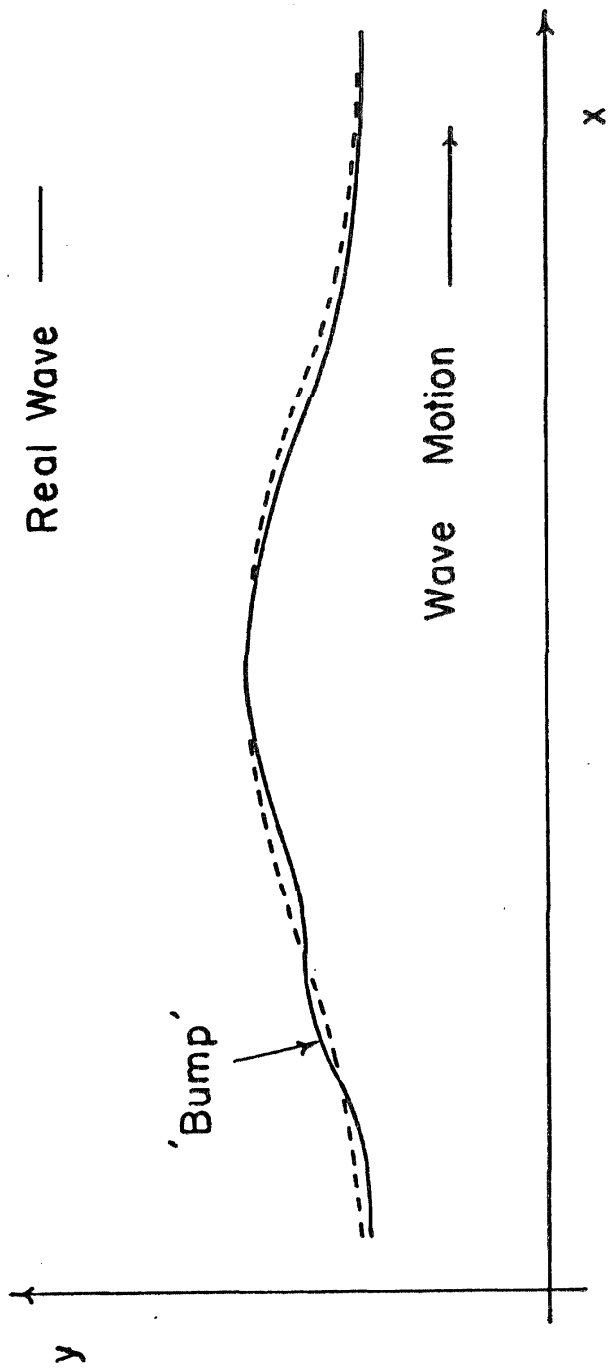

Figure IX. Solitary Wave, Real vs. Theoretical Profiles (After Generation).

$$x = A \tanh Bt \tag{46}$$

where A and B are parameters of the wave. This includes the approximation that x is small compared to t, i.e., $x \approx 0$, used when the theoretical velocity expression is integrated with respect to time to get the wavemaker motion.

The following truncation of this function is used so that the wavemaker motion requires only a finite time

$$x = \begin{cases} -A \text{ if } Bt < -10 \\ A \tanh Bt \text{ if } |Bt| < 10 \\ A \text{ if } Bt > 10 \end{cases} \tag{47}$$

From Figure X, it is seen that the main part of the function is preserved, but the infinite 'tails' are cut off.

A solitary wave of any particular H/d can be generated with the above wavemaker motion. An example is shown in Figure XI. The computed wave is lower in amplitude than the second order theory it is compared with, since it is generated from the first order theory which has less area under its profile. (Refer to Figure I.) This tends to redistribute itself so the resulting profile is consistently lower in amplitude, but more similar in shape to the second order curve. For practical comparisons, the difference is small. However, one can always get the H/d of the generated wave by measurement and use that in lieu of the nominal value. The results here use the nominal value.

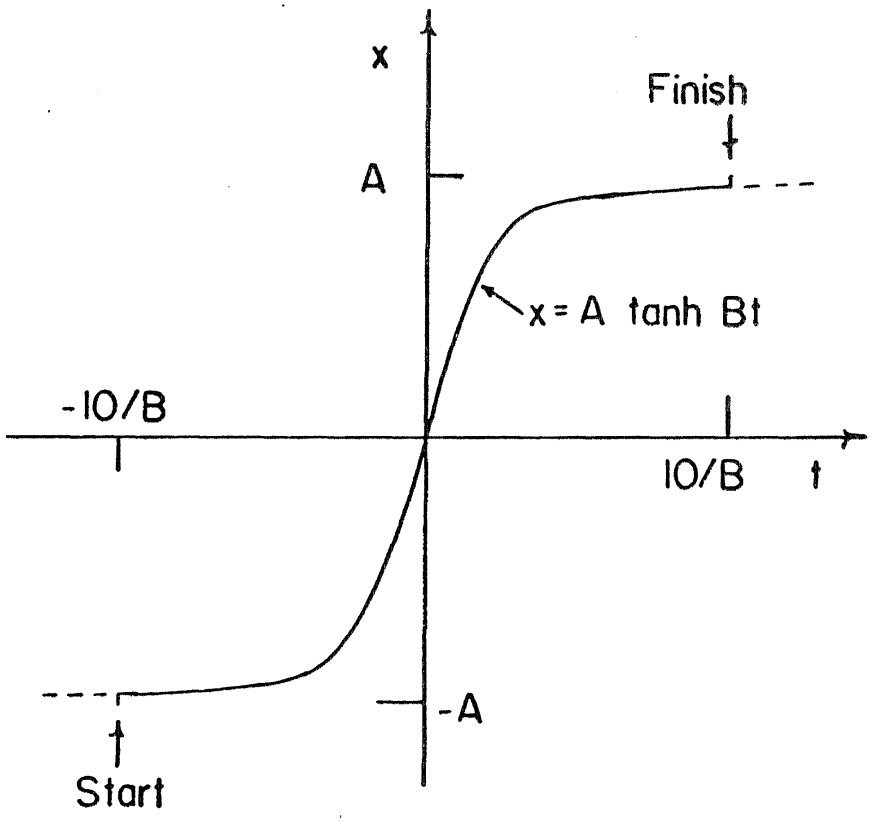

Figure X. Truncation of Wavemaker Motion in Time for Solitary Wave Generation

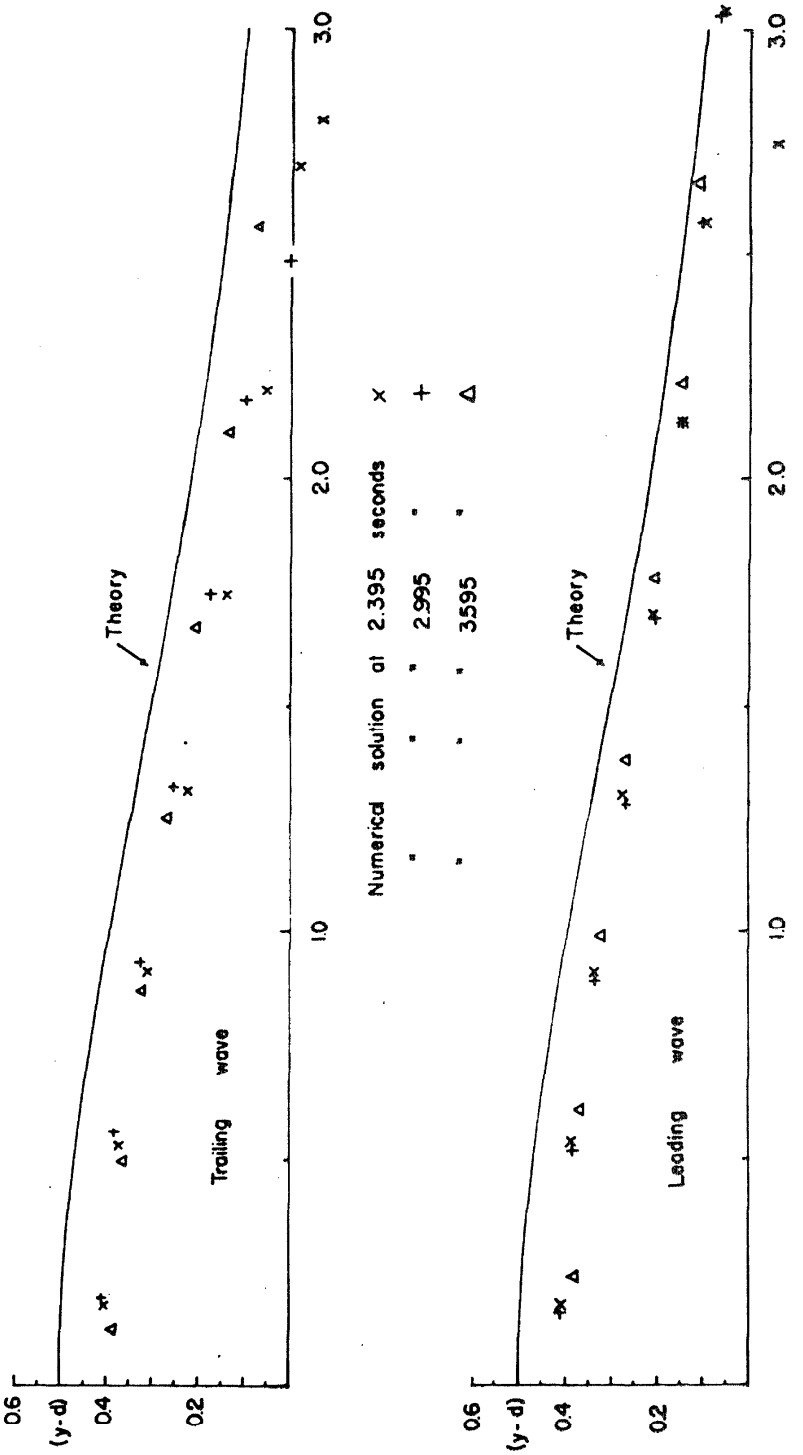

Figure XI. Comparison of Numerical Solution for Solitary Wave and Second Order Theory, H/d = 0.5.

The generation procedure could have been improved by having the wavemaker motion based on the constrained flow theory given in Appendix B. However, the solitary wave investigations were completed before this was found and computing costs prevented repeating the calculations. However, even in this case some generation error will still result from the time truncation required.

Solitary Waves - Run-up Profiles

Figures XII(a to i) show a sequence of profiles for a solitary wave run-up calculation. The 'bump' behind the wave can clearly be seen in Figure XII(b). As the solution progresses, it can be seen that the run-up takes place mainly in a thin sheet of water expanding up the beach, as shown in Figures XII(e,f). In Figures XII(g,h), the thin sheet of water should return down the beach. However, the function used to interpolate between the discrete elements to obtain a smooth curve gives an incorrect profile, (shown in dashes), especially in Figure XII(g). This is because too few points define the profile, a common numerical problem.

Importance of the Vertical Kinetic Energy

The same problem was recalculated with the terms for the vertical kinetic energy reduced by a factor of ten. This is shown in the sequence, Figures XIII(a to c). Figure XIII(a) corresponds to Figure XII(a) in time, and so on. The wave that results is different, thus indicating that the vertical kinetic energy terms have a significant influence on the waveform. Note that in XIII(c), the front of the wave

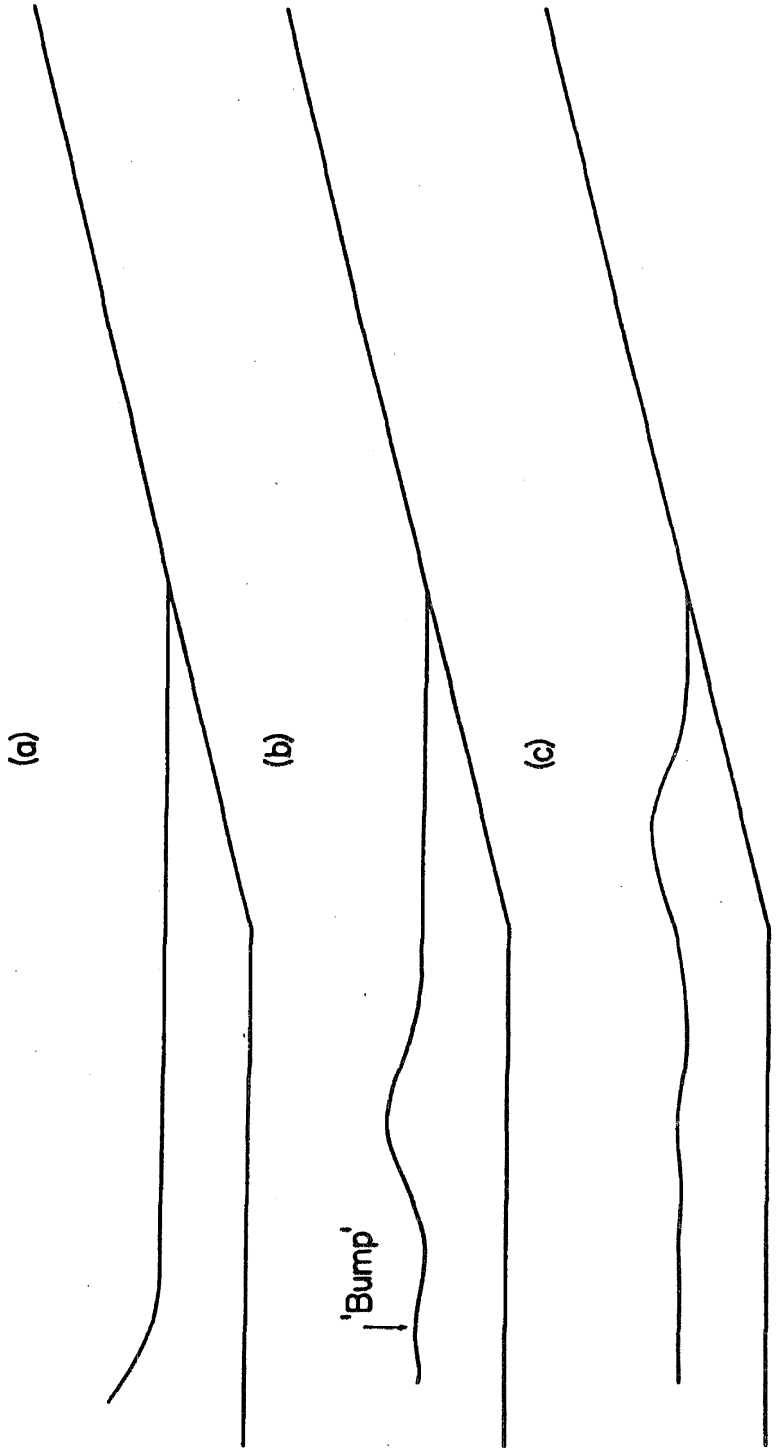

Figure XII(a,b,c). Solitary Wave Run-up Profiles, H/d = 0.5, Slope = 0.1
(Scale Distorted).

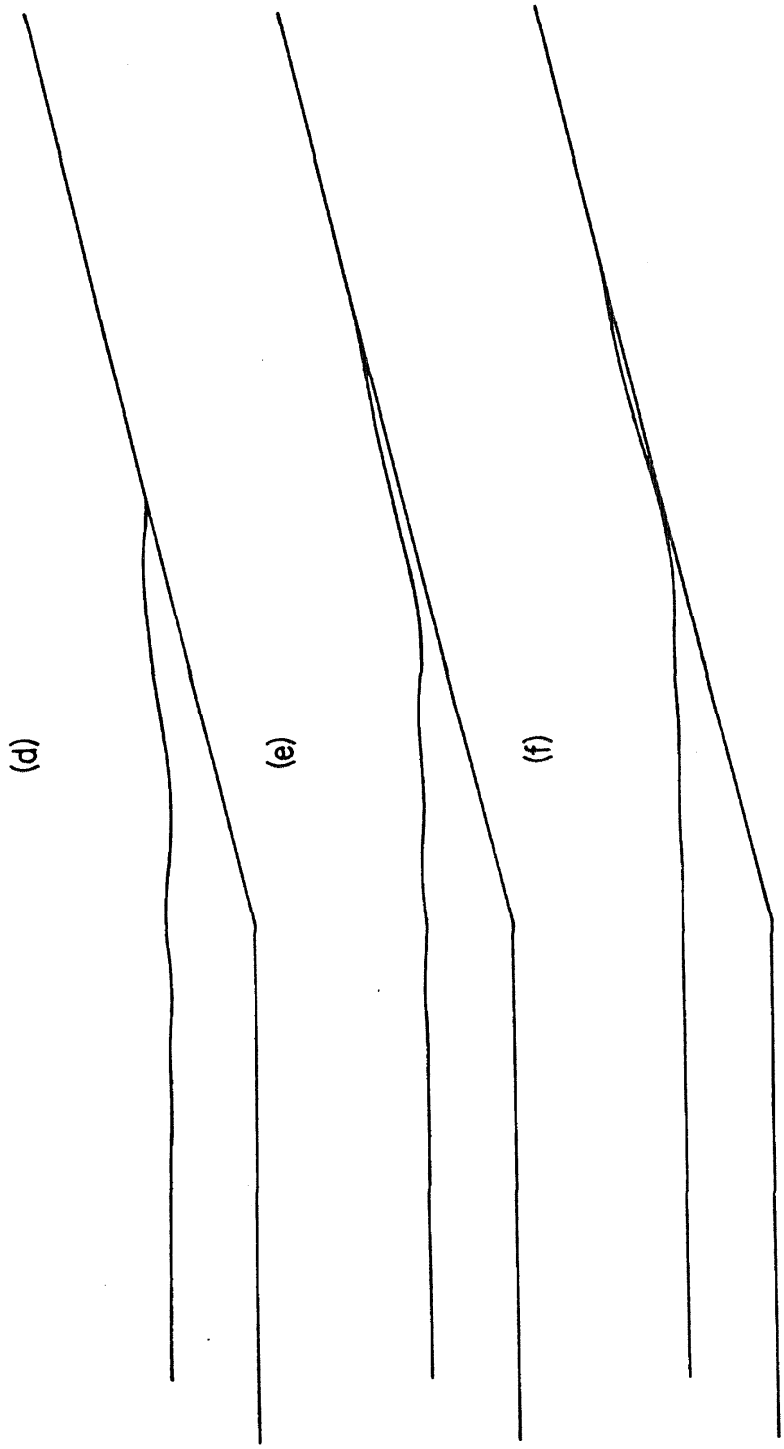

Figure XII(d,e,f). Solitary Wave Run-up Profiles.

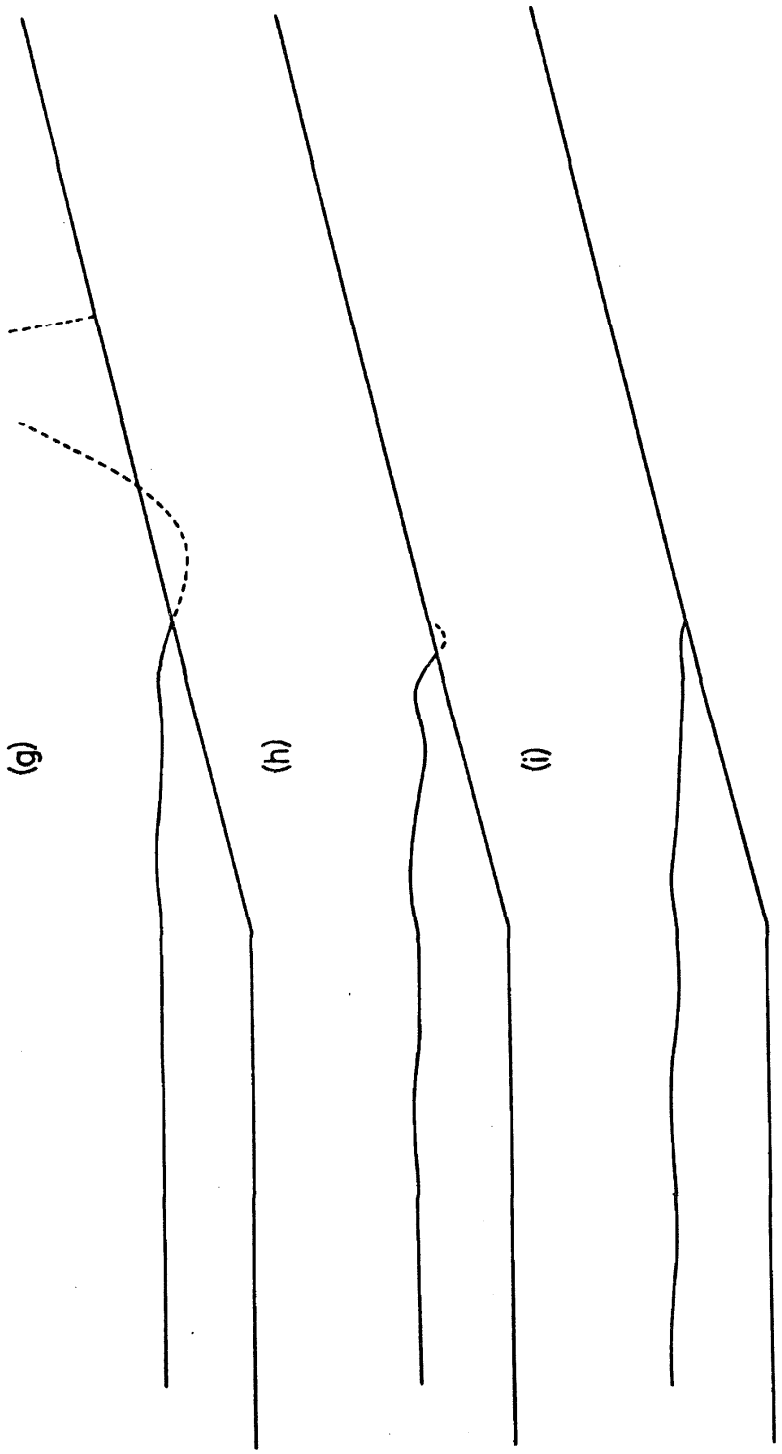

Figure XII(g,h,i). Solitary Wave Run-up Profiles.

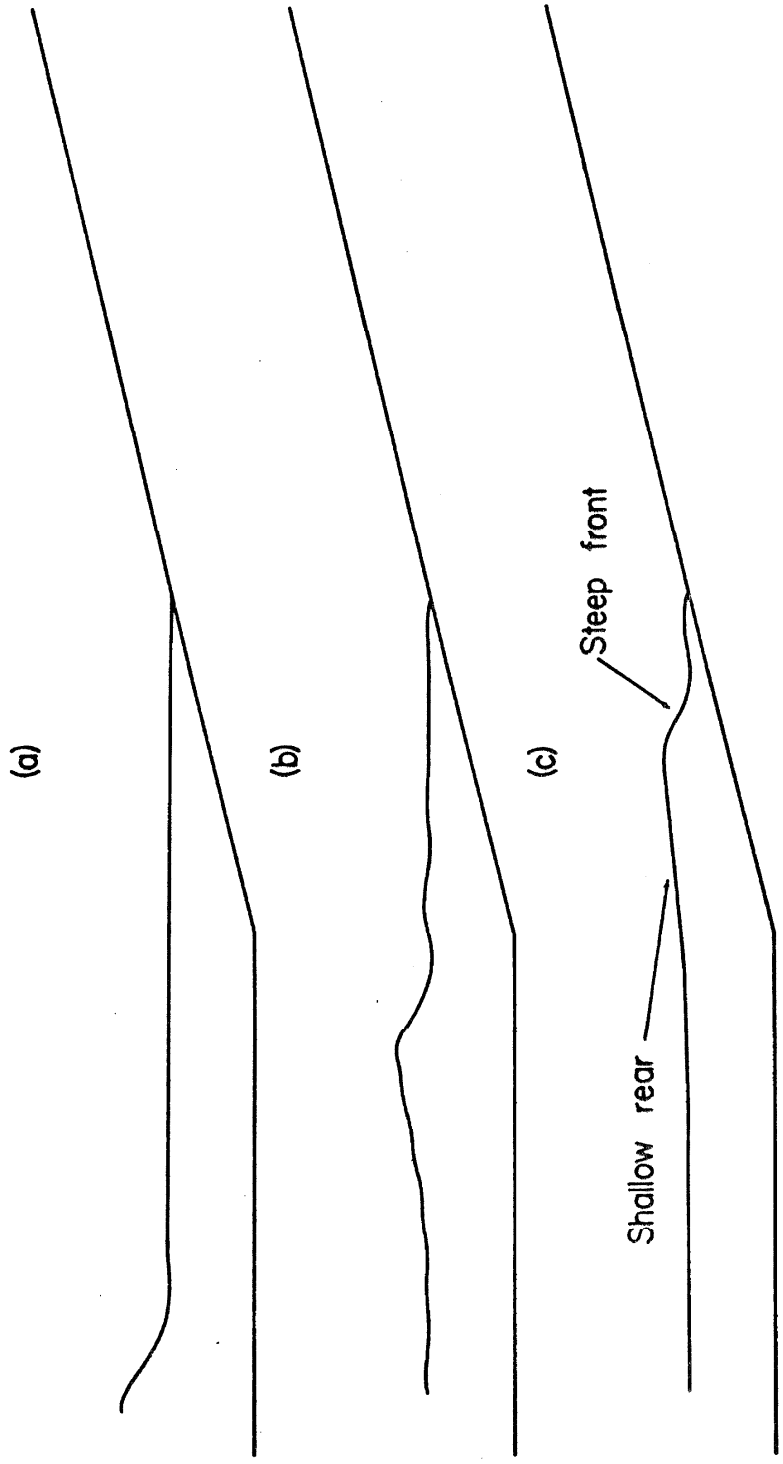

Figure XIII(a,b,c). Solitary Wave Run-up Profiles with Vertical Kinetic Energy Reduced, H/d = 0.5, Slope = 0.1 (Scale Distorted).

has steepened and the back slope has become quite gentle. In XII(c), the basic symmetry of the solitary wave is still evident. This shows that when the vertical kinetic energy is neglected the waves tend to steepen and break earlier than they should. It bears out LeMéhauté's (13) observation that the shallow water theory, with no representation of the vertical kinetic energy, tends to predict breaking too early.

Comparison of Experiments and Computation for Solitary Wave Run-up

The experimental results for the run-up of solitary waves on smooth beaches of constant slope are summarized by Kishi and Saeki (11). The results are given by

$$R/d = K(H/d)^{\delta} \tag{48}$$

where d is the still water depth, H the generated solitary wave height, and R is the run-up. K and δ are functions of the beach slope and are given by Kishi and Saeki for their work, as well as for that of Hall and Watts (5) and Kaplan (8). Examining how well this law compares with the data of Hall and Watts, one sees that the scatter of data points is only a few per cent. Thus, this law can be considered a good summary of the experimental data and useful for comparison purposes.

The computer model was tested on slopes of 0.3, 0.1, and 0.03, which covered the mid-range of the data available. Figures XIV(a,b,c) give the computed points obtained with various values of the bottom friction and the 'artificial viscosity' parameters. The

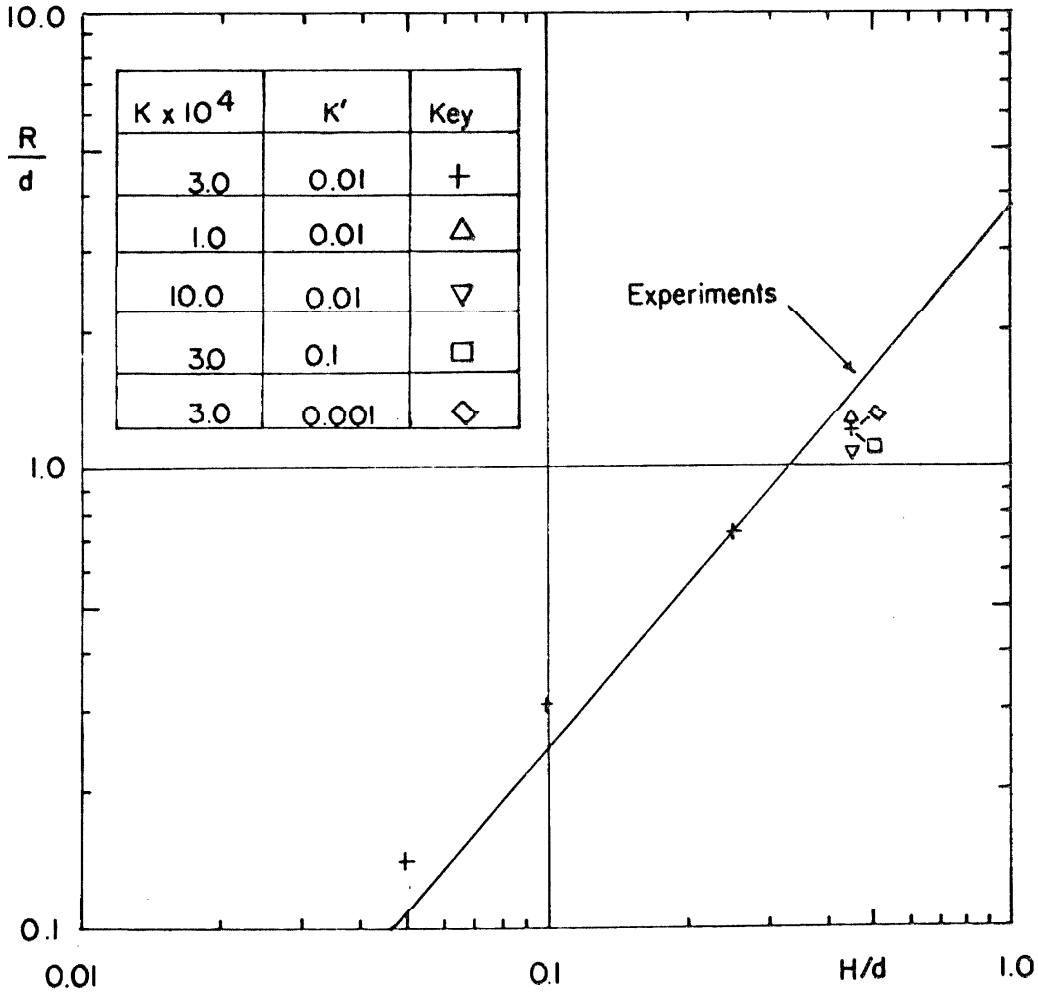

Figure XIV(a). Solitary Wave Run-up, Comparison of Experiments and Computations, Slope = 0.3.

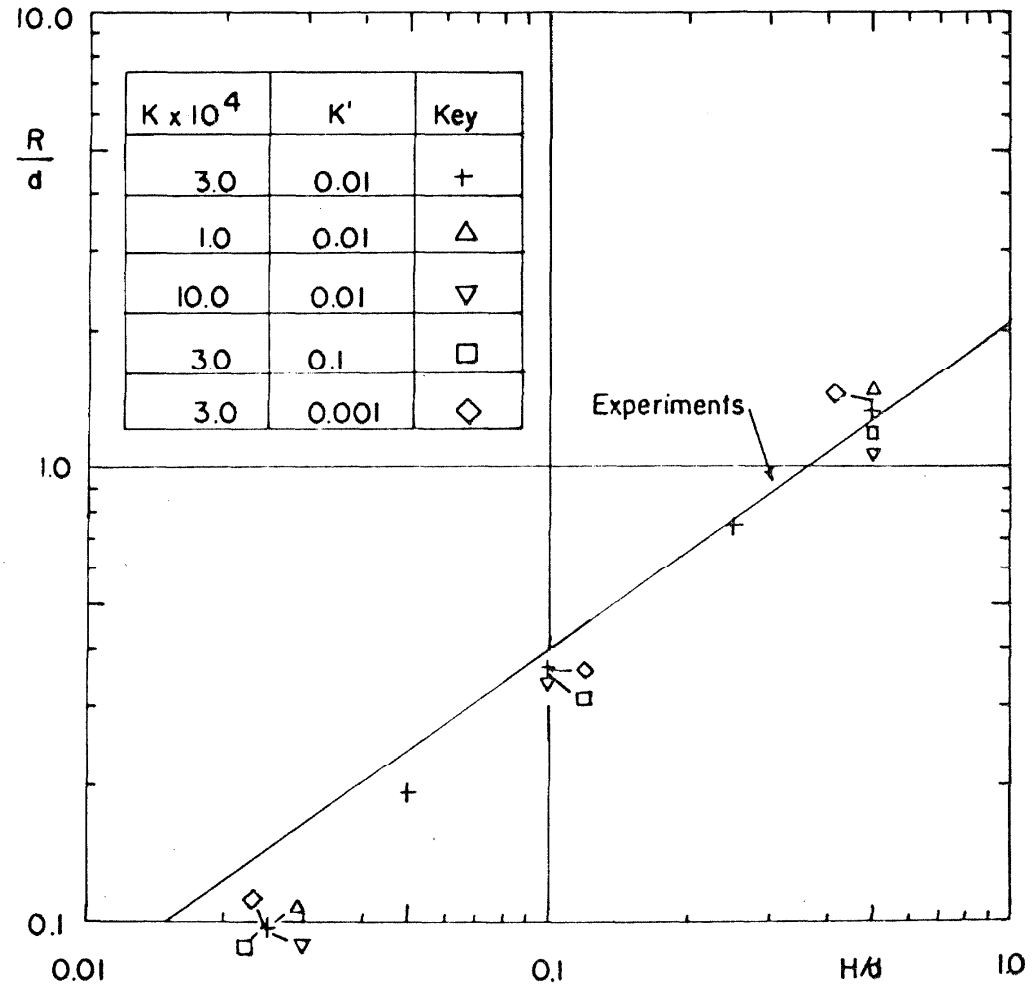

Figure XIV(b). Solitary Wave Run-up, Comparison of Experiments and Computations, Slope = 0.1.

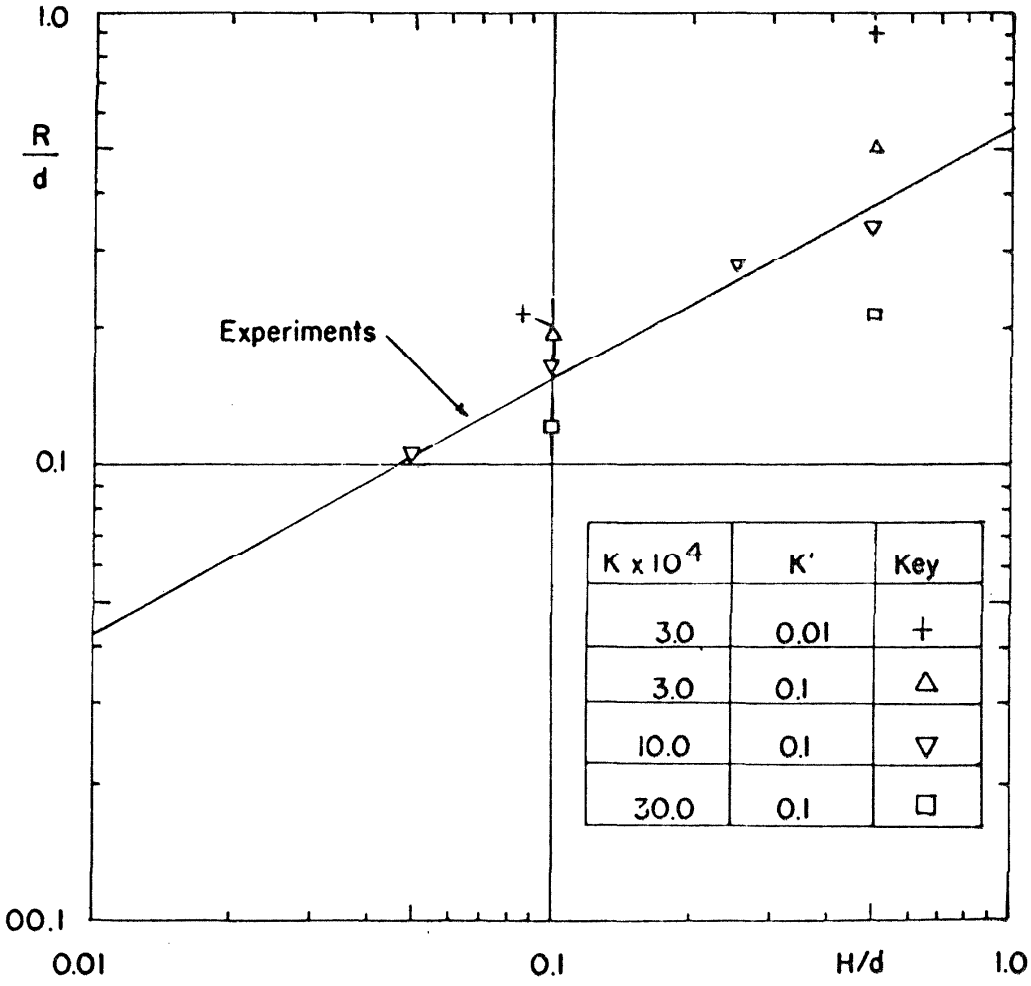

Figure XIV(c). Solitary Wave Run-up, Comparison of Experiments and Computations, Slope = 0.03.

straight line represents the experimental results.

In examining the results, it should be noted that the values of the parameters used are reasonable for trying to reproduce the experimental data. The friction coefficient can be estimated from the following considerations. For rough boundaries in open channel flow Rouse (16) gives the friction coefficient f as

$$1/\sqrt{f} = 2.03 \log_{10}(d/r) + 2.11 \tag{49}$$

where d is the depth and r the roughness of the surface. For comparatively smooth surfaces used for the experiments, an $r = 10^{-4}$ feet seems reasonable. If one estimates the friction force on the elements in the shallow water near the beach, i.e., on the triangular element, the depth is about 0.1 feet. Hence

$$1/\sqrt{f} \approx 2 \log_{10}(10^{-1}/10^{-4}) + 2$$

$$\approx 8 \quad \text{or} \quad f \approx 1/64 \tag{50}$$

The friction shear stress is $\tau = fu^2/8$. Since the element is of unit width the coefficient of the friction term is $\approx (1/64)(1/8) = 2 \times 10^{-3}$. This is of the same order as the values shown in the results.

Of course, this friction calculation is approximate in several respects. First, the experimental model was on such a small scale, the flow along the bottom was probably laminar. However, the friction rule used to calculate f is for turbulent flow. Also, the flow here is unsteady, while the rule is for steady flow. Last, the coefficient is evaluated for the shallow water near the beach. The

friction coefficient would be smaller in the deeper water, away from the beach. However, the same coefficient was used for the entire flow, thus overestimating the friction in deeper water. This is not serious, since the friction force there is much smaller than the other forces in the deeper water. (It is obvious the inertial and pressure forces increase with depth.) Thus, estimating the friction correctly for the shallow water is probably the best compromise.

The shocks in these run-up flows are usually fairly weak. Their thickness is about the same as the water depth, i.e., one foot. The shock width of $2\ell = 1.0$ gives $\ell^2 = 0.25$. Thus, 'artificial viscosity' coefficients of 0.1 and 0.01 used here are reasonable.

For steeper slopes, the effects of these quantities can be seen to be small anyhow, since the points change only slightly as the quantities are varied. Most of the error here in calculating the run-up is probably due to the flow being constrained. For shallower slopes, the errors become small compared to the variations in the run-up caused by the 'artificial viscosity' and bottom friction coefficients. The effects of these terms is quite clear, more dissipation of energy results in smaller run-ups. However, the 'correct' choice of these parameters can provide good agreement with experiments.

Some of the computations were repeated with more elements to test for truncation error, which for those cases was found to be small. Extra runs were also made with different lengths between the wave generator and the beach slope. The run-ups were slightly smaller due to the wave losing more energy to the dissipative terms before reaching the shoreline.

Bore Run-up Results

In addition to the solitary wave results, comparisons were made with the experimental results of Miller (14) for the run-up of bores. In these calculations, as in the experiments, the wavemaker piston is moved with constant velocity to generate a shock of a given Froude number. The relations used to give the piston velocity are based on the theory of infinitesimal (width) shocks, again, as in the experiments. The friction factor f was evaluated for the experiments by Miller. The slight difference between the friction factor values of Miller and those used in the computations are not important, since Miller's data indicated the run-up was not very sensitive to the bottom friction.

Figures XV(a,b,c) summarize the calculations. The results for the 15^{o} and 5^{o} slopes are reasonably good. Some error is due to the way the computer output was evaluated in these cases. For the 2^{o} slope, only partial results were obtained. When very strong shocks, i.e., higher Froude numbers, were attempted, large variations in the local depth near the beach resulted. This caused the local element width to become very small, and would have required very small time steps to satisfy the stability criteria. This would have required very long computer times to obtain the run-up data.

The only variable in the numerical calculation that is not in the experiment is the shock width. This does not seem to be an important factor if the choice of coefficient allows the formation of a reasonably smooth transition with small downstream undulations. Figures XVI(a to i) show the sequence of a bore running into a beach

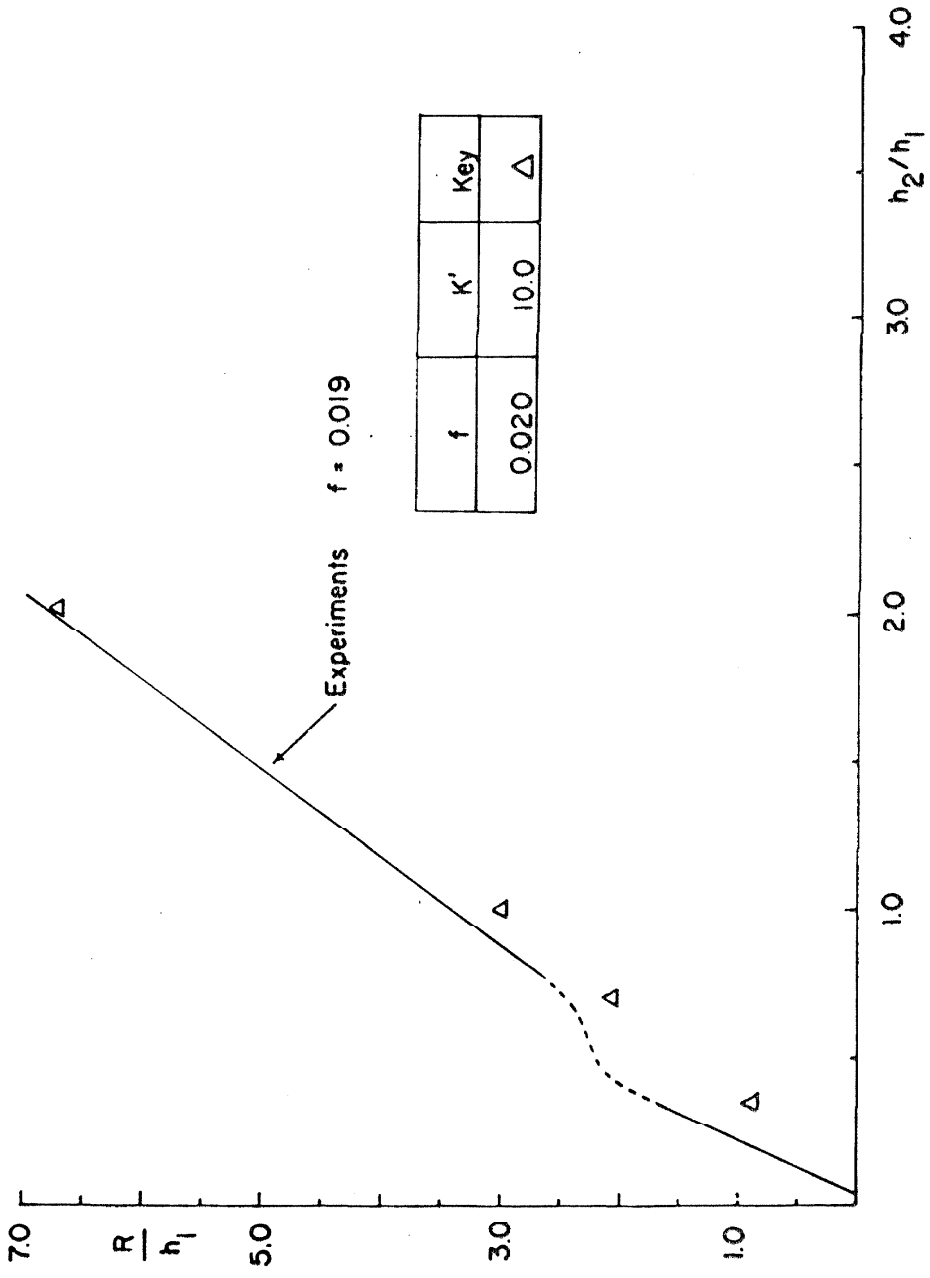

Figure XV(a). Bore Run-up, Comparison of Experiments and Computations, Slope = 15°.

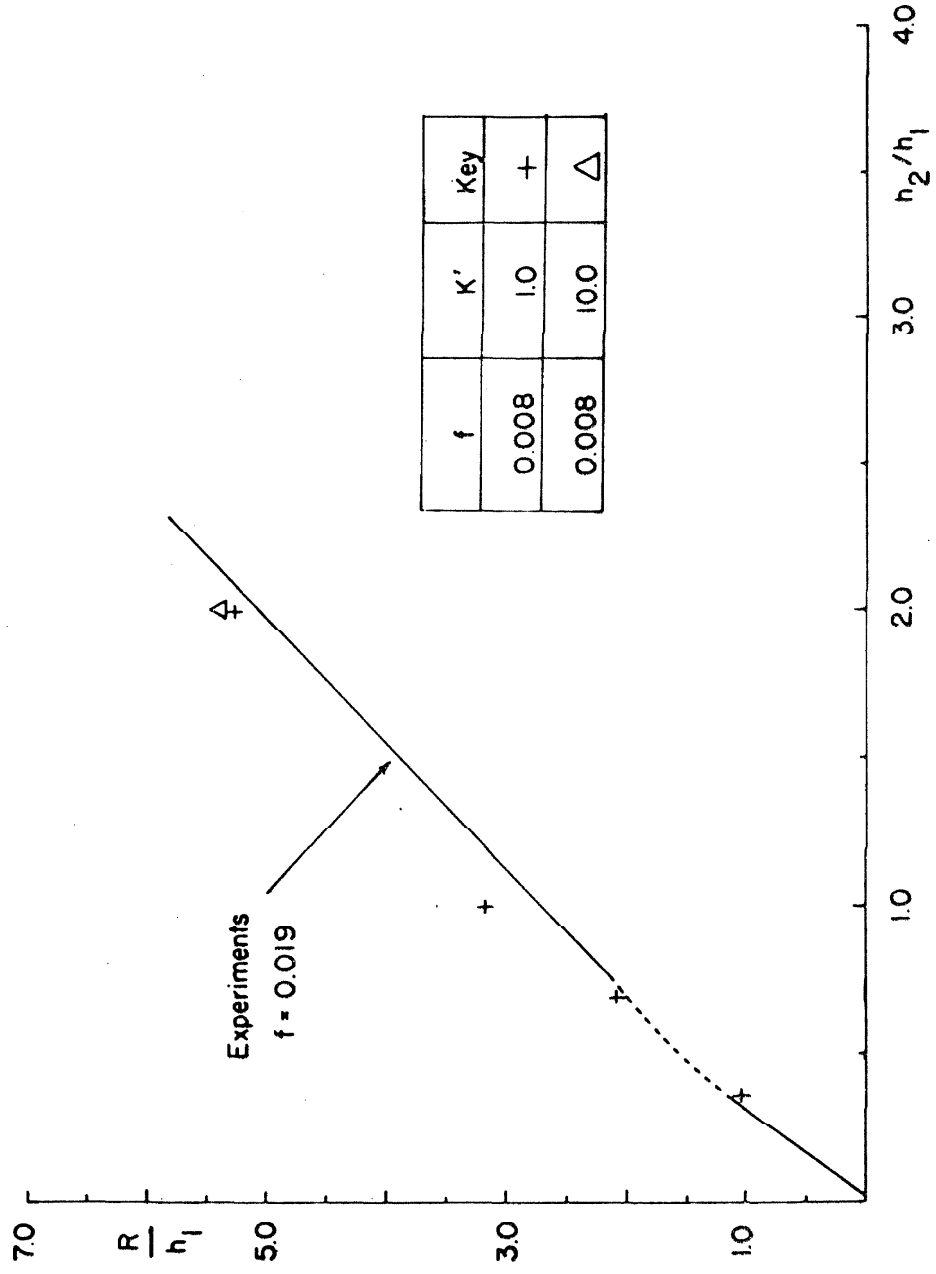

Figure XV(b). Bore Run-up, Comparison of Experiments and Computations, Slope = 5^{o}.

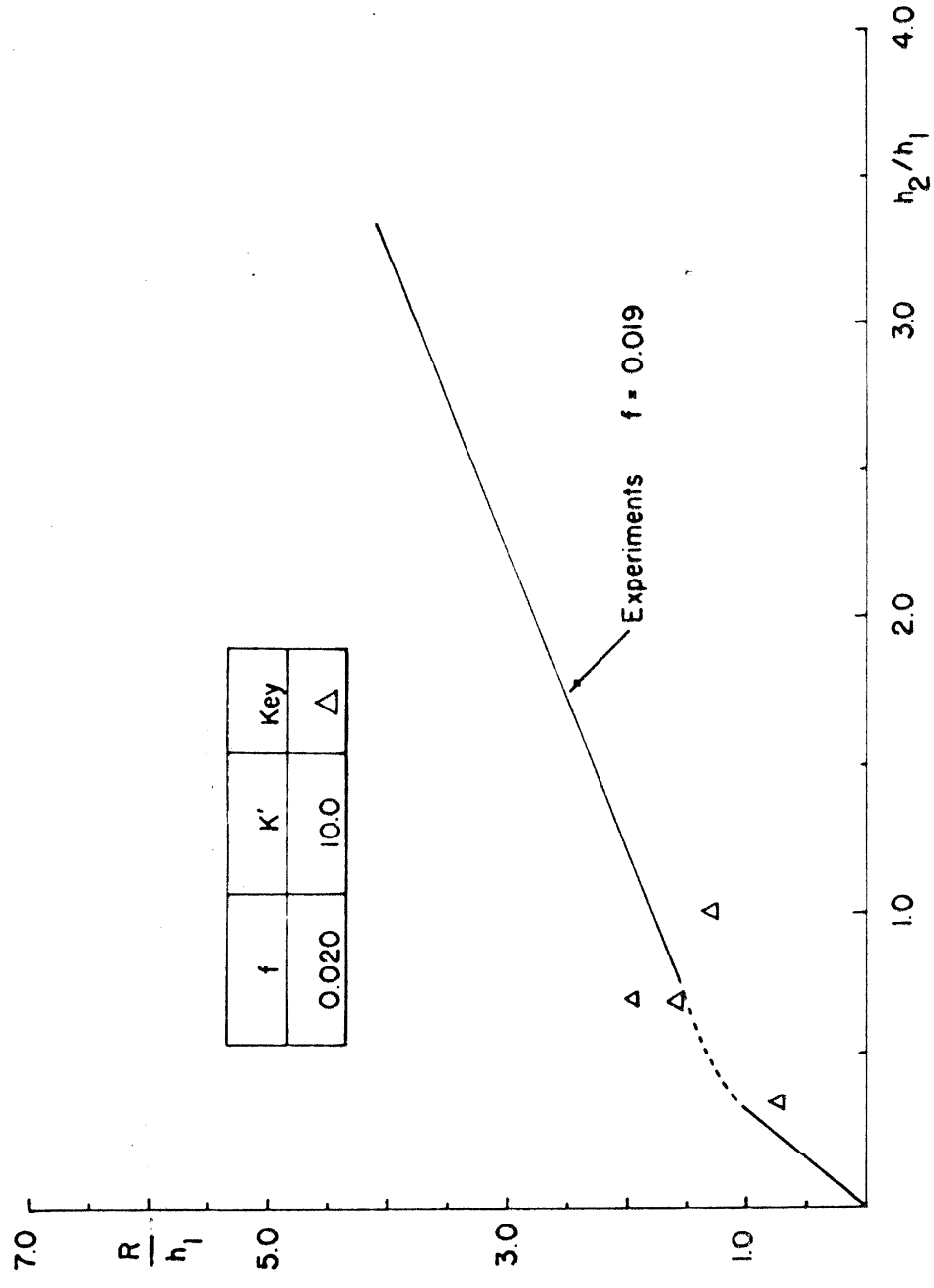

Figure XV(c). Bore Run-up, Comparison of Experiments and Computations, Slope = 2^{o}.

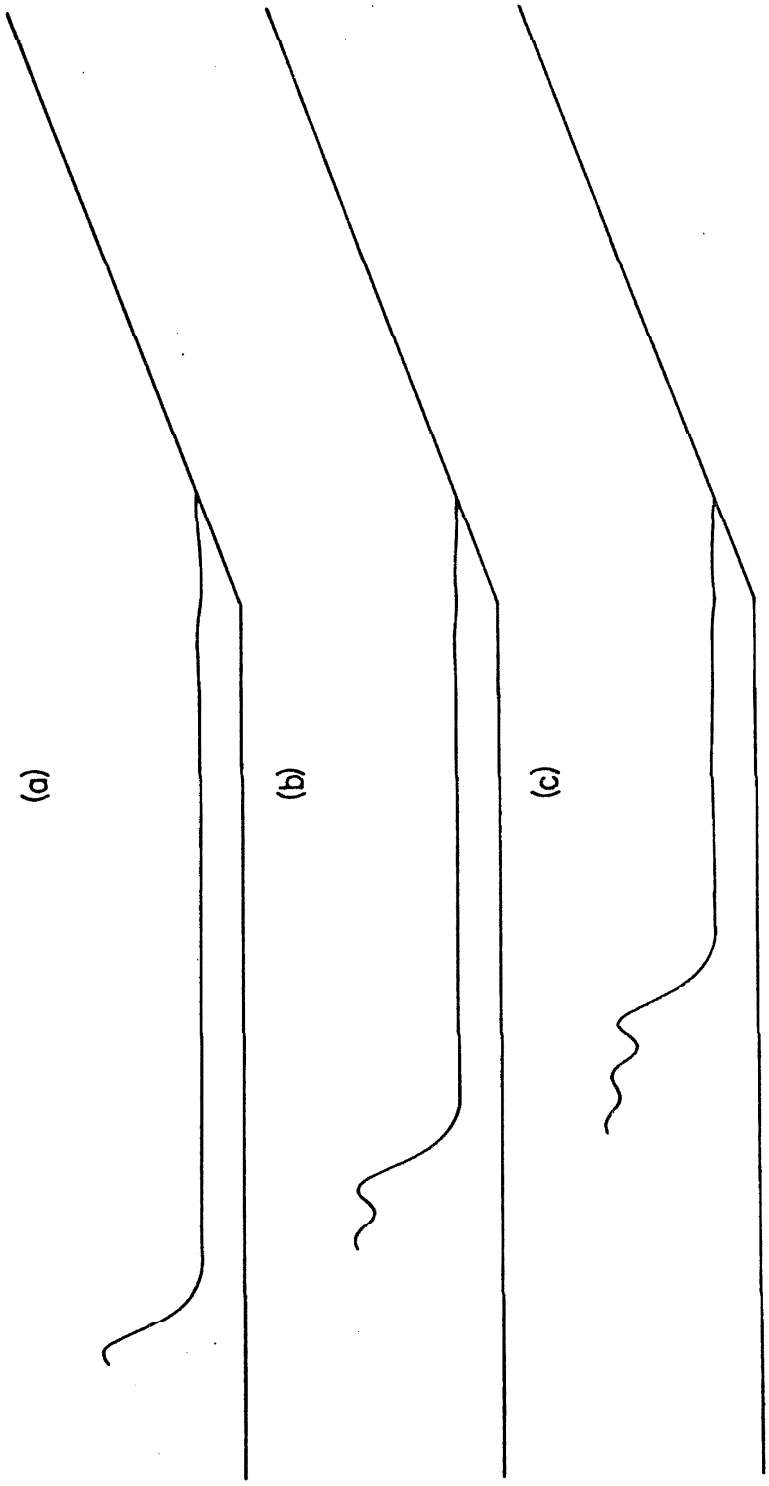

Figure XVI(a,b,c). Bore Run-up Profiles, Fr = 2.5, Slope = 5^{o}, $(\ell/h_1)^2 = 10.0$ (Scale Distorted).

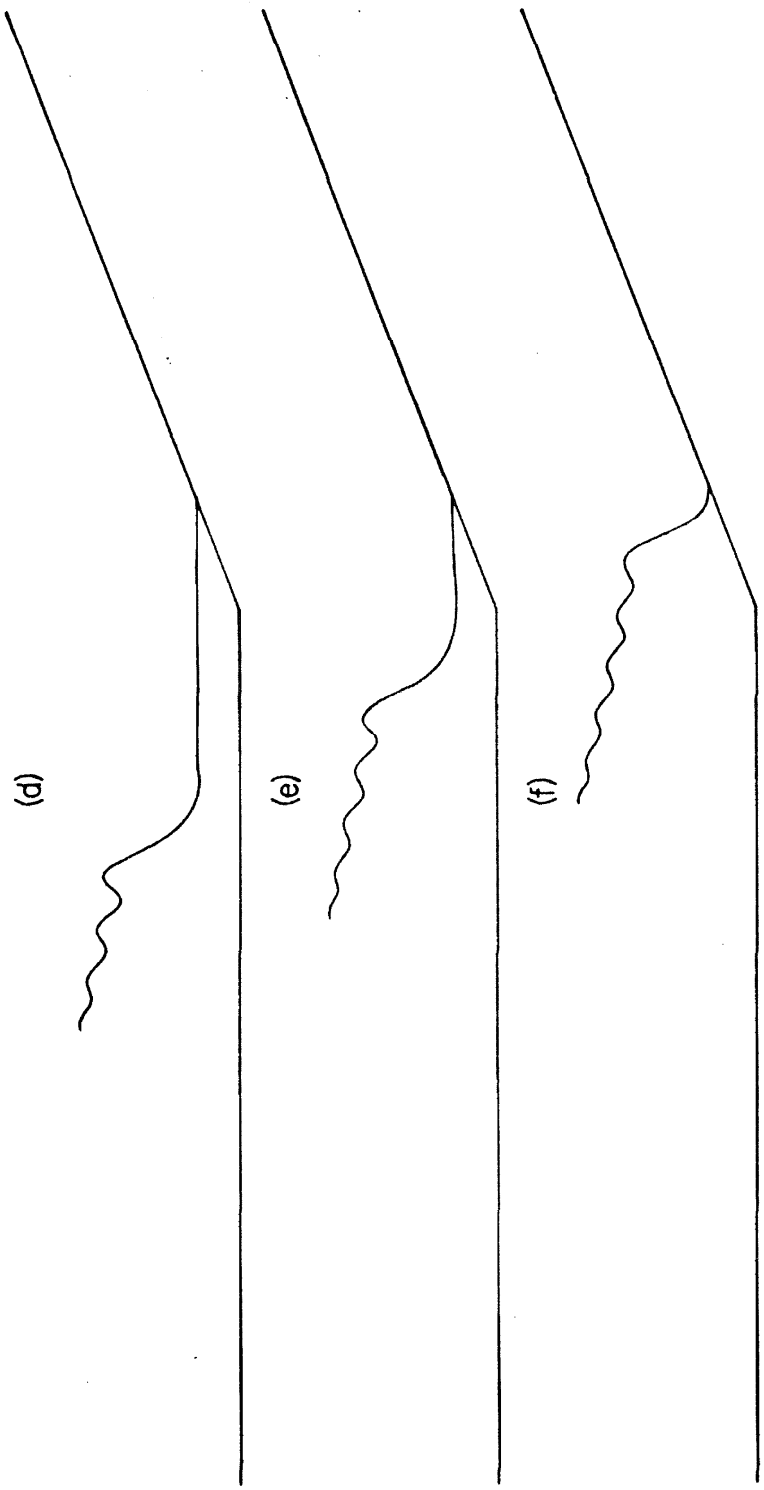

Figure XVI(d,e,f). Bore Run-up Profiles.

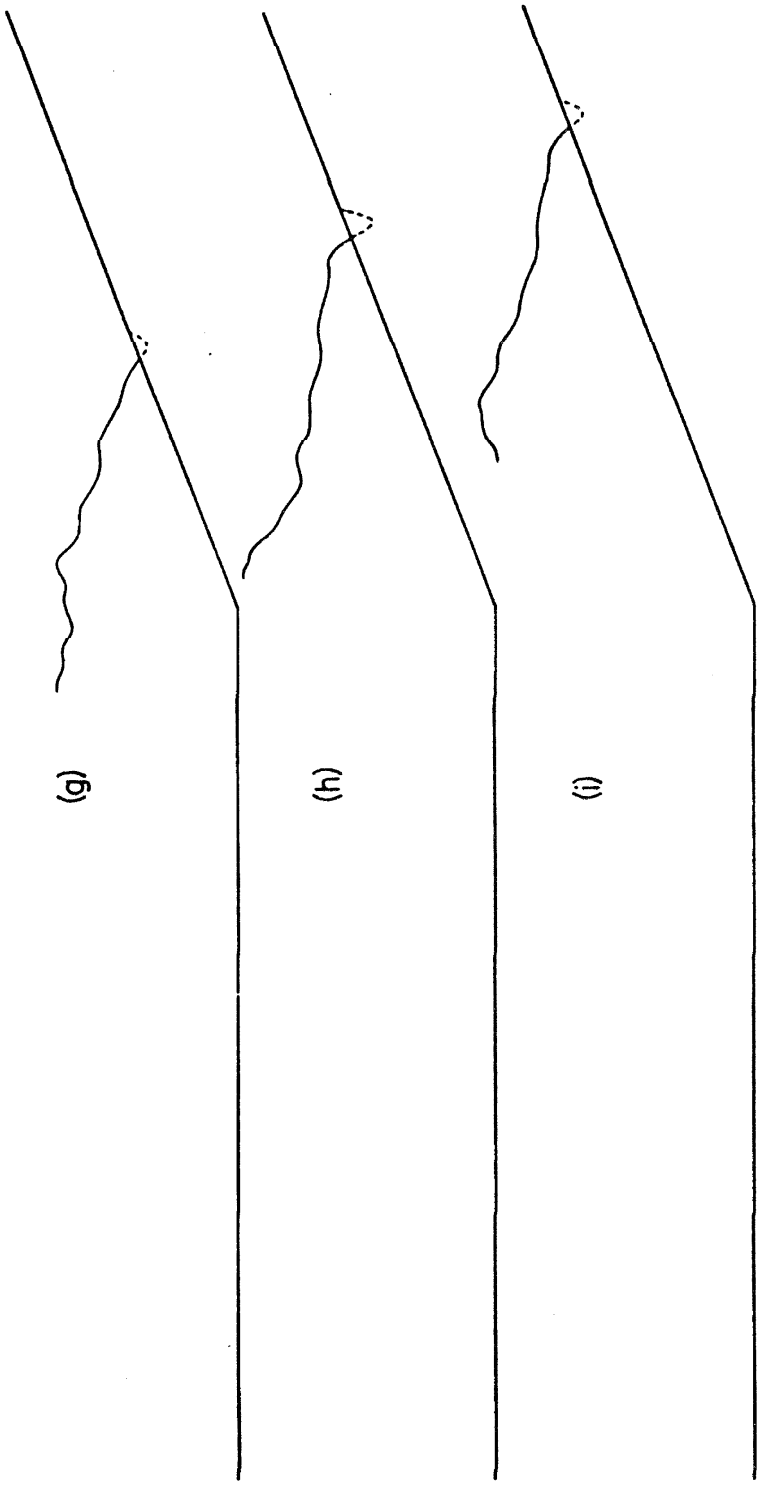

Figure XVI(g,h,i). Bore Run-up Profiles.

using an adequate 'artificial viscosity' term. Figures XVII(a to i) show the same problem with a considerably smaller coefficient and the resulting oscillations downstream of the shock. Surprisingly, the resulting run-ups are nearly the same.

Tsunami-like Wave Run-up

In addition to these checks with known experimental results, the model was used to investigate some aspects of a tsunami problem. The problem proposed was the investigation of the run-up produced by possible offshore bottom faulting on the continental shelf. The proposed motion of the bottom is shown in Figure XVIII, assuming the bottom to have been level initially. The negative of this motion was also considered, giving rise to waves of the opposite sign in amplitude.

Since the continental shelf depths vary, different cases were considered with water depths of 30, 100, and 300 feet. For simplicity, the bottom deformation was considered to produce only a vertical motion of the water, and so the surface profile appears with the same shape as the bottom. This is approximately correct when the deformation is small compared to the depth and the length of the deformation is large compared to the depth. In fact, the bottom deformation may be neglected in studying the propagation of the wave resulting from this initial free surface shape.

In small amplitude linear wave theory, an initial surface profile may be considered as the sum of two waves of one-half the above

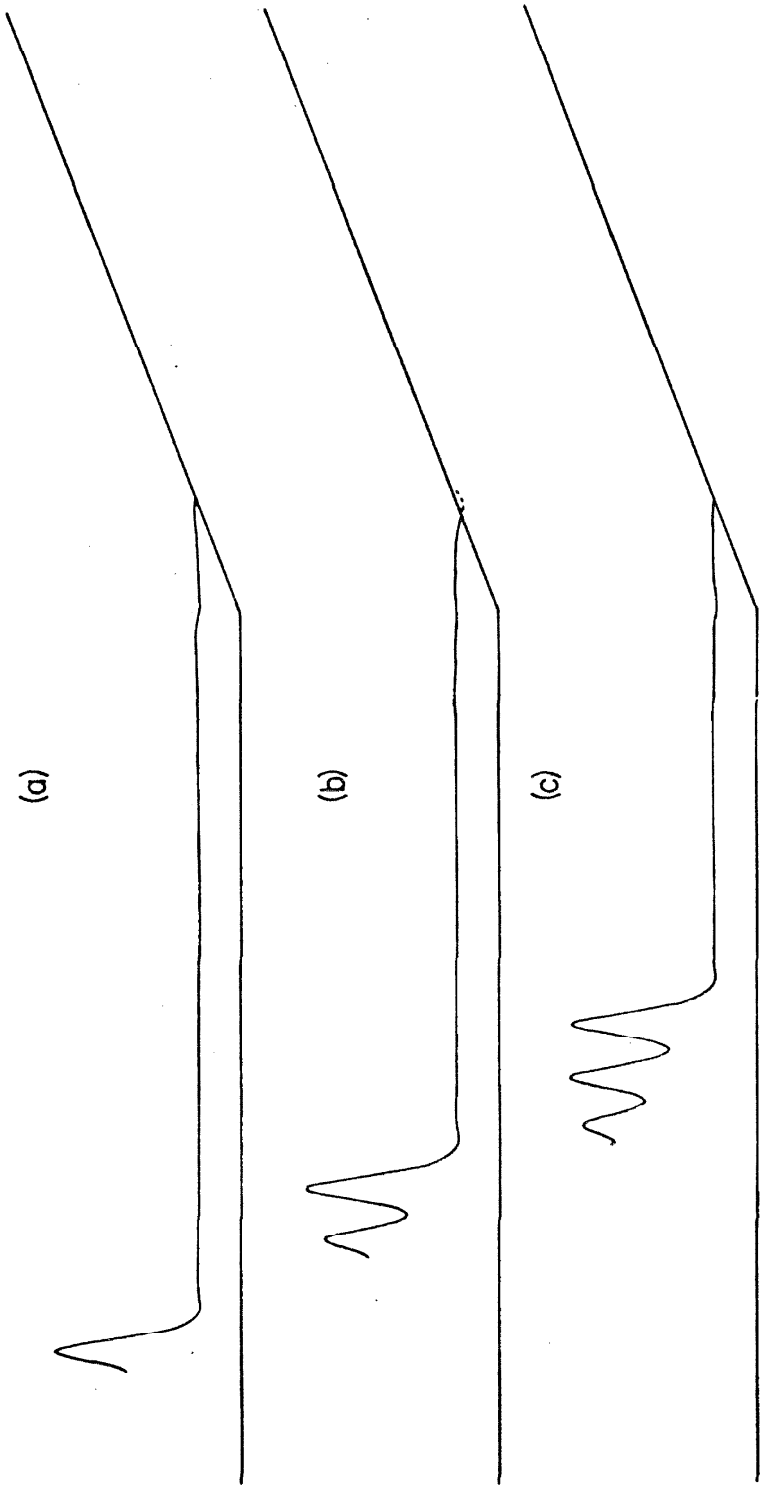

Figure XVII(a,b,c). Bore Run-up Profiles, Fr = 2.5, Slope = 5^{o}, $(\ell/h_1)^2 = 1.0$
(Scale Distorted).

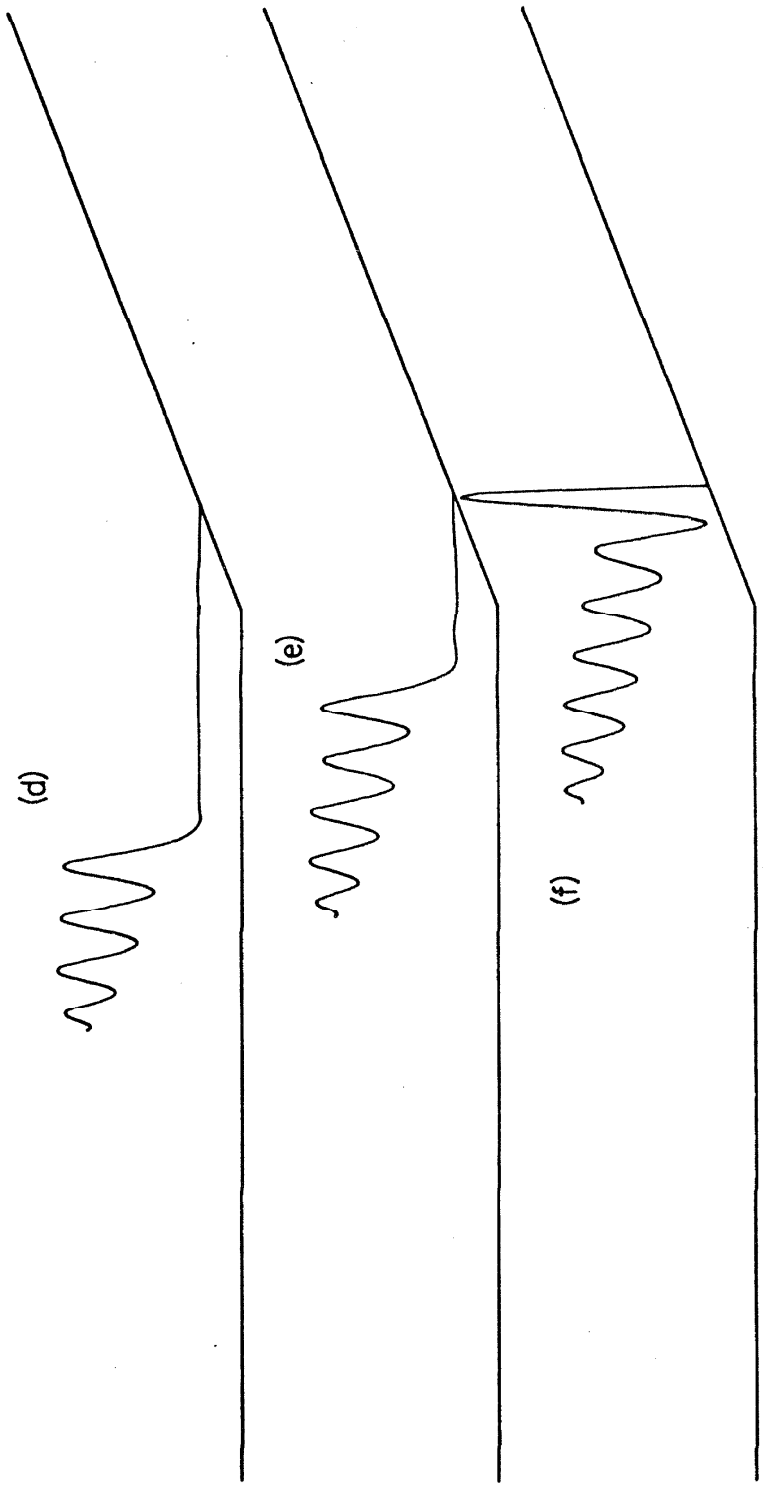

Figure XVII(d,e,f). Bore Run-up Profiles.

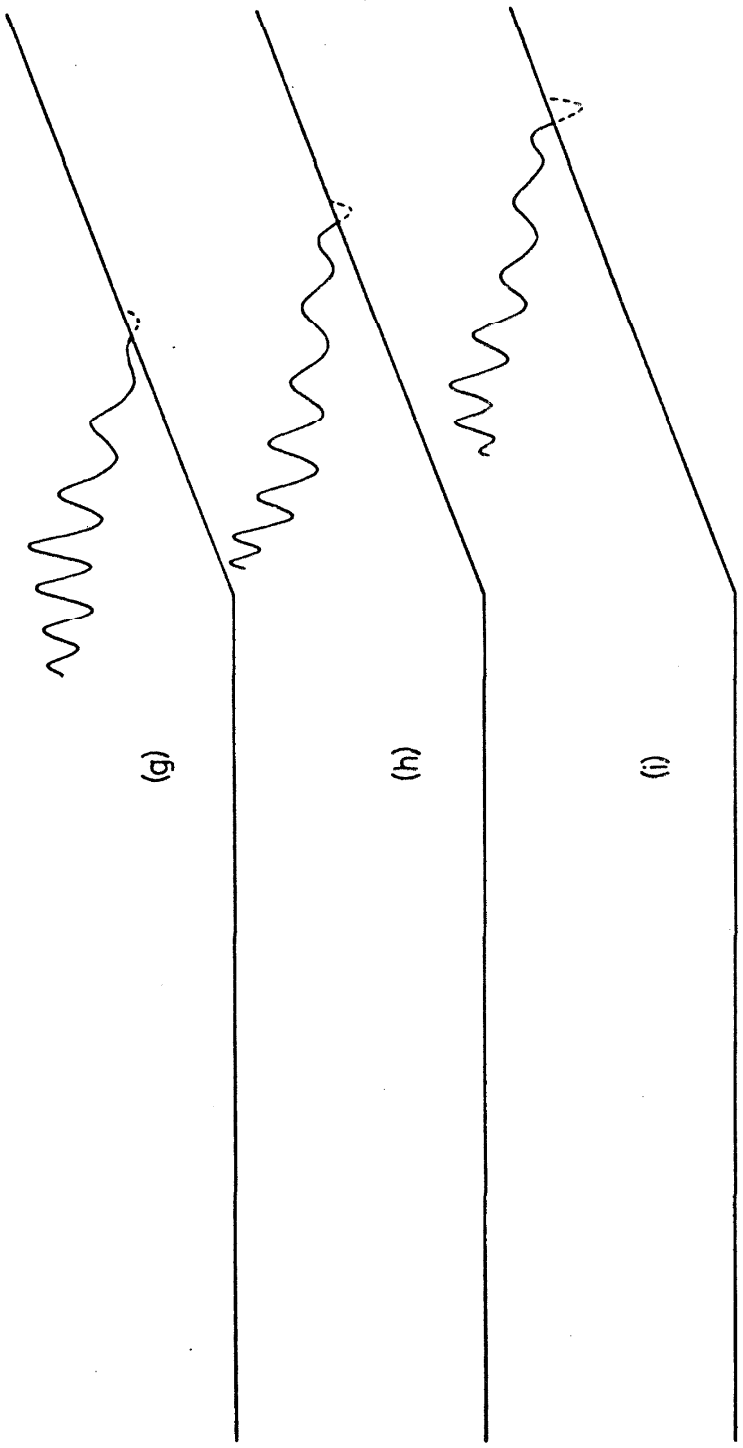

Figure XVII(g,h,i). Bore Run-up Profiles.

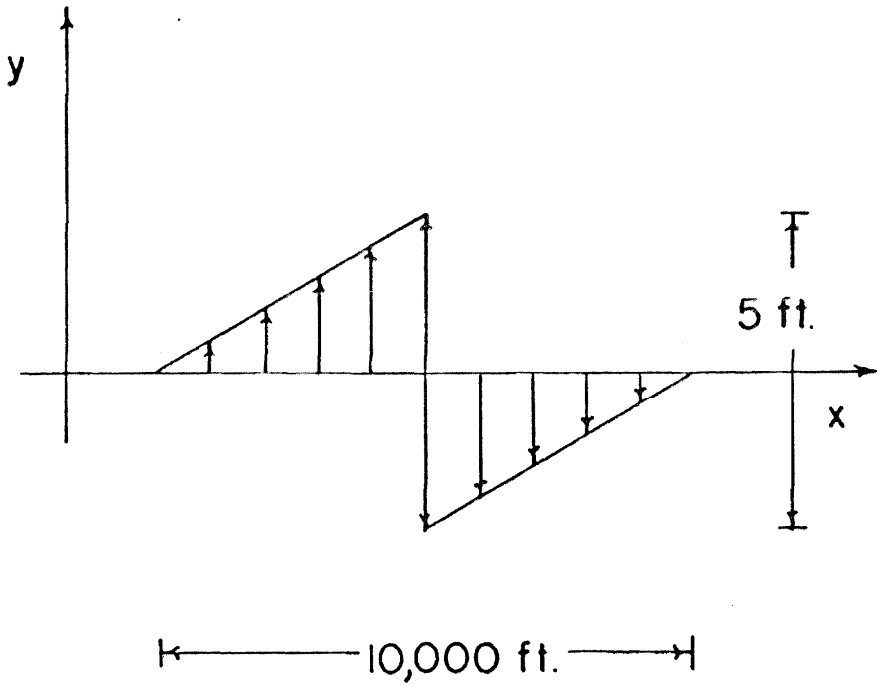

Figure XVIII. Bottom Deformation for Sample Tsunami Calculation.

amplitude. After $t = 0$, they move apart in the opposite direction as two separate but superposed solutions. One moves seaward and is not included in the analysis. The other is considered to propagate to a sloping beach where the run-up is investigated. Slopes of 1/10, 1/30, 1/100, and 1/300 were considered.

In investigating some cases, the errors involved near the transition from the flat bottom to a steep slope were found to be as large as the wave itself. This could have been resolved by using more elements, to reduce essentially the truncation error. However, this is costly in terms of computer time. To avoid this problem, a tank of uniform slope was considered. However, this meant the depth of the wavemaker was different than the original case. This was compensated for by transforming the wave to the correct proportions for that depth, so its effect would be the same as the original wave.

The shock width in these problems was made about 2 to 3 times $\overline{DX}$, the initial element width. In some cases, narrower shocks would have been more realistic, but as pointed out earlier, the numerical results tend to become unstable if the shock widths are made too small.

The bottom friction was initially left out of these calculations except as noted later.

The tabulated results are presented in Table I. In most cases, a leading positive wave produces a larger run-up than a leading negative wave. When the negative portion is first, a shock develops from the positive crest that follows which seems to dissipate the energy

TABLE I

Run-up for Tsunami-like Waves
(No Friction)

Beach Slope	Depth Offshore in feet		
	300 ft.	100 ft.	30 ft.
1/10	3.8		
	7.9		
1/30	10.2	7.1	
	7.5	8.7	
1/100	2.9	9.0	7.5
	1.2	4.0	
1/300		4.9	

Note: Run-up in feet. Top number is for positive leading wave. Bottom number is for negative leading wave.

in the wave.

To try to see if the results had any significance, the deep water size of the waves were calculated and the results plotted on the dimensionless plot (R/d vs. Slope, Figure XIX) used by Savage (17) to consolidate experimental data on the run-up or periodic (sinusoidal) waves. The deep water size is calculated on the basis that the wave is sinusoidal with the same wave length and height, using small amplitude theory. For comparison, the results of Savage are shown, along with the theoretical run-up of nonbreaking waves given by Keller (10).

The results appear to fit in as an extension of the results of Savage for small H_o/L_o. That is, for a given initial wave steepness (in deep water), the run-up increases (along the non-breaking curve) with decreasing beach slope. However, at a given slope (smaller for less steep waves), the wave begins to break, reducing the run-up on even shallower slopes. Hence the curves for constant H_o/L_o fall below the non-breaking curve, when breaking occurs.

Of course, this is only an approximate comparison, since the computed wave is not sinusoidal in shape and not part of a periodic train. However, the model could be used to investigate sinusoidal wave run-up for these low initial steepness waves. The important thing to note is that the large run-up tends to result from low steepness waves on shallow slopes.

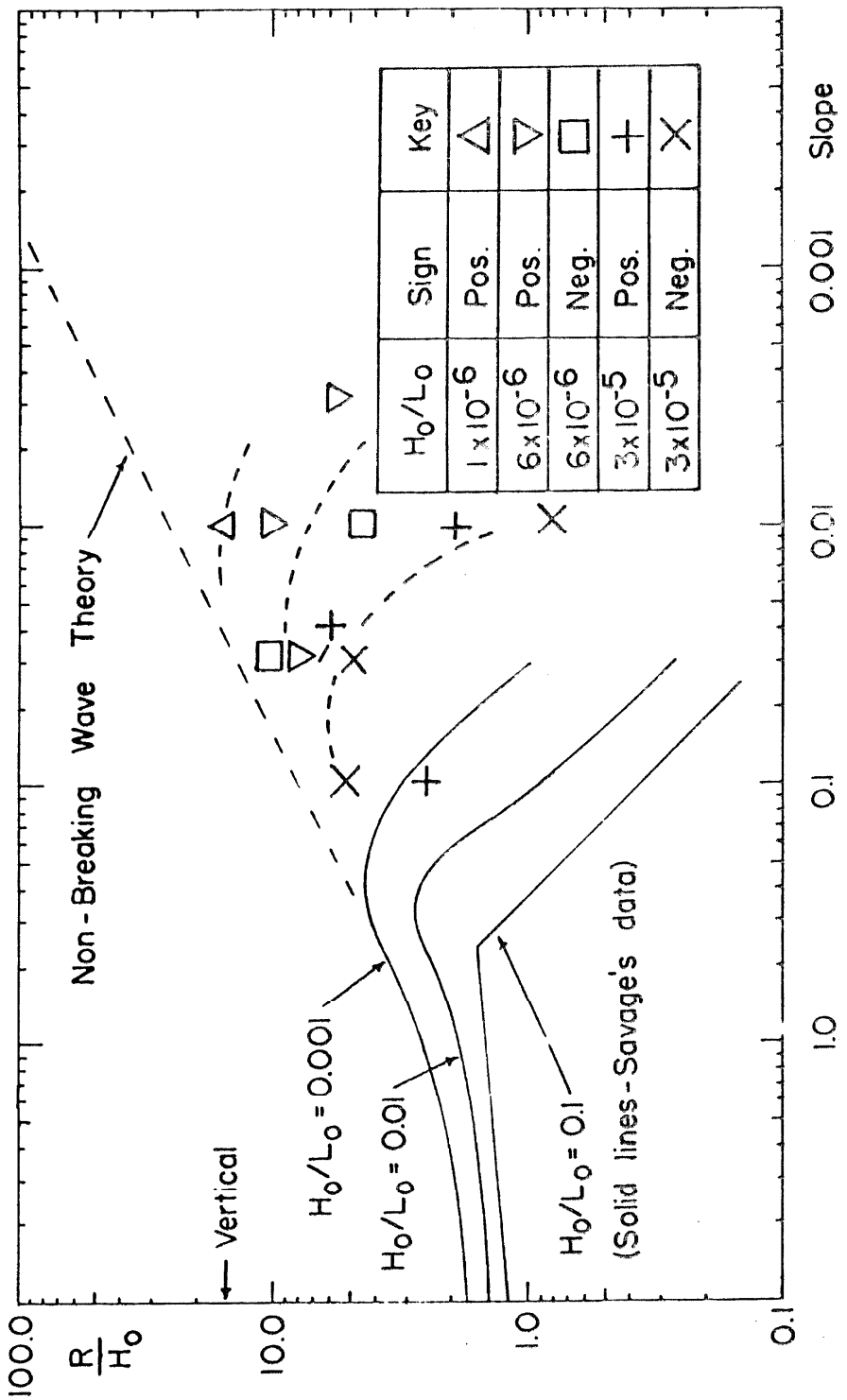

Figure XIX. Dimensionless Run-up Chart with Data from Sample Tsunami Calculations

Frictional Effects on Tsunami-like Run-up

To examine the effects of friction on such potential tsunami run-ups, certain solutions were recomputed with two values of the friction coefficient. This, it was hoped, would show the beginning of frictional effects and represent realistic values in a real problem. (It should be remembered the friction factor f is related to the friction coefficient K by $f = 8K$.)

The results are summarized in Table II. The run-up is seen to be more sharply reduced by friction on shallow slopes. This is similar to the results for solitary waves. It is especially important because on shallow slopes, the run-up can approach the large values of magnification indicated by the non-breaking wave theory, if little or no friction is present. The friction is the main means of reducing these large values.

The results for the same wave, on one slope, but generated at different depths, do not indicate any strong relationship between the initial wave steepness and the run-up reduction due to friction.

Tsunami-like Wave Run-up Profiles

To conclude this section, Figures XX (a to i) are presented. This is a sequence of profiles for the tsunami run-up on a 1/30 slope with an initial depth of 300 feet. It should be noted that the plot emphasizes the vertical. In Figure XX(a), the tsunami wave is seen to enter from the left (top). There is a small truncation error at the right near the beach, but this will be lost in the incoming wave. By Figure XX(f), the positve portion of the wave has been concentrated

TABLE II

Reduction in Run-up Due to Friction
(As a Fraction of Zero Friction Value)

At Constant Depth of 100 Feet

Friction Coefficient	Beach Slope		
	1/300	1/100	1/30
10^{-4}	0.90	0.94	1.0
10^{-3}	0.50	0.72	0.98

At Constant Slope of 1/100

Friction Coefficient	Depth in feet		
	300 ft	100 ft	30 ft
10^{-4}	0.99	0.94	0.97
10^{-3}	0.89	0.72	0.80

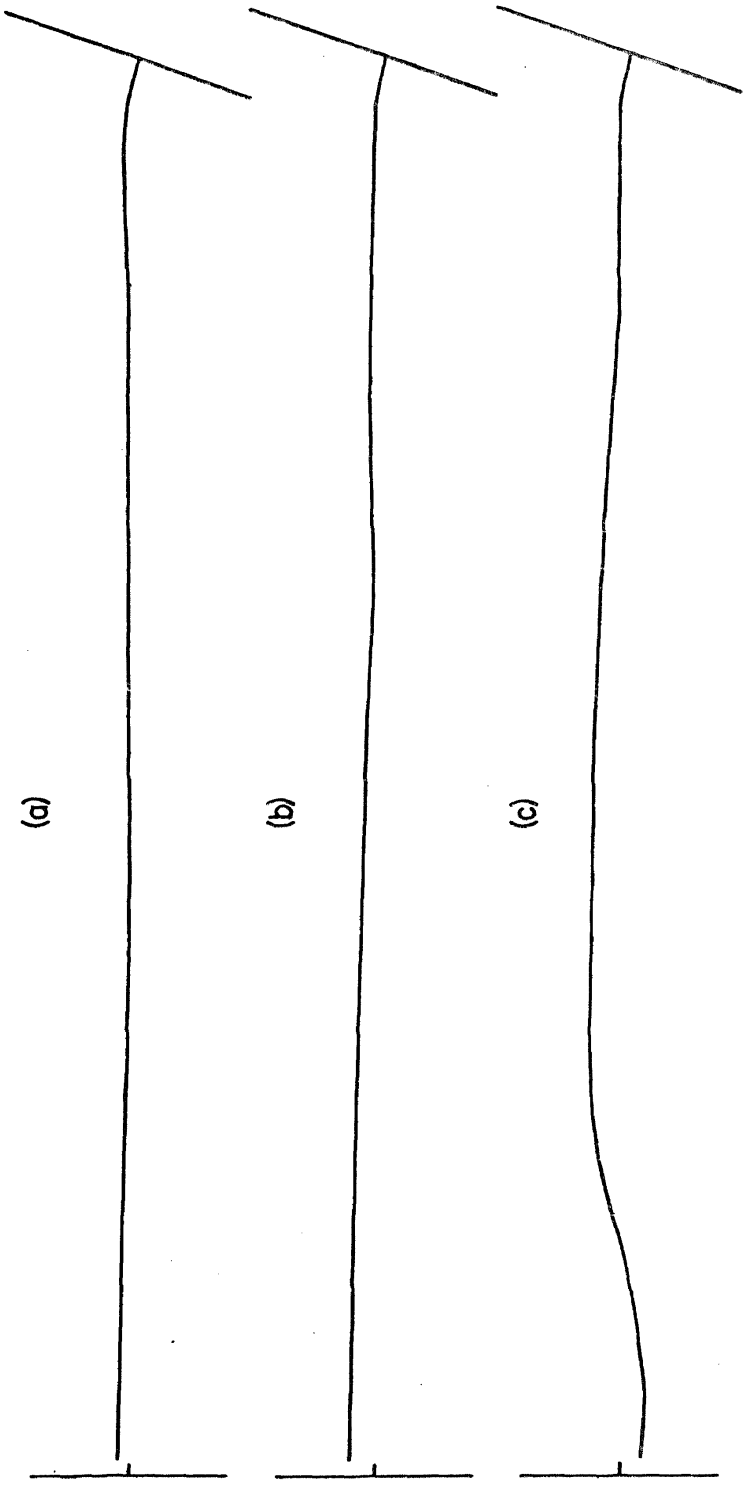

Figure XX(a,b,c). Sample Tsunami Run-up Profiles, Depth = 300 ft, Slope = 1/30 (Scale Distorted).

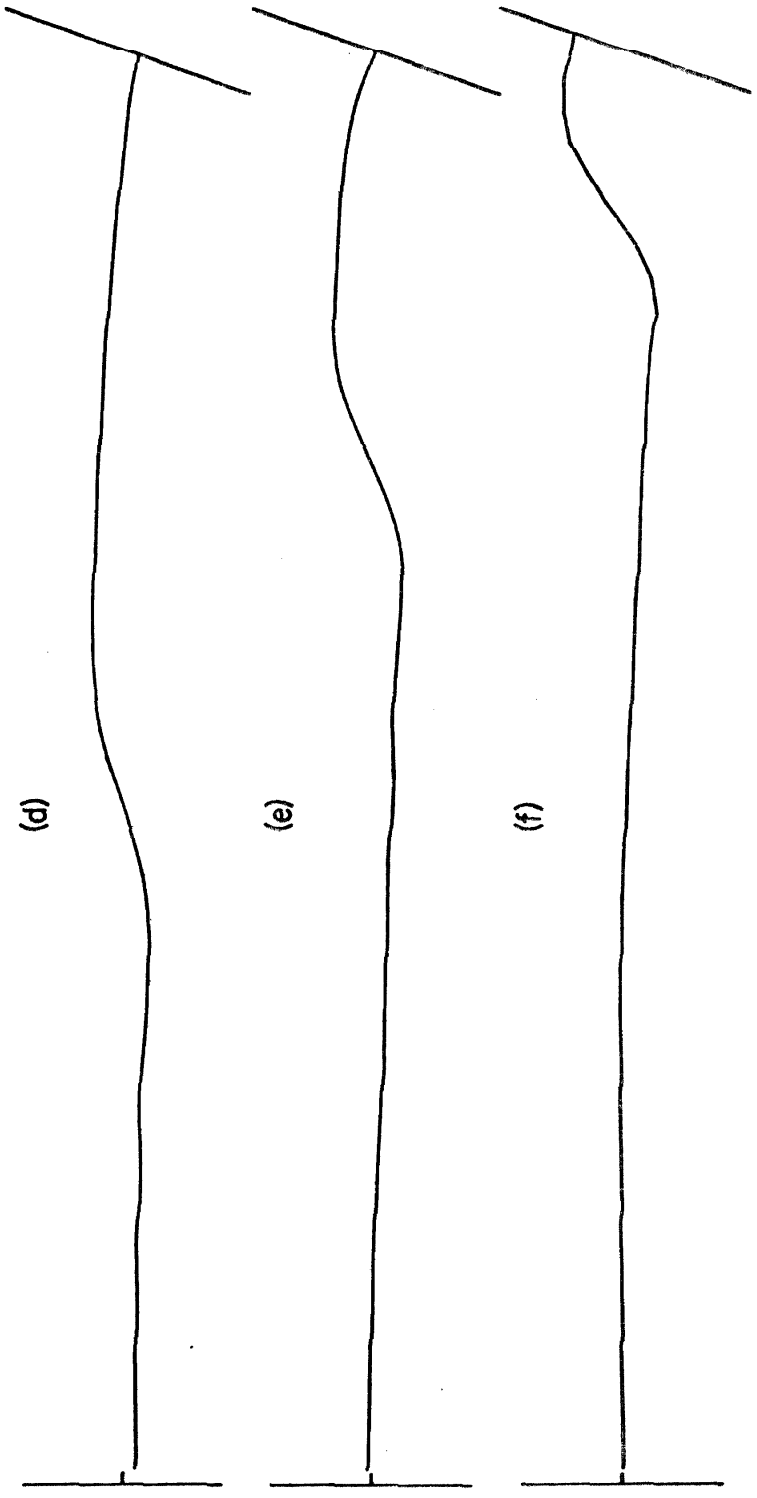

Figure XX(d,e,f). Sample Tsunami Run-up Profiles.

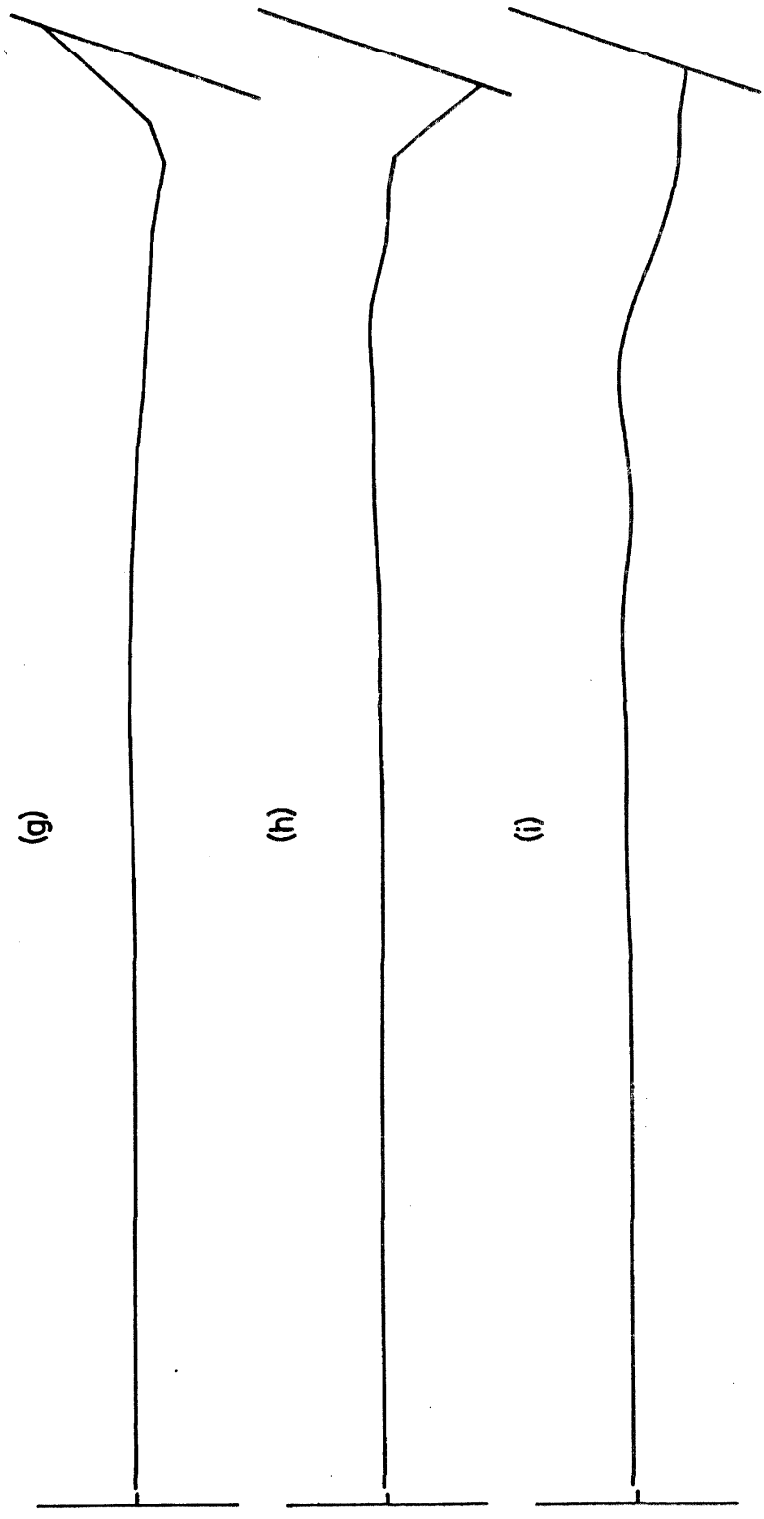

Figure XX(g,h,i). Sample Tsunami Run-up Profiles.

at the beach. It surges upwards, and then a backflow occurs. No breaking or bore formation seems to take place here. However, this is not surprising. The results for this case plot on the Savage run-up chart very close to the solution line for the non-breaking wave theory. Since that is based on shallow water theory, all of which is included in the formulation of this model, the model can account for this case perfectly.

SUMMARY, CONCLUSIONS, AND RECOMMENDATIONS

A mathematical model was developed for computing the run-up of long waves on a sloping beach. The model approximates the flow perpendicular to the beach by one in which the horizontal velocity is constrained to be constant in depth. This approximation gives good results for long (shallow water) waves and is also shown to give good results for the propagation and run-up of solitary waves. The formulation includes the kinetic energy of vertical motion, which is not included in formulations commonly used for studying the run-up problem. It is shown that the inclusion of this kinetic energy leads to equations that allow the propagation of a solitary-like wave. The inclusion of this kinetic energy also modifies the wave shape and gives a more realistic determination of the breaking of the wave than is given by the commonly used shallow water theory.

The model can treat hydraulic shocks by including an 'artificial viscosity' term in the equations. This allows energy dissipation in the shock, but conserves mass and momentum across the shock. It is shown that the proposed model approximately represents the formation and propagation of shocks.

The effect of bottom friction is taken into account in the model and it is shown that even small values of bottom friction can significantly effect the wave run-up on shallow slopes. This indicates that methods of increasing bottom friction may provide practical means for reducing the potential danger of tsunami run-up.

Calculations were made of the run-up of tsunami-like waves of very small initial steepness and it was found that these waves had relatively large run-ups. These waves were generated by a dipole-like displacement of the simulated ocean floor and it was found that a positive leading wave generally causes a larger run-up than a negative leading wave.

For further systematic studies of various aspects of the run-up problem, it is felt that this model will complement experimental model studies by virtue of its special properties. One is its flexibility, in that by reprogramming the computer, a variety of waveforms and flow regions can be examined. Also, the computer model can go beyond the constraints of real experiments, especially in examining very small initial steepness waves on very small slopes.

On the other hand, the computer model requires much care in its use to avoid computational errors. Careful choice of the 'artificial viscosity' and bottom friction coefficients is important. It seems more work needs to be done in this area, especially in an improved bottom friction rule.

The numerical analysis of the problem and the actual algorithms used also need to be restudied with the intent of reducing the computational time. This would mean obtaining an algorithm requiring the fewest operations to integrate over one time step, as well as determining the time step size adequate to satisfy the stability criteria without being wastefully small. Improvements in computers in terms of speed, memory size, and 'parallel' processing capability will tend to improve the relative merits of using this model to investigate run-up

problems.

More complicated contours can be studied by extending the present model derivation to a general bottom profile, which adds terms to the equations and increases the numerical computations. Perhaps a slightly more complex situation, where the flow is still constrained, but has more 'degrees of freedom,' such as

$$u(x, y, t) = u_0(x, t) + yu_1(x, t) + y^2u_2(x, t) \tag{51}$$

should be looked at as a basis for a more advanced model.

The present equations could be used to obtain solutions for the steady state periodic wave run-up. The analysis used here for transient waves would not be very efficient for getting this solution, but a modified analysis aimed particularly at steady state solutions should be developed.

APPENDIX A

Shock Thickness Using 'Artificial Viscosity' with the Shallow Water Equations

The equations governing the constrained flow, where the vertical kinetic energy is neglected, but the 'artificial viscosity' term is added are

$$h_+ + (uh)_x = 0 \tag{A.1}$$

$$(uh)_+ + (u^2h + \tfrac{1}{2}gh^2 + \ell^2 h(u_x)^2)_x = 0 \tag{A.2}$$

These equations are valid for a coordinate system moving at any fixed speed. Fixing the coordinates to a shock, the flow appears steady and the flow quantities are functions of x only, i.e., $h = h(x)$, $u = u(x)$, giving

$$(uh)' = 0 \tag{A.3}$$

$$(u^2h + \tfrac{1}{2}gh^2 + \ell^2 h(u')^2)' = 0 \tag{A.4}$$

as two O.D.E.'s to be solved. These can be integrated at once to

$$A + uh = 0 \tag{A.5}$$

$$B + u^2h + \tfrac{1}{2}gh^2 + \ell^2 h(u')^2 = 0 \tag{A.6}$$

where A and B are constants. For a shock-like solution, it is desired that far away from the shock (centered at $x = 0$), the flow quantities become constant values. Hence, the following conditions

are imposed.

As	$x \to -\infty$	$u \to u_1$	$h \to h_1$	$u' \to 0$
	$x \to \infty$	$u \to u_2$	$h \to h_2$	$u' \to 0$

This leads to the shock conditions

$$u_1 h_1 = u_2 h_2 \tag{A.7}$$

$$u_1^2 h_1 + \frac{1}{2} g h_1^2 = u_2^2 h_2 + \frac{1}{2} g h_2^2 \tag{A.8}$$

which may be solved for h_1 in terms of u_1 and u_2

$$h_1 = \frac{2u_1 u_2^2}{g(u_1 + u_2)} \tag{A.9}$$

The constants A and B are evaluated

$$A = -u_1 h_1 = -\frac{2(u_1 u_2)^2}{g(u_1 + u_2)} \tag{A.10}$$

$$B = -(u_1^2 h_1 + \frac{1}{2} g h_1^2)$$

$$= -\left(\frac{2u_1^2 u_2^2 (u_1^2 + u_1 u_2 + u_2^2)}{g(u_1 + u_2)^2}\right) \tag{A.11}$$

Since

$$H = -A/u \tag{A.12}$$

then

$$\ell^2 (u')^2 + u^2 + \frac{1}{2} gh + B/h = 0$$

$$\ell^2 (u')^2 = -u^2 + \frac{1}{2} \frac{gA}{u} + \frac{Bu}{A}$$

$$\ell^2(u')^2 = \frac{-u^3(u_1+u_2) - u_1^2u_2^2 + u^2(u_1^2+u_1u_2+u_2^2)}{u(u_1+u_2)}$$

$$\ell^2(u')^2 = (u_1-u)(u-u_2)[1 + u_1u_2/(u(u_1+u_2))] \qquad (A.13)$$

To get a rough idea of the solution, we plot

$$\frac{du}{dx} = -\frac{1}{\ell}\sqrt{(u_1-u)(u-u_2)\left(1 + \frac{u_1u_2}{u(u_1+u_2)}\right)} \qquad (A.14)$$

between u_1 and u_2, assuming $u_1 > u_2$. See Figure A. We can also plot its inverse -dx/du. See Figure B. If at $x = 0$, $u = (u_1+u_2)/2$, then x(u) looks like Figure C, where from the original boundary conditions we know the asymptotes. A more conventional representation of the shock profile is given in Figure D.

The so-called 'slope width' of the shock, δ, can be evaluated by using the value of du/dx at $x = 0$

$$\frac{du}{dx} = \frac{1}{\ell}\sqrt{\left(\frac{u_1-u_2}{2}\right)^2\left(1 + \frac{2u_1u_2}{(u_1+u_2)^2}\right)} \qquad (A.15)$$

The quantity $1 + 2u_1u_2/(u_1+u_2)^2$ varies between 1.0 and 1.25, so

$$\frac{du}{dx} \approx \frac{1}{\ell}\,\frac{u_1-u_2}{2} \qquad (A.16)$$

Thus the 'slope width' δ is found

$$\frac{u_1-u_2}{\delta} \approx \frac{1}{\ell}\,\frac{u_1-u_2}{2} \qquad (A.17)$$

$$\delta \approx 2\ell \qquad (A.18)$$

This shows the basic nature of the 'artificial viscosity' term.

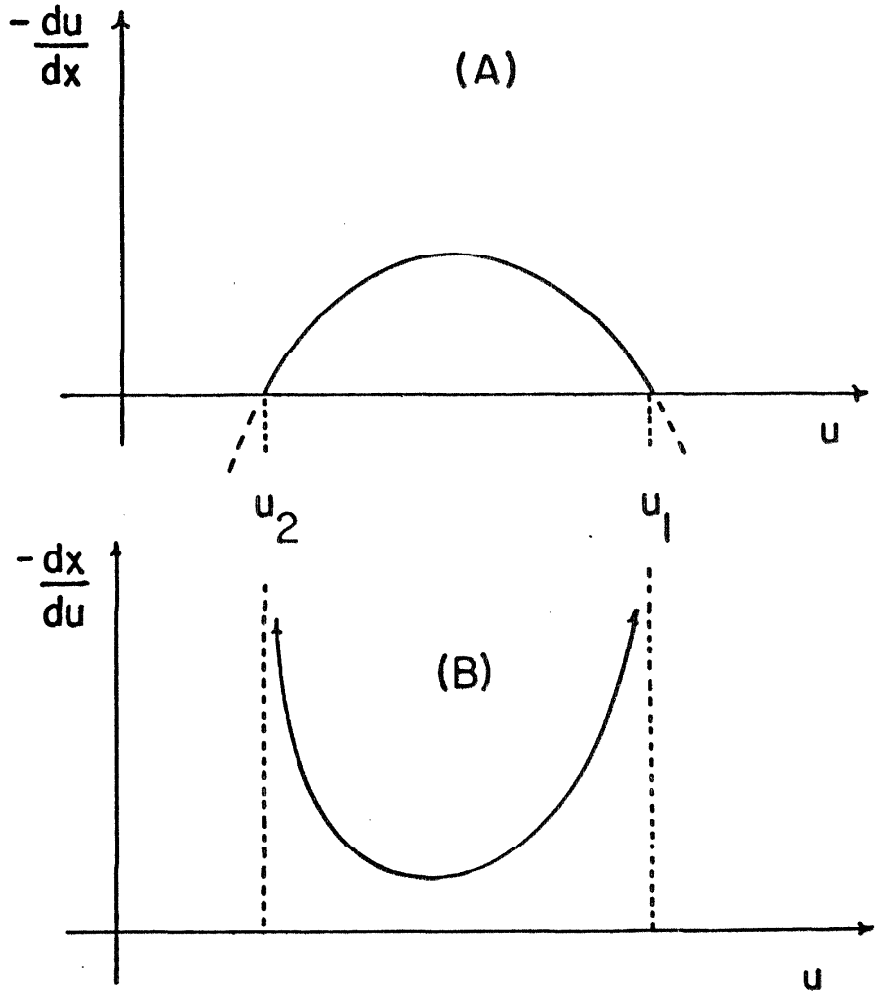

Figures A and B.

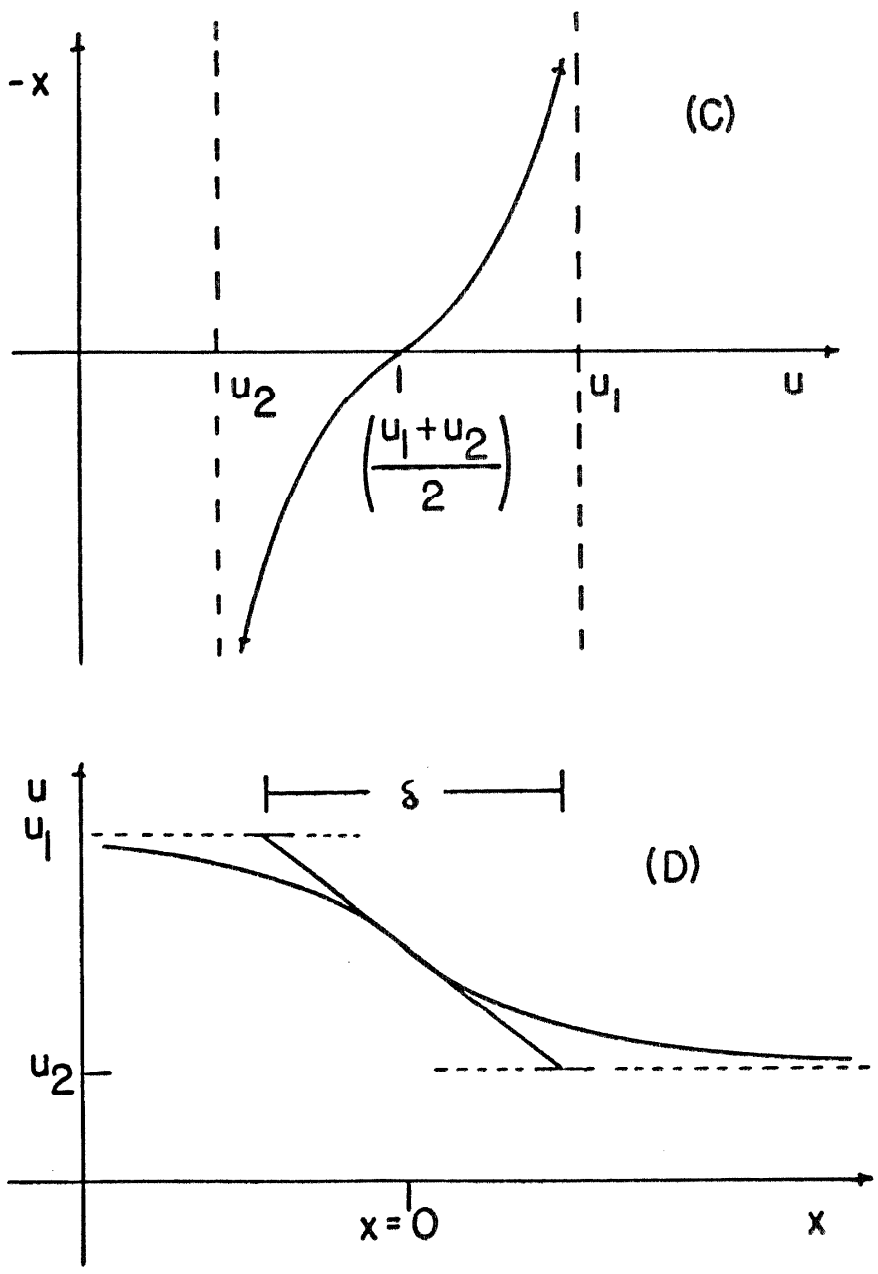

Figures C and D.

The shocks tend to be constant in width and independent of the shock strength when this term is used.

When the terms representing the kinetic energy of the vertical flow are introduced in equation (A. 2) to give the constrained flow, the analytic solution for the shock becomes more difficult to obtain and interpret. However, the numerical solutions discussed in the text show the overall shock behavior is correct and similar to the results shown here for the shallow water equations.

APPENDIX B

Permanent Waveform for Constrained Flow

The equations of motion for constrained flow can be integrated to give a solution for a permanent waveform. So far as is known this solution has not been derived before. The equations for constrained flow as derived are

$$h_+ + (uh)_x = 0 \tag{B.1}$$

$$(uh)_+ + \left(u^2h + \frac{1}{2}gh^2 + \frac{1}{3}h^3(u_x^2 - u_{x+} - uu_{xx})\right)_x = 0 \tag{B.2}$$

These equations are valid when translating at any fixed speed. If we choose the coordinates moving with the wave of permanent form, the flow is steady and $u = u(x)$, $h = h(x)$. The equations become O.D.E.s

$$(uh)' = 0 \tag{B.3}$$

$$\left(u^2h + \frac{1}{2}gh^2 + \frac{1}{3}h^3\left((u')^2 - uu''\right)\right)' = 0 \tag{B.4}$$

which are integrated to

$$uh - A = 0 \tag{B.5}$$

$$u^2h + \frac{1}{2}gh^2 + \frac{1}{3}h^3\left((u')^2 - uu''\right) - B = 0 \tag{B.6}$$

At $x = \pm \infty$, one lets the flow approach a uniform flow $u = u_o$, $h = h_o$, and $u'' = u' = 0$.

Thus

$$A = u_o h_o \tag{B.7}$$

$$B = u_o^2 h_o + \frac{1}{2} g h_o^2 \tag{B.8}$$

Rewriting the equations

$$3u^2/h^2 + 3g/h + \left((u')^2 - uu''\right) - 3B/h^3 = 0$$

$$1/h = u/A$$

Eliminating h

$$3u^4/A^2 + 3gu/A - 3Bu^3/A^3 - \left((u')^2 - uu''\right) = 0 \tag{B.9}$$

Since x does not appear explicitly, using

$$u'' = u'(du'/du) \tag{B.10}$$

reduces the order of the equation. Rearranging, one obtains

$$\frac{d(u')^2}{du} - \frac{2}{u}(u')^2 = \frac{6u^3}{A^2} - \frac{6Bu^2}{A^3} + \frac{6g}{A}$$

$$\frac{d}{du}\left(\frac{u'}{u}\right)^2 = \frac{6u}{A^2} - \frac{6B}{A^3} + \frac{6g}{Au^2} \tag{B.11}$$

Integrating

$$\left(\frac{u'}{u}\right)^2 = \frac{3u^2}{A^2} - \frac{6Bu}{A^3} - \frac{6g}{Au} + \text{constant} \tag{B.12}$$

since at $x = \pm \infty$, $u = u_o$ and $u' = 0$, we can evaluate the constant. If on the right-hand side, the values of A and B are substituted, and $c_o^2 = gh_o$ is defined, then

$$\left(\frac{u'}{u}\right)^2 = \frac{3}{(u_o h_o)^2}(u - u_o)\left[u - \left(u_o + \frac{c_o^2}{u_o}\right) + \frac{c_o^2}{u}\right]$$

or

$$(u') = \frac{\sqrt{3}}{u_o h_o}(u - u_o)\sqrt{u\left(u - \frac{c_o^2}{u_o}\right)} \tag{B.13}$$

The branch selected is such that $u' > 0$ for $(c_o^2/u_o) < u < u_o$, so that the profile is some sort of positive wave, with $h > h_o$.

If we take the crest of the wave at $x = 0$, the $du/dx = 0$ there. Since the other zero is at $x = \pm \infty$, $u = u_o$, then $u = c_o^2/u_o$ at $x = 0$. Thus the integral can be written

$$\int_{\frac{c_o^2}{u_o}}^{u} \frac{du}{(u_o - u)\sqrt{u\left(u - \frac{c_o^2}{u_o}\right)}} = \int_o^x \frac{\sqrt{3}\,dx}{u_o h_o} \tag{B.14}$$

to find the function $u(x)$. Both sides may be integrated

$$\frac{1}{\sqrt{u_o^2 - c_o^2}} \cosh^{-1}\left(\frac{2u_o(uu_o - c_o^2)}{(u_o - u)c_o^2} + 1\right) = \frac{\sqrt{3}\,x}{u_o h_o} \tag{B.15}$$

Inverting gives

$$\frac{u}{u_o} = \frac{1 + \cosh\left(\frac{x\sqrt{3}}{u_o h_o}\sqrt{u_o^2 - c_o^2}\right)}{2\frac{u_o^2}{c_o^2} + \cosh(\;) - 1}$$

The wave profile $h(x)$ is found by using $hu = u_o h_o$

$$\frac{h}{h_o} = \frac{\frac{2u_o^2}{c_o^2} + \cosh(\;) - 1}{1 + \cosh(\;)} \tag{B.16}$$

Since at $x = 0$, the maximum height of $H + h_o$ is obtained because $\cosh(0) = 1$, then

$$\frac{H + h_o}{h_o} = \frac{u_o^2}{c_o^2} \tag{B.17}$$

This gives the speed of the permanent wave as a function of its size

$$u_o = c_o\left(1 + \frac{H}{h_o}\right)^{1/2} = \sqrt{gh_o}\left(1 + \frac{H}{h_o}\right)^{1/2} \tag{B.18}$$

The profile can then be found as

$$h - h_o = H \frac{2}{1 + \cosh\left(\frac{\sqrt{3}\,x}{h_o}\sqrt{\frac{H}{H + h_o}}\right)} \tag{B.19}$$

APPENDIX C

How 'Artificial Viscosity' Implies Energy Dissipation

The equations governing the constrained flow, where the vertical kinetic energy is neglected, with the 'artificial viscosity' term (F) added, are

$$h_+ + (uh)_x = 0 \tag{C. 1}$$

$$(uh)_+ + (u^2h + \frac{1}{2} gh^2 + F)_x = 0 \tag{C. 2}$$

Consider in addition, an energy flux equation:

$$\underbrace{\left(\frac{u^2h}{2} + \frac{gh^2}{2}\right)}_{A}{}_+ + \Bigg(u \underbrace{\left(\frac{u^2h}{2} + \frac{gh^2}{2}\right)}_{B} + \underbrace{u \frac{gh^2}{2}}_{C} \Bigg)_x + D = 0 \tag{C. 3}$$

where the terms are interpreted as follows.

A represents the rate of change in time of the total kinetic and potential energy for a fixed region of width dx.

B represents the transport of kinetic and potential energy across the boundary of that region.

C represents the work done on the boundary of the region by the pressure force.

D is the rate at which energy is dissipated in the region, i. e., the local energy dissipation rate.

Solving for D with (C. 1), (C. 2), and (C. 3) one finds

$$D = F_x u \tag{C. 4}$$

as mentioned in the text.

This discussion has been simplified by the omission of the kinetic energy of the vertical flow. However, this will only appear as additional terms in equations (C. 2), (C. 3), and (C. 4). The basic nature of D will still be represented by the portion of the expression $F_x u$.

APPENDIX D

Small Amplitude Waves for Constrained Flow

The equations for the constrained flow

$$h_+ + (uh)_x = 0 \tag{D. 1}$$

$$(uh)_+ + \left(u^2h + \frac{1}{2}\, gh^2 + \frac{h^3}{3}\,(u_x{}^2 - u_{x+} - uu_{xx})\right)_x \tag{D. 2}$$

can be linearized for small amplitudes by considering $h = \eta + d$ where d is constant and $d > > \eta$. If this is substituted in (D. 1) and (D. 2) and only first-order terms in u and η are retained, one has

$$\eta_+ + u_x d = 0 \tag{D. 3}$$

$$u_+ d + g\eta_x - \frac{d^3}{3}\, u_{xx+} = 0 \tag{D. 4}$$

Eliminating u gives

$$\eta_{++} - gd\eta_{xx} - \frac{d^2}{3}\, \eta_{xx++} = 0 \tag{D. 5}$$

The dispersion relation for this equation can be written as,

$$c = \frac{\omega}{k} = \left(\frac{gd}{1 + \frac{(dk)^2}{3}} \right)^{\frac{1}{2}} \tag{D. 6}$$

where c is the phase velocity, ω the angular frequency and k the wave number. The corresponding relation for small amplitude potential flow theory is

$$c = \frac{\omega}{k} = \left(\frac{g}{k}\, \tanh\, kd \right)^{\frac{1}{2}} \tag{D. 7}$$

For long waves, $kd < < 1$, both expressions give the classical $c = \sqrt{gd}$. The expression (D. 6) approximates (D. 7) for larger kd with increasing error, ($kd = 1$, difference $\approx 1\%$; $kd = 2$, difference $\approx 5\%$).

Hence, small amplitude wavelengths less than about 3-5 times the depth are no longer accurately modelled. The constrained flow gives these waves a lower phase velocity than the potential theory predicts. This obviously results from the poor approximation of the flow field of the potential flow as the wavelengths decrease.

APPENDIX E

Description of Computer Programs

The computer system used for the actual calculations was an IBM 7094 system, in use at Caltech until mid-1969. The program is written in Fortran and should be adaptable to other computers. A complete copy of a typical program with several variations is given as an addendum to this description, but it does not represent the entire collection of programs used.

The main control program (WWP for Water Wave Program) can be outlined broadly as follows:

1. All the data relevant to specifying the problem are read from a series of cards. These data define the geometry of the 'wave tank' modelled, the size of the finite elements, and the size of the integration time steps. Also included are the parameters governing the excitation applied to the initially 'quiet' tank via the 'wavemaker' input. Certain additional data indicate what results the computer should supply as output from the calculation.

2. Other fundamental quantities are calculated from the input data. Especially important is the definition of the Lagrangian variables (x_i's and $\dot{x}_i$'s) with the correct initial values and the calculations of the c_i's. Naturally, space has been reserved for these arrays of numbers with appropriate dimensioning statements in the program.

3. The stepwise integration of the system in time is begun. The integration is initially by Runga-Kutta but after several time steps, Adam's method is used, since the time step size is equal and the

computation is reduced. Two important subroutines used in this calculation are the excitation (DRIVE) and the evaluation of the equations of motion (FUNC for Function).

a. DRIVE supplies the instantaneous acceleration of the wavemaker as a function of time to produce the input waveform. Three different subroutines are given as examples. The first produces a constant velocity wavemaker motion to generate a bore of given strength. The second produces the approximation to the solitary wave described in the main text. The last produces a single square wave pulse. In all cases, the parameters describing the input waveform are taken from the initial data. Some calculation could be eliminated by doing the preliminary calculations involved in DRIVE only once, so at subsequent time steps only the time dependent portion of the function is recalculated.

b. FUNC supplies the evaluation of the right-hand side of the first order system of ordinary differential equations being solved. Hence, most of the complex algebraic expressions involved in the system appear in FUNC. This includes the inversion of the matrix [A] needed to evaluate the expression $[A]^{-1}\{B\} + [A]^{-1}\{f\}$, (44) in the text.

Since the evaluation of FUNC represents most of the computation done in the solution of this problem, careful attention should be given to reducing the execution time of this subroutine.

At each time step, a check is made to see if it is appropriate to output some data and/or terminate the calculation. Both cases are

covered in the next section.

4. A vast amount of data is generated in a repetitive numerical integration of the sort described here. Only a part of it is interesting and is taken as output.

One basic output used in this program is graphical presentation of the profiles of the free surface of the flow at fixed intervals in time. This is done by interrupting the integration and using the x_i's to calculate the profile, which is given to a plotting subroutine. The integration is then resumed.

Specific variables of interest may be stored at fixed time intervals to be presented graphically as time functions when the calculation is complete. In this program, the water level at the beach is so presented.

Main Program - WWP

```
$IBFTC WWP
      COMMON
     1/WALL/N,XO,R,N2,G,DRD,DRE,X1,T,DRA,DRC,XF(500),M,PI2,CO3,TA,TG,DX,
     2DRB,D
     3/WFUNC/XP(500),C(250),X(500),TF
      DIMENSION WT(10),WO(10),WA(10),TJ(500),TK(500),TL(500),TC(500),
     1TB(500),H(250),HT(7500) ,AREA(969),DUMMY(1)
     2,TMA(500),Z(50),Y(50)
C     INPUT TITLES
      CALL RCD (NWT,WT,NWO,WO,NWA,WA)
  101 CONTINUE
C     INPUT PARAMETERS
      CALL RCD (R,D,AL,TT)
      WRITE(6,1001)R,D,AL,TT
 1001 FORMAT (1HO,E15.8)
      CALL RCD (N,NT,NP,NH)
      WRITE (6,1002) N,NT,NP,NH
 1002 FORMAT(1HO,I8)
C     INPUT DRIVE PARAMETERS
      CALL RCD (DRA,DRB,DRC,DRD,DRE)
      WRITE(6,1001)DRA,DRB,DRC,DRD,DRE
C     PRELIMINARY RESULTS
      HN=FLOAT(NH)
      PT=HN*D
      PB=0.0
      PB1=2.0*PB-PT
      PT1=2.0*PT-PB
      NO=10*N
      TA =SIN(AL)/COS(AL)
      TG=32.2*TA
      RT=R+D/TA
      RP=R+HN*D/TA
      RP2=RP/2.0
      DX=RT/FLOAT(N)
      N2=2*N
C     INITIAL CONDITIONS
      DO 1 I=1,N
      XF(I)=DX*FLOAT(I-1)
      NI=N+I
    1 XF(NI)=0.0
      N1=N-1
      DO 2 I=1,N
    2 IF (((XF(I)+XF(I+1))/2.0).GE.R) GO TO 3
      WRITE (6,1003)
 1003 FORMAT (1H1,5HERROR)
    3 CONTINUE
      M=I
      DO 4 I=1,N1
      H(I)=D
      IF(I.GE.M) H(I)=H(I)-((XF(I)+XF(I+1))/2.0-R)*TA
    4 CONTINUE
      H(N)=D-(XF(N)-R)*TA
      DO 5 I=1,N1
    5 C(I)=H(I)*(XF(I+1)-XF(I))
      C(N)=H(N)**2/(2.0*TA)
      CI=H(N)
      DT=TT/FLOAT(NT)
      D2=2.0*D
      NSBP=NT/NP
      PI=3.14159
      PI2=2.0*PI
```

```
      G=32.2
      XO=0.0
      X1=0.0
C     BEGIN CALCULATION
C     BEGIN  RK
      DO 6 J=1,3
      DUMM=DUMMY(J)
      T=DT*FLOAT(J-1)
      CALL DRIVE
      TF=T
      DO 7 I=1,N2
    7 X(I)=XF(I)
      CALL FUNCT
      DO 8 I=1,N2
      TC(I)=DT*XP(I)
      IF(J.EQ.1) TJ(I)=XP(I)
      IF(J.EQ.2) TK(I)=XP(I)
      IF(J.EQ.3) TL(I)=XP(I)
    8 X(I)=XF(I)+TC(I)/3.0
      TF=T+DT/3.0
      CALL FUNCT
      DO 10 I=1,N2
      TB(I)=XP(I)*DT
   10 X(I)=XF(I)+2.0*TB(I)/3.0
      TF=T+2.0*DT/3.0
      CALL FUNCT
      DO 11 I=1,N2
   11 XF(I)=XF(I)+TC(I)/4.0+3.0*DT*XP(I)/4.0
    6 CONTINUE
C     END RK BEGIN ADAMS
      DO 12 J=4,NT
      DUMM=DUMMY(J)
      T=DT*FLOAT(J-1)
      CALL DRIVE
      TF=T
      DO 13 I=1,N2
   13 X(I)=XF(I)
      CALL FUNCT
      DO 14 I=1,N2
      XI=55.0*XP(I)-59.0*TL(I)+37.0*TK(I)-9.0*TJ(I)
      XF(I)=XF(I)+DT*XI/24.0
      TJ(I)=TK(I)
      TK(I)=TL(I)
      TL(I)=XP(I)
   14 CONTINUE
C     PICTURE DECISION
      NM=MOD(J,NSBP)
      IF (NM.EQ.0) GO TO 50
   51 CONTINUE
      HT(J)=CI+(XF(N)-R)*TA
   12 CONTINUE
      GO TO 61
   62 CONTINUE
      GO TO 101
   50 CONTINUE
C     PICTURE SEQUENCE
      DO 15 I=1,N1
      H(I)=C(I)/(XF(I+1)-XF(I))
      IF(I.GE.M)  H(I) =H(I)+(((XF(I)+XF(I+1))/2.0)-R)*TA
      IF (H(I).GT.HTM)  HTM=H(I)
   15 CONTINUE
```

```
      H(N)=CI+(XF(N)-R)*TA
      IF (H(N).GT.HTM)  HTM=H(N)
      DO 91 I=1,N1
   91 TMA(I)=(XF(I)+XF(I+1))/2.0
      TMA(N)=XF(N)+CI/TA
      DO 16 I=1,50
      Z(I)=RP*FLOAT(I-1)/50.0
      Y(I)=0.0
      IF (Z(I).GE.R) Y(I)=TA*(Z(I)-R)
   16 CONTINUE
      CALL PLOTA(PAREA,0.0,RP,PB,PT,1)
      CALL PLOTB (Z,Y,6H000008,50)
      CALL PLOTB (TMA,H,6H00000*,N)
      CALL PLOTC (WT,NWT,WO,NWO,WA,NWA)
      WRITE(6,1004)T
 1004 FORMAT (1HO,15HWAVE PROFILE AT,1X,F7.3,1X,7HSECONDS)
      GO TO 51
   61 CONTINUE
      HTM=0.0
      DO 64 I=1,NT
   64 IF(HT(I).GT.HTM) HTM=HT(I)
      WRITE(6,1010) HTM
 1010 FORMAT(1H1,4HHTM=,5X,E15.8)
       PT=2.0*HTM-D
      PB=3.0*D-2.0*HTM
      CALL PLOTA(PAREA,0.0,TT,PB,PT,1)
      DO 63 I=1,NT
      T=DT*FLOAT(I-1)
      CALL PLOTB (T,HT(I),6H00000*,1)
   63 CONTINUE
      CALL PLOTC(WT,NWT,WO,NWO,WA,NWA)
      GO TO 62
       END
```

Function Subroutine - FUNC

```
$IBFTC FUNCT
      SUBROUTINE FUNCT
      COMMON
     1/WALL/N,XO,R,N2,G,DRD,DRE,X1,T,DRA,DRC,XF(500),M,PI2,CO3,TA,TG,DX,
     2DRB,D
     3/WFUNC/XP(500),C(250),X(500),TF
      DIMENSION A(500,3),B(500),Y(500)
      DO 7 I=1,N
    7 IF (((X(I)+X(I+1))/2.0).GE.R) GO TO 8
      WRITE (6,1001)
 1001 FORMAT(1H1,5HERROR)
    8 CONTINUE
      M=I
      DO 1 I=1,N
      NI=I+N
      XP(I)=X(NI)
    1 CONTINUE
      XP(N+1)=XO
      N1=N-1
      A(1,1)=0.0
      DO 2 I=3,N
      A(I-1,1)=C(I-1)/4.0-C(I-1)**3*DRA/(3.0*(X(I)-X(I-1))**4)
      II=I-1
      IF(II.GE.M) A(I-1,1)=A(I-1,1)+C(I-1)*TA**2*DRA/4.0
    2 CONTINUE
      DO 3 I=2,N1
      A(I-1,2)=C(I)/4.0+C(I-1)/4.0+C(I)**3*DRA/(3.0*(X(I+1)-X(I))**4)
     1+C(I-1)**3*DRA/(3.0*(X(I)-X(I-1))**4)
      II=I-1
      IF(II.GE.M) A(I-1,2)=A(I-1,2)+C(I-1)*TA**2*DRA/4.0
     1-C(I-1)**2*TA*DRA/(X(I)-X(I-1))**2
      IF(I.GE.M) A(I-1,2)=A(I-1,2)+C(I)*TA**2*DRA/4.0
     1+C(I)**2*TA*DRA/(X(I+1)-X(I))**2
    3 CONTINUE
      A(N-1,2)=(C(N)+C(N-1)/4.0)*(1.0+TA**2*DRA)
     1+C(N-1)**3*DRA/(3.0*(X(N)-X(N-1))**4)-C(N-1)**2*TA*DRA/
     2(X(N)-X(N-1))**2
      DO 4 I=2,N1
      A(I-1,3)=C(I)/4.0-C(I)**3*DRA/(3.0*(X(I+1)-X(I))**4)
      IF(I.GE.M) A(I-1,3)=A(I-1,3)+C(I)*TA**2*DRA/4.0
    4 CONTINUE
      A(N-1,3)=0.0
      DO 5 I=2,N1
      NI=N+I
      B(I-1)=-2.0*C(I)**3*(X(NI+1)-X(NI))**2*DRA/(3.0*(X(I+1)-X(I))**5)
     1+2.0*C(I-1)**3*(X(NI)-X(NI-1))**2*DRA/(3.0*(X(I)-X(I-1))**5)
     2-C(I)**2*G/(2.0*(X(I+1)-X(I))**2)
     3+C(I-1)**2*G/(2.0*(X(I)-X(I-1))**2)
     4-1.00*DRD*SIGN((X(NI)+X(NI+1))**2,X(NI)+X(NI+1))*DX
     5-DRD*SIGN((X(NI)+X(NI-1))**2,X(NI)+X(NI-1))*DX
     6-DRE*C(I)*HYSD(X(NI)-X(NI+1))*((X(NI+1)-X(NI))/(X(I+1)-X(I)))**2
     7/(X(I+1)-X(I))
     8+DRE*C(I-1)*HYSD(X(NI-1)-X(NI))*((X(NI)-X(NI-1))/(X(I)-X(I-1)))**2
     9/(X(I)-X(I-1))
      II=I-1
      IF(II.GE.M) B(I-1)=B(I-1)-C(I-1)**2*(X(NI)-X(NI-1))**2*TA*DRA
     1/(2.0*(X(I)-X(I-1))**3)-C(I-1)*TG/2.0
      IF(I.GE.M) B(I-1)=B(I-1)-C(I)**2*(X(NI+1)-X(NI))**2*TA*DRA
     1/(2.0*(X(I+1)-X(I))**3)-C(I)*TG/2.0
    5 CONTINUE
      B(1)=B(1)-(C(1)/4.0-C(1)**3*DRA/(3.0*(X(2)-X(1))**4))*XO
```

```
      B(N-1)=2.0*C(N-1)**3*(X(N2)-X(N2-1))**2*DRA/(3.0*(X(N)-X(N-1))**5)
     1+C(N-1)**2*G/(2.0*(X(N)-X(N-1))**2)
     2-C(N-1)**2*(X(N2)-X(N2-1))**2*TA*DRA/(2.0*(X(N)-X(N-1))**3)
     3-(C(N)+C(N-1)/2.0)*TG
     4-DRD*SIGN(X(N2)**2,X(N2))
     5-DRD*SIGN((X(N2)+X(N2-1))**2,X(N2)+X(N2-1))*DX
     6+DRE*C(N-1)*HYSD(X(N2-1)-X(N2))*((X(N2)-X(N2-1))/(X(N)-X(N-1)))**2
     7/(X(N)-X(N-1))
      CALL ALGEQN(N-1,A,B,Y)
      DO 6 I=1,N1
      NI=I+N
      XP(NI+1)=Y(I)
    6 CONTINUE
      RETURN
       END
```

Heavyside Function

```
$IBFTC HYS      DECK
      FUNCTION HYSD(X)
      IF(X) 1,2,3
    1 HYSD=0.0
      RETURN
    2 HYSD=0.5
      RETURN
    3 HYSD=1.0
      RETURN
       END
```

Matrix Inversion Subroutine

```
$IBFTC ALG      DECK
      SUBROUTINE ALGEQN(N,A,B,Y)
      DIMENSION  A(500,3),B(500),Y(500),P(500),Q(500)
      P(1)=-A(1,3)/A(1,2)
      Q(1)=B(1)/A(1,2)
      DO 1 I=2,N
      P(I)=-A(I,3)/(A(I,2)+A(I,1)*P(I-1))
    1 Q(I)=(B(I)-A(I,1)*Q(I-1))/(A(I,2)+A(I,1)*P(I-1))
      Y(N)=Q(N)
      DO 2 I=2,N
      J=N+1-I
    2 Y(J)=Y(J+1)*P(J)+Q(J)
      RETURN
       END
```

Bore Input Subroutine - DRIVE

```
$IBFTC DRIVE
      SUBROUTINE DRIVE
      COMMON
     1/WALL/N,XO,R,N2,G,DRD,DRE,X1,T,DRA,DRC,XF(500),M,PI2,CO3,TA,TG,DX,
     2DRB,D
      FR=DRB
      HR=0.5*(SQRT(1.0+8.0*FR**2)-1.0)
      UB=FR*SQRT(32.2*D)
      UW=UB*(1.0-1.0/HR)
      CO6=UW/DRC
      CO5=R/UB
      XO=CO6*EXP(-T/DRC)*HYSD(CO5-T)-HYSD(T-CO5)*CO6*EXP(-(T-CO5)/DRC)
      RETURN
       END
```

Solitary Wave Input Subroutine

```
$IBFTC DRIVE   DECK
      SUBROUTINE DRIVE
      COMMON
     1/WALL/N,XO,R,N2,G,DRD,DRE,X1,T,DRA,DRC,XF(500),M,PI2,CO3,TA,TG,DX,
     2DRB,D
      CO4=SQRT(G*D)*(1.0+0.5*DRB/D)
      CO5=SQRT(3.0*G*DRB)*CO4*DRB/D**2
      CO6=SQRT(3.0*DRB/(4.0*D**3))*CO4
      ARG=CO6*T-5.0
      IF(ARG.GE.5.0) ARG=0.0
      XO=-CO5*TANH(ARG)*4.0/((EXP(ARG)+EXP(-ARG))**2)
      RETURN
       END
```

Square Wave Pulse Input Subroutine

```
$IBFTC DRIVE
      SUBROUTINE DRIVE
      COMMON
     1/WALL/N,XO,R,N2,G,DRD,DRE,X1,T,DRA,DRC,XF(500),M,PI2,CO3,TA,TG,DX,
     2DRB,D
      C=DRB*20.0/DRC
      ARG=T/(2.0*DRC)
      IF(ARG.GT.1.0) GO TO 1
      IF(ARG.LT.0.05) GO TO 2
      IF(ARG.GT.0.45.AND.ARG.LT.0.55) GO TO 3
      IF (ARG.GT.0.95) GO TO 2
    1 CONTINUE
      XO=0.0
      RETURN
    2 CONTINUE
      XO=C
      RETURN
    3 CONTINUE
      XO=-C
      RETURN
       END
```

APPENDIX F

Notation

A	constant
[A]	system matrix function (square matrix)
B	constant
{B}	system right-hand side (column matrix)
c, c_o	local wave speed (in general and at infinity)
c_i, c_n	volume (ith and nth elements)
Cons	constant
d	still water depth
$\overline{DT}$	time step size
$\overline{DX}$	initial element width
f	friction factor
{f}	driving function (column matrix)
F	'artificial viscosity' force at a cross section
Fr	Froude number
g	gravity constant
h, h_o	depth of water (in general and at infinity)
h_1, h_2	depth of water (upstream and downstream of shock)
h_i, h_n	depth of water (ith and nth element)
H	height of solitary wave above still water
H_o	deep water height of wave above still water
He	Heavyside function
k	wave number
K	friction coefficient, constant
K'	'artificial viscosity' coefficient

KE_{hor}, KE_{vert}	kinetic energy (horizontal and vertical)
ℓ	shock width parameter
L_i	Lagrangian of ith element
L_o	deep water wave length of wave
$\overline{LT}$	total Lagrangian
N	number of elements
$\overline{NT}$	number of time steps
p	pressure
P	total horizontal pressure force at a vertical cross section
PE	potential energy
r	roughness
R	intercept of beach slope on x-axis, run-up above still water level
S	beach slope
t	time
u	horizontal velocity
v	vertical velocity
x, x_i, x_n	horizontal coordinate (in general, ith and nth elements)
y	vertical coordinate
α	angle of beach from horizontal
δ	constant
τ	shear stress on bottom

APPENDIX G

References

1. Amein, M., "Bore Inception and Propagation by the Nonlinear Wave Theory," Proceedings of Ninth Conference on Coastal Engineering, American Society of Civil Engineers, 1964, pp. 70-81.

2. Carrier, G. F., "Gravity Waves on Water of Variable Depth," Journal of Fluid Mechanics, Vol. 24, Part 4, April, 1966, pp. 641-659.

3. Chow, V. T., "Hydraulic Jump and Its Use as Energy Dissipator," Open-Channel Hydraulics, McGraw-Hill, New York, 1959, p. 400.

4. Freeman, J. C., and LeMéhauté, B., "Wave Breakers on a Beach and Surges on a Dry Bed," Journal of the Hydraulics Division, A.S.C.E., Vol. 90, No. 2, March, 1964, pp. 187-216.

5. Hall, J. V., and Watts, G. M., "Laboratory Investigation of the Vertical Rise of Solitary Waves on Impermeable Slopes," Technical Memo No. 33, Beach Erosion Board, Corps of Engineers, U.S. Army, March, 1953.

6. Iida, K., "Magnitude, Energy, and Generation Mechanisms of Tsunamis, and a Catalog of Earthquakes Associated with Tsunamis," Proceedings of Tsunami Meetings Associated with the Tenth Pacific Science Congress, National Academy of Sciences, July, 1963, pp. 7-18.

7. Kajiura, K., "On the Partial Reflection of Water Waves Passing Over a Bottom of Variable Depth," See (6), pp. 206-230.

8. Kaplan, K., "Generalized Laboratory Study of Tsunami Run-up," Technical Memo No. 50, Beach Erosion Board, Corps of Engineers, U.S. Army, Jan., 1955.

9. Keller, H. B., Levine, D. A., and Whitham G. B., "Motion of a Bore Over a Sloping Beach," Journal of Fluid Mechanics, Vol. 7, Part 2, Feb. 1960, pp. 302-316.

10. Keller, J. B., "Tsunamis-Water Waves Produced by Earthquakes," See (6), pp. 154-166.

11. Kishi, J., and Saeki, H., "The Shoaling, Breaking, and Run-up of Solitary Waves on Impermeable Rough Slopes," Proceedings of the Tenth Conference on Coastal Engineering, A.S.C.E.,

Vol. I, 1966, pp. 322-348.

12. Laitone, E. V., "The Second Approximation to Cnoidal and Solitary Waves," Journal of Fluid Mechanics, Vol. 9, Part 3, Nov., 1960, pp. 430-444.

13. LeMéhauté, B., Koh, R., and Hwang, L., "A Synthesis on Wave Run-up," Journal of Waterways and Harbors Division, A.S.C.E., Vol. 94, No. WW1, Feb., 1968, pp. 77-92.

14. Miller, R., "Experimental Determination of Run-up of Undular and Fully Developed Bores," Journal of Geophysical Research, Vol. 73, No. 13, July, 1968, pp. 4497-4510.

15. Richtmyer, R. D., and Morton, K. W., "Fluid Dynamics in One Space Variable," Difference Methods for Initial Value Problems, Second Edition, Interscience, New York, 1967, p. 313.

16. Rouse, H., "Surface Resistance," Elementary Mechanics of Fluids, John Wiley, New York, 1946, p. 214.

17. Savage, R. P., "Wave Run-up on Roughened and Permeable Slopes," Journal of Waterways and Harbors Division, A.S.C.E., Vol. 84, Part 3, May, 1958, pp. 1640-1641.

18. Saville, T., "Wave Run-up on Shoreline Structures," Journal of Waterways and Harbors Division, A.S.C.E., Vol. 82, Part 2, April, 1956, pp. 925-1.

19. Stoker, J. J., "Water Waves, the Mathematical Theory with Applications," Interscience, New York, 1957.

20. Takahasi, R., "On Some Model Experiments on Tsunami Generation," See (6), pp. 235-248.

21. Vitousek, M., "Proposed Mid-Ocean Tsunami Gage and Oceanography Instrument System," See (6), pp. 131-133.

22. Von Neumann, J., and Richtmyer, R. D., "A Method for the Numerical Calculation of Hydrodynamic Shocks," Journal of Applied Physics, Vol. 21, March, 1950, pp. 232-237.

23. Wadati, K., Hiron, T., and Hisamoto, S., "On the Tsunami Warning Service in Japan," See (6), pp. 138-145.

24. Whitham, G. B., "On the Propagation of Shock Waves Through Regions of Non-uniform Area or Flow," Journal of Fluid Mechanics, Vol. 4, Part 3, July, 1958, pp. 337-360.

25. Wiegel, R. L., "Research Related to Tsunamis Performed at the Hydraulic Laboratory, U.C. Berkeley," See (6), pp. 174-197.

26. Wiegel, R. L., "Tsunamis," Oceanographic Engineering, Prentice-Hall, New Jersey, 1964, pp. 95-107.